POLITECNICO DI MILANO

Facoltà di Ingegneria Industriale

Corso di Laurea in Ingegneria Aeronautica

FEM modeling of bolted connections for road restraint systems

Relatore: Prof. Marco Anghileri
Correlatore:

Tesi di Laurea di:
Dario GUARINO   Matr. 739692

Anno Accademico 2013/2014

ii

Indice

Elenco delle figure

Elenco delle tabelle

Sommario

Il lavoro di tesi si prefigge l'obiettivo di sviluppare un modello in grado di rappresentare, servendosi di un codice ad elementi finiti, una giunzione bullonata, tipica dei collegamenti delle barriere stradali.

Il corretto comportamento della giunzione è di fondamentale importanza per il buon funzionamento del sistema di ritenuta, che dev'essere in grado di ridirigere il veicolo fuori controllo minimizzando le sollecitazioni cui sono soggetti gli occupanti: da ciò l'esigenza, in numerosi casi, della rottura dei collegamenti, tipicamente tra nastro e paletti.

Si intende creare un modello in grado di migliorare le prestazioni della soluzione comunemente adottata, caratterizzata da un semplice punto di saldatura, introducendo, ad esempio, la possibilità di considerare connesioni multiple e l'utilizzo di un precarico per rappresentare gli sforzi dovuti alla coppia di serraggio necessaria per il collegamento.

Lo scopo finale è quello di migliorare l'accuratezza delle simulazioni "full scale" per ottenere una migliore correlazione con i crash test reali, necessari nell'iter di progetto di una barriera stradale.

Durante tutto il lavoro si fa riferimento alla norma europea EN 1317.

Il lavoro inizia effettuando prove sperimentali "ad hoc", successivamente confrontate con test numerici di dettaglio per trovare il miglior compromesso tra accuratezza dei risultati e costo computazionale.

Infine il modello viene integrato nelle simulazioni di crash test completi.

Parole chiave: sicurezza stradale, giunzioni bullonate, sistemi di ritenuta stradale, Ls-Dyna, crash test, EN 1317.

Abstract

The objective of this thesis is to develop a Finite Element Model able to represent a bolted junction, the typical connection used for road restraint systems.

The proper behavior of the junction is of extreme importance to allow the road barrier to work as intended, being able to redirect the errant vehicle minimizing the stresses for the passengers; because of this, in many cases there is the need to have the failure of some connections, typically between beam and posts.

The aim is to create a model that improves the actual solution, characterized by a simple weld point, introducing, for instance, the possibility to model multiple connections and the use of a preload to represent the stresses due to the tightening torque.

The final goal is to improve the accuracy of "full scale" simulations, to have a perfect correlation between numerical analysis and real crash tests, necessary during the design phase of a road restraint system.

During the whole work the reference norm is the EN 1317.

The first step of the work consists in dedicated experimental tests, followed by a series of numerical simulations to achieve the best compromise between accuracy and computational cost.

Finally the model is integrated in full scale simulations.

Keywords: Road safety, bolted connections, road restraint systems, Ls-Dyna, crash test, EN 1317.

Estratto in italiano

0.1 Obiettivi del lavoro

L'obiettivo di questo lavoro di tesi è creare un modello ad elementi finiti di una connessione bullonata, da utilizzare in simulazioni numeriche di crash test di barriere di sicurezza stradali, per migliorare le previsioni del comportamento del sistema di ritenuta.
Al fine di validare la tecnica di modellazione è stata condotta una campagna di test sperimentali da confrontare con i risultati dei modelli numerici.
Allo stato attuale le giunzioni non sono modellate nelle rappresentazioni numeriche in scala reale: il bullone è sostituito da uno o piu punti di saldatura, spotweld, al fine di unire palletto, nastro ed eventualmente l'elemento distaziatore della barriera; per ciascuna connessione è necessario uno spotweld.
Uno degli obiettivi del nuovo modello è dare la possibilità di collegare tutte le parti desiderate usando un singolo bullone, come accade nella realtà; ovviamente, per rendere ciò possibile, la modellazione dei componenti dev'essere modificata per riprodurre correttamente le controparti reali: in particolare, i fori devono essere aggiunti e la griglia di calcolo adattata alla nuova geometria.
Nella fase iniziale dell'iter di progetto di una barriera stradale le informazioni disponibili riguardo i bulloni sono limitate: tipicamente si è a conoscenza unicamente del diametro e della classe. E' dunque necessario che il modello sia adeguato, prestandosi a rapide modifiche e necessitando, per funzionare, le sole informazioni di cui si é in possesso.

0.2 Organizzazione del lavoro

Il lavoro di tesi è suddiviso in 9 capitoli:

- Capitolo 0: estratto in italiano del lavoro

- Capitolo 1: introduzione, presentazione generale del lavoro, descrizione approfondita di una barriera stradale;
- Capitolo 2: stato dell'arte per la modellazione delle giunzioni;
- Capitolo 3: descrizione dei test sperimentali effettuati, della modalità di prova e dei risultati ottenuti;
- Capitolo 4: presentazione dei modelli numerici di dettaglio creati, nelle diverse configurazioni adottate: modelli con elementi bidimensionali
- Capitolo 5: presentazione dei modelli numerici di dettaglio creati, nelle diverse configurazioni adottate: modelli con elementi tridimensionali;
- Capitolo 6: risultati dei test di dettaglio e confronto con i dati sperimentali;
- Capitolo 7: il comportamento del modello di bullone è studiato applicandolo ad analisi in scala reale, confrontando i risultati numerici con quelli di crash test al vero;
- Capitolo 8: conclusioni e sviluppi futuri.

0.3   Tipologia e descrizione dei sistemi di ritenuta

L'importanza dei sistemi di ritenuta stradale è chiara considerando il numero di veicoli che percorre la rete stradale: 300 milioni, per oltre 5 milioni di chilometri nella sola unione europea; l'impatto economico di incidenti, feriti e morti è stimato intorno al 2% del PIL del continente, corrispondente a circa 250 milioni di euro. I sistemi di ritenuta sono considerati come i più flessibili tra i sistemi di sicurezza, poichè sono in grado di contenere differenti tipi di veicoli in molteplici configurazioni: da una piccola vettura ad un autoarticolato, con la possibilità di essere equipaggate con parti dedicate alla protezione per i motociclisti. Lo scopo di un sistema di ritenuta stradale è quello di minimizzare le conseguenze dell'impatto di un veicolo errante.

I termini chiave per descrivere il comportamento e le prestazioni di una barriera stradale, riportati nella normativa di riferimento EN-1317, sono:

- Livello di contenimento
- Larghezza di lavoro
- Deflessione dinamica
- Intrusione del veicolo
- Severità di impatto
- Redirezione

0.4 Stato dell'arte

Durante l'impatto tra veicolo e sistema di ritenuta i bulloni sono soggetti
ad elevate forze e momenti che causano notevoli sforzi e deformazioni, con
conseguente possibile cedimento della giunzione stessa, che tipicamente può
avvenire per rottura del bullone o per deformazione del foro permettendo
alla vite di essere sfilata.
In alcuni casi il cedimento della giunzione é necessario per il corretto funzionamento del sistema ritenuta, evitando che questo diventi, nel peggiore
dei casi, una rampa per il veicolo che vi impatta.

(a) *t = 0.0 s.*   (b) *t = 0.1 s.*

(c) *t = 0.2 s.*   (d) *t = 0.3 s.*
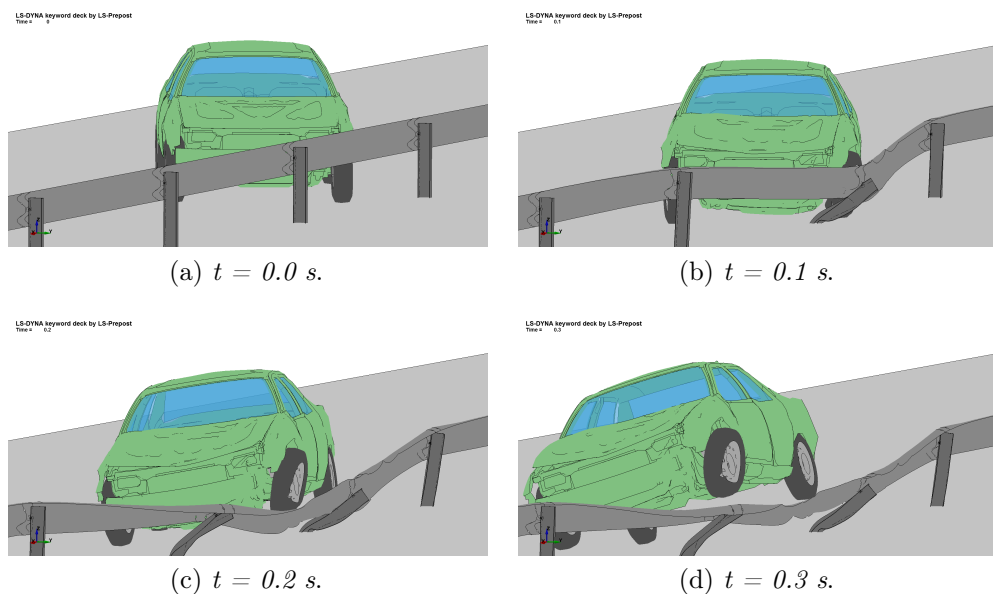
Figure 1: Comportamento del veicolo in caso di mancato cedimento della giunzione

Uno dei requisiti che deve avere il nuovo modello é la versatilità: deve
infatti permettere di studiare sia il comportamento del bullone in caso di
test di dettaglio, sia come la singola giunzione ha effetto sull'intero sistema
di ritenuta.

0.5   Prove sperimentali

La macchina in figura 2 si trova nei laboratori del CRM [1] ed é stata utilizzata per condurre i test.

Figure 2: Macchina per test di trazione

Una volta preparati tutti i componenti necessari allo svolgimento delle prove sono stati tirati 9 bulloni, ripartiti su quattro configurazioni di prova differenti.

(a) *Sega a nastro.*
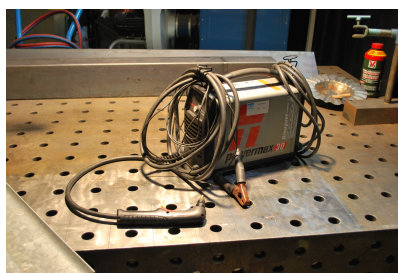
(b) *Plasma Cutter.*

(c) *Nastro dopo le operazioni di taglio.*
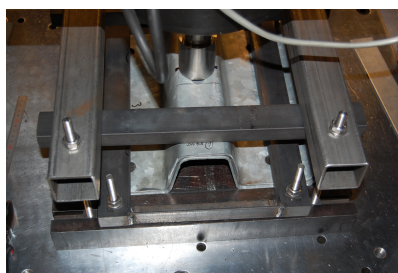
(d) *Nastro vincolato.*

Figure 3: Materiale di prova

---

[1]Centro di ricerca sulla metallurgia di Arcelor-Mittal, Liegi

Prima di procedere con i risultati delle prove un'importante considerazione é necessaria: sebbene nominalmente tutti uguali, i bulloni M10 si sono rivelati diversi tra loro, infatti, in alcuni casi, sono state riscontrate delle differenze tra le dimensioni della filettatura di bulloni e dadi; ciò ha influenzato l'esito di alcune prove. Purtroppo ci si é resi conto di tale problema solo al termine della prima giornata di lavoro.

0.5.1 M10 4.6 - Risultati

Nelle tabelle 1 e 2 sono presenti la lista delle parti utilizzate ed i risultati ottenuti.

	Spessore	Diametro del foro o dimensione di riferimento
Nastro singolo	3.0 mm	60 x 18 mm
Nastro doppio	6.0 mm	60 x 18 mm
Rondella	2.3 mm	10.6 mm interno, 20 mm esterno
Piattino copri asola	5.0 mm	12 mm

Table 1: M10 - Parti utilizzate

	Carico massimo [N]	Spostamento [mm]
Singolo nastro 1	29812.9	9.550
Singolo nastro 2	28796.4	13.405
Singolo nastro 3	28929.2	10.424
Doppio nastro 1	31503.8	4.960
Doppio nastro 2	31346.9	6.074
Doppio nastro 3	34416.1	7.172

Table 2: M10 - Risultati

In un caso il bullone si é rotto, mentre negli altri due é stato sfilato a seguito della rottura del piattino copri asola.

Usando due nastri sovrapposti in un caso il bullone si é rotto, mentre nei restanti due ha ceduto la filettatura.

(a) *M10.*   (b) *Piattino copri asola.*
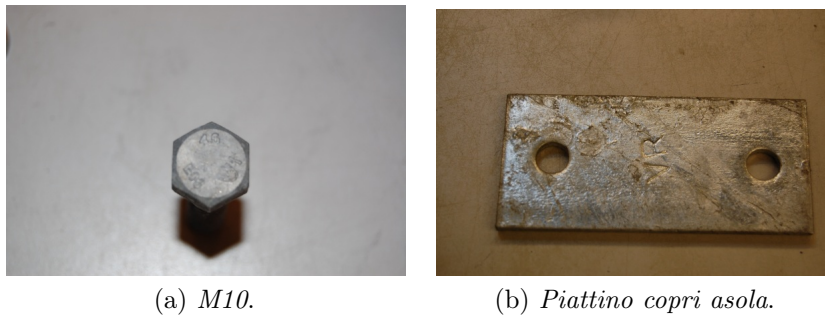
Figure 4: M10
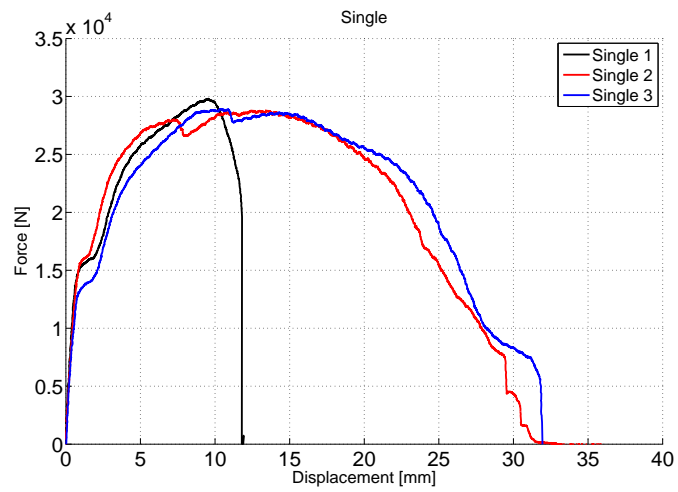
Figure 5: M10 - Nastro singolo

(a) *Bullone rotto.*   (b) *Piattino rotto.*
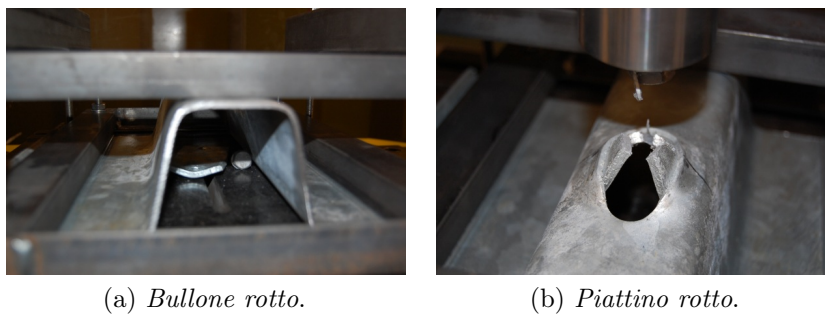
Figure 6: M10 - Dopo il test
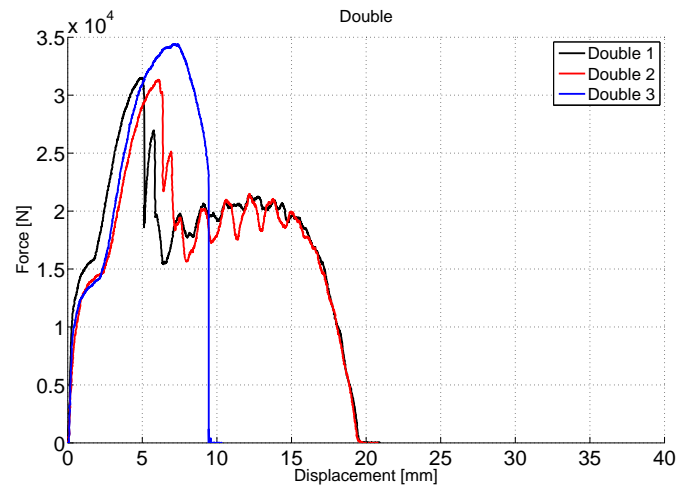
Figure 7: M10 - Doppio nastro
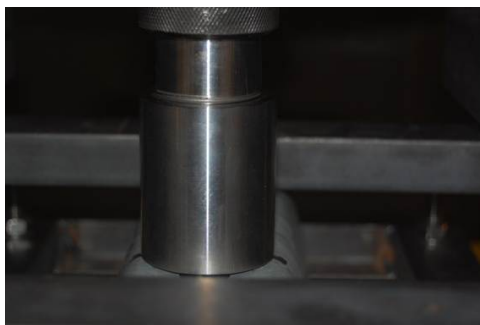
(a) *Primo stadio.*   (b) *Ultimo stadio.*

Figure 8: M10 - Prima e dopo la prova

0.5.2   M16 5.8 - Risultati

La configurazione di prova é la stessa usata con gli M10; in questo caso solamente tre prove sono disponibili, due con il bullone in posizione centrata rispetto al foro ed una con la vite ad un'estremità. In entrambi casi sono stati usati due nastri sovrapposti.

	Spessore	Diametro del foro o dimensione caratteristica
Nastro singolo	2.5 mm	60 x 18 mm
Nastro doppio	5.0 mm	60 x 18 mm
Piattino copri asola	5.0 mm	18 mm

Table 3: M16 - Parti utilizzate

Figure 9: M16 e piattino copri asola

	Carico massimo [N]	Spostamento [mm]
Centrato 1	82760	28.75
Centrato 2	81203	25.02
Decentrato	85489	10.75

Table 4: M16 - Risultati
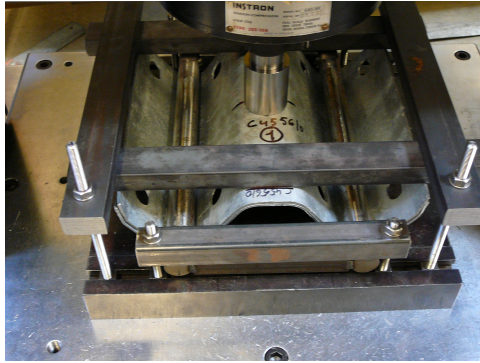
(a) *M16 - Configurazione centrata.*
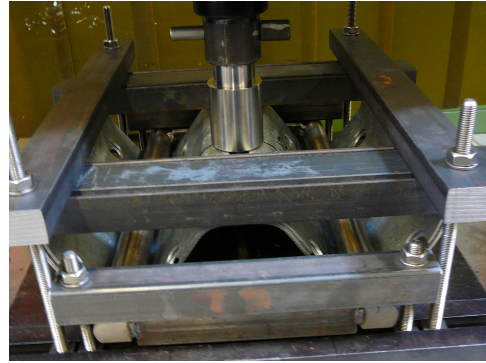
(b) *M16 - Configurazione decentrata.*

Figure 10: M16 - Risultati
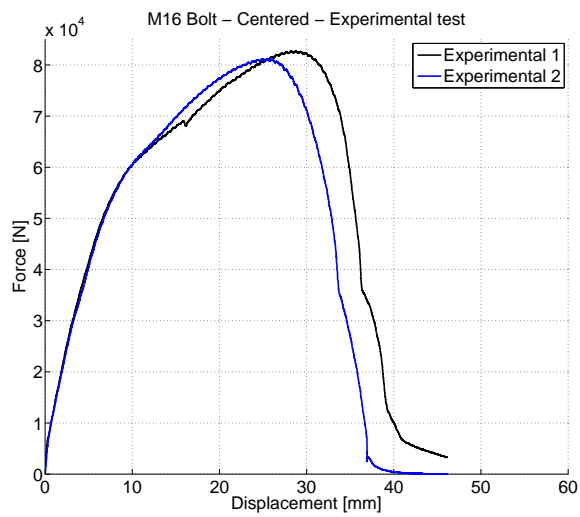
Figure 11: M16 - Configurazione centrata
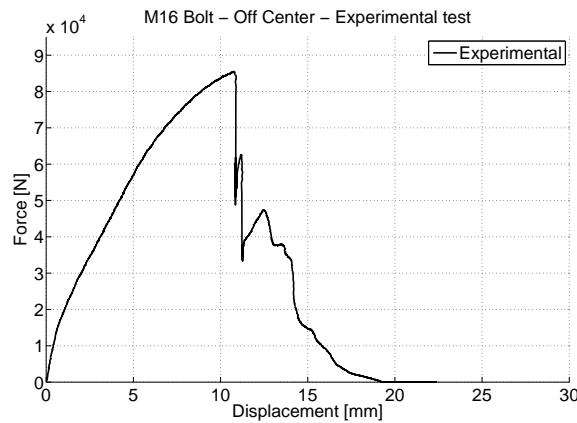
Figure 12: M16 - Configurazione decentrata

0.5.3   Analisi dei risultati

Sebbene a livello teorico le parti utilizzate avrebbero dovuto essere uguali
tra loro, i risultati ottenuti mostrano differenti comportamenti.
Questo si deve al fatto che il metodo utilizzato per classificare gli acciai
é basato sul valore minimo, nominale, garantito; ciò significa che per un
bullone di classe 4.6 lo sforzo minimo per giungere a rottura é 400 MPa. In
questo modo sono influenzati anche gli altri componenti: un acciaio S235
avrà un valore di snervamento minimo di 235 MPa, ma in teoria, secondo
la norma attuale, potrebbe avere un valore di snervamento reale di 500
MPa.
    Come mostrato in figura 13, in entrambi i casi, lo sforzo a rottura é
maggiore del minimo, anche in modo considerevole se si considera il secondo
caso. Il modello numerico proposto può facilmente tenere conto di tali
differenze, semplicemente modificando il valore di rottura tra i parametri
del materiale, che come valore predefinito utilizza quello nominale.

0.6   Descrizione del modelli numerici

I modelli numerici realizzati si differenziano per il tipo di elementi uti-
lizzati: solidi o bidimensionali. L'approccio ad elementi solidi permette
uno studio di dettaglio della giunzione e sfrutta lo schema di soluzione
implicito, garantendo stabilità della soluzione e tempi di calcolo contenuti
nonostante il gran numero di elementi presenti nel modello; l'approccio a
shell, invece, é richiesto per essere utilizzato nelle analisi in scala reale.
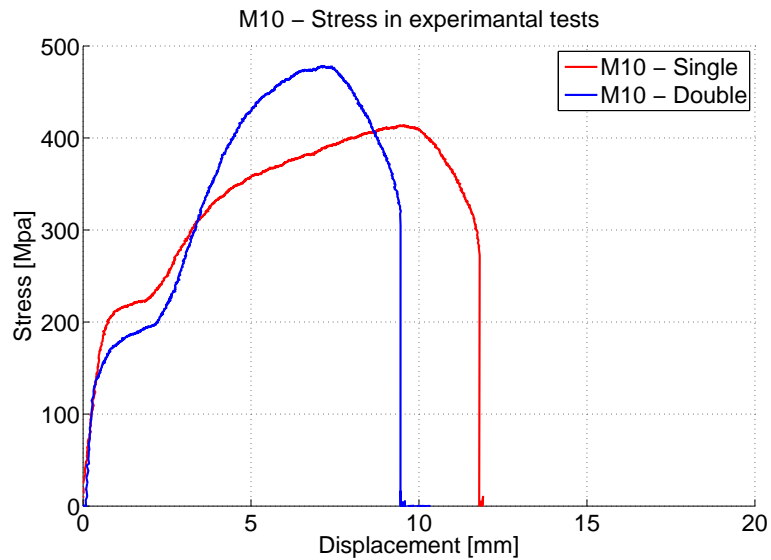
Figure 13: Sforzi nei bulloni M10

0.6.1 Modello 3D

Il modello consiste di 349.578 nodi e 294.708 elementi nel caso del bullone M16 e 140.044 nodi e 103.287 elementi per il modello di M10.

(a) *M16.*   (b) *M10.*
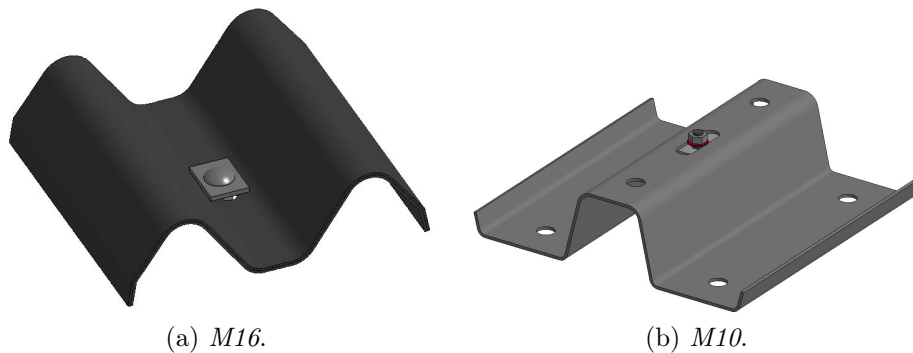
Figure 14: Modello 3D

Per favorire la convergenza della soluzione si é scelto di usare elementi sottointegrati, tipicamente non affetti da problemi di stabilità e non troppo esigenti dal punto di vista computazionale. Ciascun nastro é caratterizzato da 3 elementi lungo lo spessore.
Vincoli ed imposizione dello spostamento sono analoghi alla prova reale, come illustrato in 15.

(a) *Vincoli.*   (b) *Modalità di tiro.*
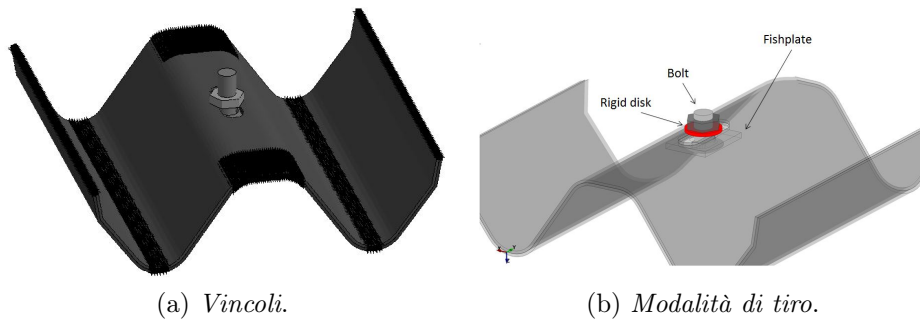
Figure 15: Condizioni al contorno

Per definire il criterio di rottura si é fatto ricorso al livello di defor-mazione plastica degli elementi: superato un valore di soglia gli elementi sono cancellati del modello; é chiaramente un criterio con dei limiti, primo fra tutti la sensibilità alle dimensioni della discretizzazione, ma nonostante ciò si é rivelato accurato ed adatto al problema.

0.6.2   Modello 2D

Il modello é generale: per passare da un bullone ad un altro é sufficiente cambiare le proprietà nelle schede di LS-Dyna, senza la necessità di modi-ficare la geometria; esso consiste in un elemento monodimensionale, per simulare il gambo del bullone e due gruppi di shell per riprodurne testa e dado. I punti di forza sono la semplicità di modellazione, un'alta efficienza computazionale e validi risultati.
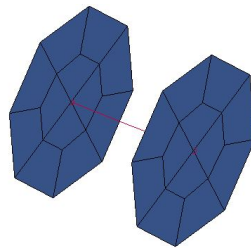
Figure 16: Modello bidimensionale

Il materiale da assegnare all'elemento rappresentante il gambo della vite é il *MAT 100: Spotweld damage failure*, che richiede in ingresso solamente due parametri per definire un criterio di rottura; entrambi sono noti a partire dalla classe della vite che si vuole riprodurre:

- σ_{rr}^{F} - Sforzo assiale a rottura

- τ^F Sforzo di taglio a rottura

usati nella seguente equazione:

$$\left(\frac{\sigma_{rr}}{\sigma_{rr}^F}\right)^2 + \left(\frac{\tau}{\tau^F}\right)^2 = 1 \tag{1}$$

Se il termine di sinistra dell'equazione diventa maggiore di 1 lo spotweld cede, causando il cedimento della giunzione.

Tale criterio considera la componente di forza assiale, le due componenti di taglio ed i momenti intorno ai 3 assi.
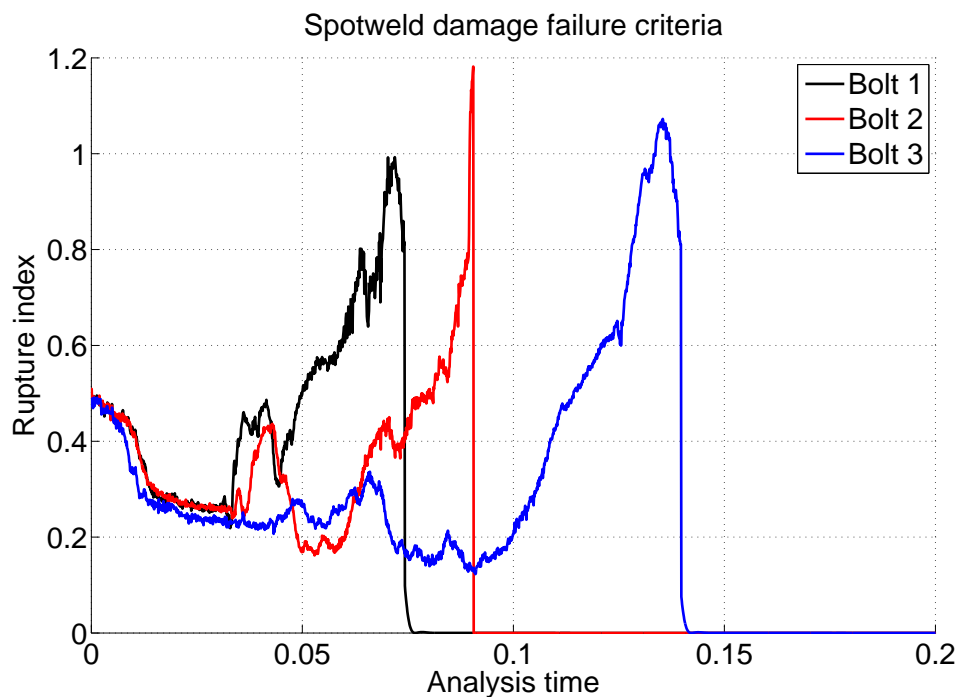
Figure 17: Cedimento del bullone

Il modello prevede la possibilità di introdurre un precarico nella vite, per simulare la coppia di serraggio data dal dado.

Per gestire accuratamente i contatti si utilizzano delle "Null Beam", elementi monodimensionali posizionati sul perimetro di ciascun foro e sovrapposte all'elemento rappresentante il gambo del bullone. Il materiale a loro assegnato é privo di massa e resistenza; hanno una funzione puramente numerica e nessun effetto strutturale.

Dopo la prima serie di test numerici due problematiche sono emerse: rottura prematura, in alcuni casi, di bulloni M10, ed eccessiva deformazione
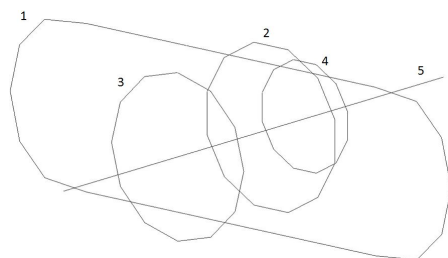
Figure 18: Null beam

di testa e dado nel caso di M16. Per ovviare a tali difetti il modello é stato modificato, aggiungendo altre 4 beam per rappresentare il gambo del bullone.
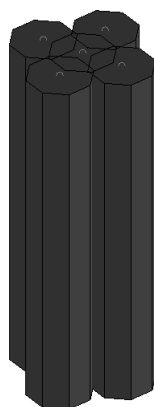
Figure 19: Modello a 5 beams

0.7   Correlazione numerico - sperimentale

In questa parte del lavoro sono confrontati i risultati dei testi numerici locali con i test sperimentali. Per esigenze numeriche la velocità di tiro durante le analisi numeriche é maggiore di quella usata durante le prove; 1 mm/s per i casi impliciti e 100 mm/s per i quelli espliciti. In 20 energia interna e cinetica sono state confrontate per assicurarsi di avere un comportamento statico.
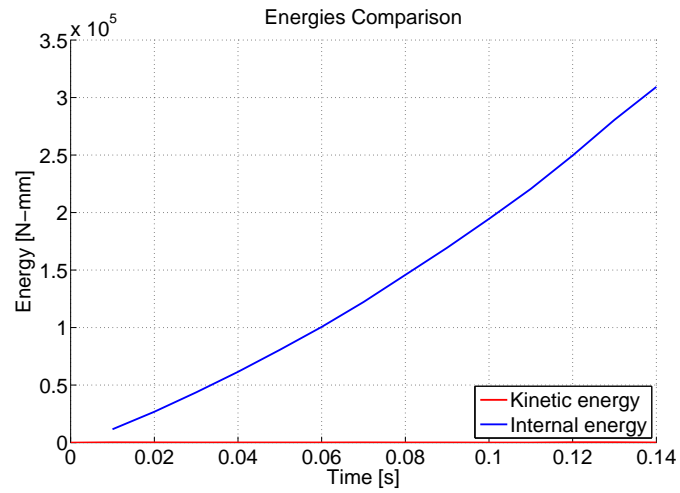
Figure 20: Confronto energie

0.7.1   M10 - 4.6

In 21 é presente l'andamento del carico, mentre in tabella 5 i valori massimi di forza assiale.

Caso	Numerico [N]	Sperimentale [N]	Δ	Errore [%]
Shell 1-beam	30635	29813	822	2.7
Shell 5-beam	29986	29813	173	0.6
Solidi	30368	29813	555	1.9

Table 5: M10 forze di picco - Nastro singolo

In figura 22, a sinistra, si nota chiaramente l'esigenza del modello a 5 beam, per evitare che la forza si concentri in un unico nodo deformando le shell circostanti in modo assolutamente non fisico e permettendo la trasmissione di momenti che in realtà sono contrastati della sezione stessa del bullone.
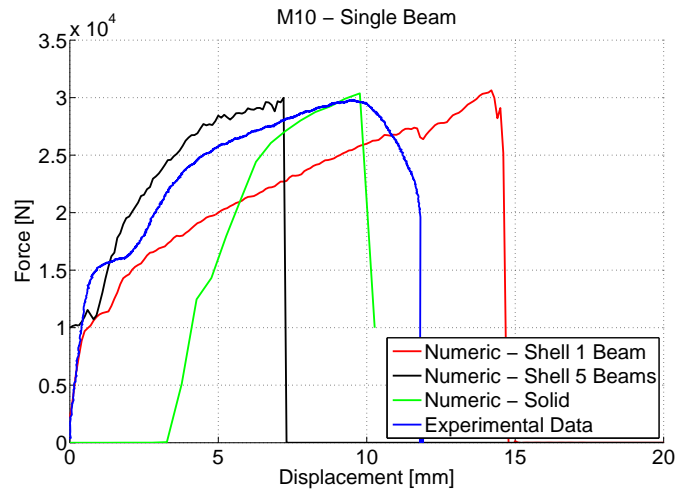
Figure 21: M10 - Singolo nastro - Risultati

(a) *Shell 1-beam.*   (b) *Solidi.*
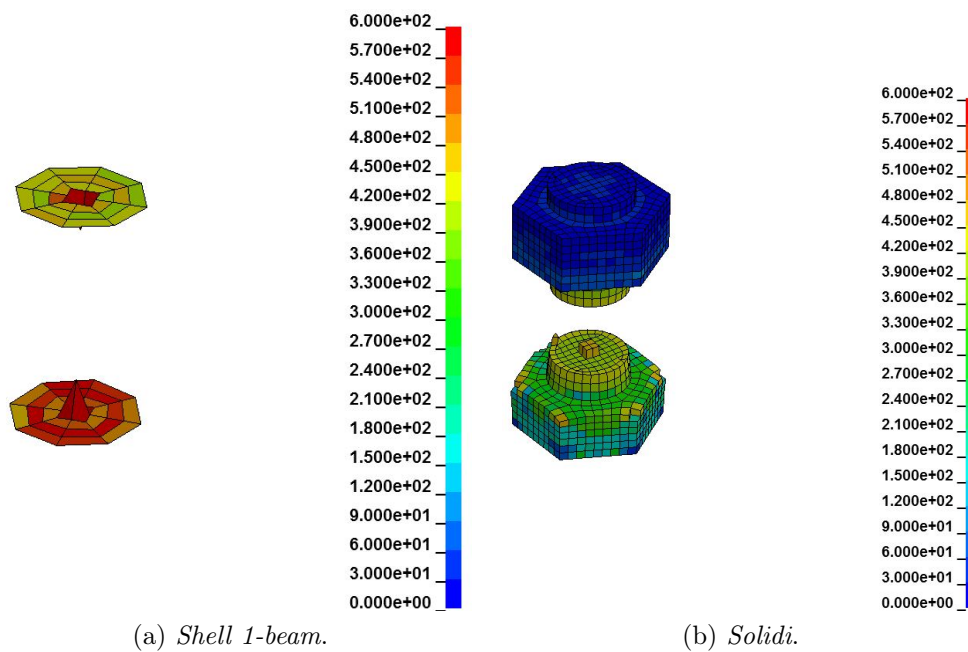
Figure 22: M10 a rottura - Nastro singolo

0.7.2   M16 - 5.8

In questo caso non si ha la rottura del bullone: i valori di picco sono ben riprodotti, mentre la pendenza delle curve potrebbe essere migliorata usando le leggi reali dei materiali al posto di quelle di acciai generici.
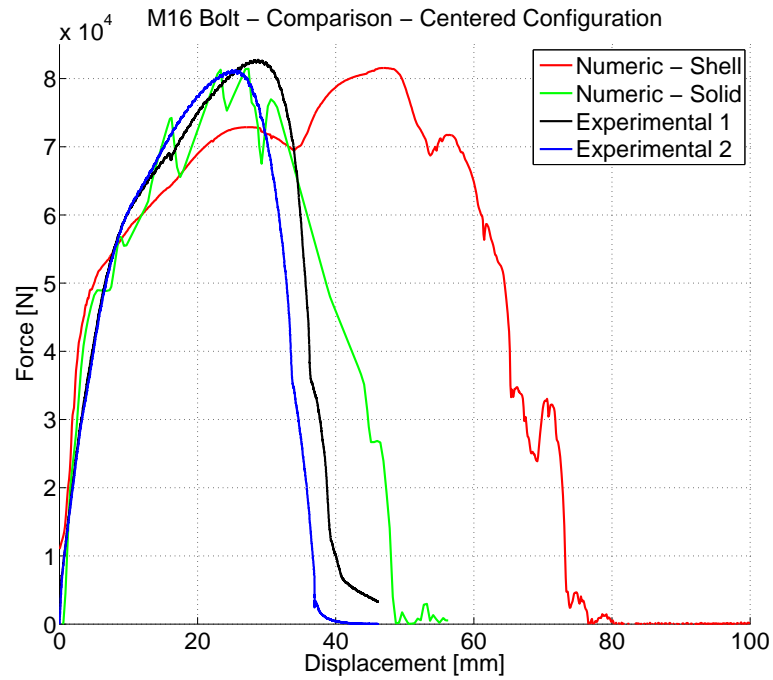
Figure 23: M16 - Bullone in posizione centrata

Caso	Numerico [N]	Sperimentale [N]	Δ	Errore [%]
Shell	81553	81981	428	0.5
Solid	81434	81981	547	0.7

Table 6: M16 a rottura - Bullone in posizione centrata

In tabella 7 invece sono riportati i tempi di calcolo di ciascuna soluzione adottata, per evidenziare l'alta efficienza degli elementi 2D.
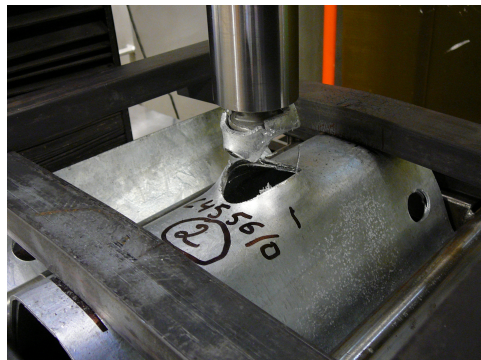
(a) *Sperimentale.*
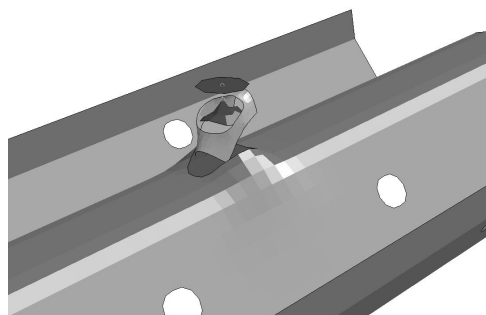
(b) *Modello a shell.*
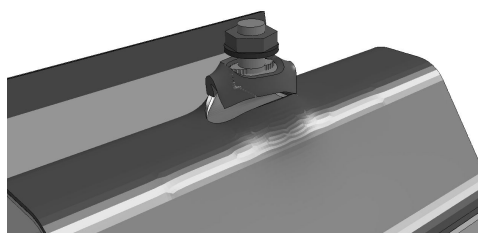
(c) *Modello a solidi.*

Figure 24: M16 - Istante finale

Modello	Tempo
M10 - Nastro singolo - 1 Beam	11m31s
M10 - Nastro singolo - 5 Beams	11m57s
M10 - Nastro singolo - Solid	24m21s
M16 - Posizione centrata - 1 Beam	11m29s
M16 - Posizione centrata - Solid	8h13m

Table 7: Tempo di calcolo

0.8   Risultati delle simulazioni in scala reale

I fattori chiave per valutare la qualità di un modello sono: il tempo computazionale e l'accuratezza dei risultati, in termini di numero di disconnesioni, larghezza di lavoro e deflessione dinamica della barriera.
Sono di seguito riportati, in parte, i risultati ottenuti.
Il caso della tabella 8, il cui nome non é riportato per motivi di confidenzialità, riguarda un veicolo da 900Kg che impatta con un angolo di 20° ad una velocità di 100 km/h.

Caso	Elementi	Tempo	Disc.	WW	DD	ASI
Spotweld	473.138	33h38m	4	0.85	0.79	0.75
1-Beam	482.013	13h47m	2	0.86	0.65	0.93
Test reale	-	-	2	0.76	0.68	0.80

Table 8: Risultati barriera A - TB11

Grazie al nuovo modello di bullone, oltre ad una sensibile diminuzione del tempo di calcolo, si ottengono valori migliori di ASI e DD.
In tabella 9 la stessa barriera é testata con un veicolo pesante da 10 tonnellate.

Caso	Elementi	Tempo	Disc.	WW	DD	ASI
Spotweld	473138	36h27m	3	1.22	1.13	3.04
1-Beam	482013	37h24m	2	1.22	1.15	1.60
Test reale			2	1.19	1.11	2.90

Table 9: Risultati barriera A - TB42

In 10, ultimo caso presentato, sono analizzate tutte le configurazioni simulate.
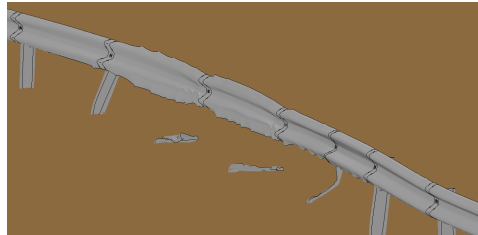
(a) .   (b) .

Figure 25: Barriera A - TB42

Nome	Elementi	Discs.	WW	DD	Angolo d'uscita	ASI
Spotweld	585.310	5	0.75	0.54	8	0.75
1-Beam	567.407	4	0.83	0.62	8	0.75
5-Beams	568.648	4	0.83	0.60	9	0.78
Solidi	670.937	3	0.82	0.61	9	0.69
Doppio	582.004	3	0.80	0.68	9	0.71
Test reale	-	4	0.8	0.7	9	0.7

Table 10: Risultati Barriera B - TB11

0.9 Conclusioni e sviluppi futuri

A seguito dei risultati ottenuti si puo' concludere che il modello di bullone funzioni e fornisca buoni risultati; l'obiettivo di avere un modello in grado di operare con le sole ridotte informazioni disponibili nella fase iniziale del progetto é stato raggiunto.

Il modello é in grado di riprodurre entrambe le modalitità tipiche di rottura caratterizzanti i sistemi di ritenuta stradale: rottura del gambo della vite e sfilamento del bullone ancora intatto.

Le numerose simulazioni condotte hanno sancito la superiorità della soluzione ad elementi bidimensionali, grazie all'alta efficienza computazionale, che la rendono utilizzabile con efficacia in tutte le configurazioni; il modello ad elementi solidi si é rivelato anch'esso accurato, ma dall'applicazione limitata ai soli test locali o barriere molto semplici. Il suo utilizzo in sistemi complessi comprometterebbe eccessivamente il tempo di calcolo.

Nel complesso, i miglioramenti apportarti alla soluzione spotweld sono considerevoli e soddisfacenti.

Se in futuro venissero condotte ulteriori compagne sperimentali sarebbe possibile studiare casi specifici, come il caso di bullone soggetto a pura trazione.

Con l'aumento delle prestazioni dei calcolatori, negli anni a venire la soluzione ad elementi solidi potrebbe essere sempre più diffusa, a patto di essere in grado di riprodurre accuratamente il comportamento del materiale in situazioni critiche, come la rottura.

Chapter 1

Introduction

1.1 Objectives of the work

The objective of this work is to create a new finite element model of bolted connections, to be used in full scale dynamic simulations of full scale crash tests of road safety barriers, to improve the capability to predict the behavior of the restraint system.

In order to validate the modeling technique, experimental tests were carried out and compared with numerical results.

Usually the junctions are not modeled in full scale crash test simulations: the bolt is replaced by one or more spotwelds that link together post, beam, and eventually a spacer and a backstrip; for each connection one spotweld is needed (beam to spacer, spacer to post, beam to post...etc).

One of the goals of the new model will be the possibility to connect all the parts with just one bolt, as it is in reality. Obviously the geometry of all the involved parts must be modified to represent the real components: in particular the holes will be added and the mesh of the pieces adapted to the new geometry.

Since the first phase of the work it is important to take into account the fact that the final model should be the best compromise between accuracy and computational time.

During the whole development of a road restraint system, flexibility and easiness of use of the tools to realize the numerical model are a key factor. Typically, in the initial design phase of a new barrier, the amount of available information from the manufacturer is limited; considering junctions, the only data provided concern:

- the diameter of the bolt;

- the class of the bolt.

Both these parameters, during the design and optimization of the product, are changed several times, hence it is mandatory to have a model quickly modifiable.
The pursuit of the state of the art is the final goal of this master thesis work.

1.2   Organization of the work

This thesis is divided in 9 chapters:

- Chapter 0 - Short summary, in Italian.

- Chapter 1 - Introduction: objectives of the work and general overview of road restraint systems, a brief classification of the products, terminology and norm EN 1317;

- Chapter 2 - State of the art: importance of bolts and available solutions to model a junction;

- Chapter 3 - Experimental tests: the test configuration is described and the results presented;

- Chapter 4 - Local numerical models: 3D configuration;

- Chapter 5 - Local numerical models: 2D configuration;

- Chapter 6 - Results of local tests: all the results of the numerical simulations are shown, for the all cases presented in chapter 4 and 5. The results are compared with the experimental data of chapter 3;

- Chapter 7 - Results of full scale simulations: the behavior of the junction model is analyzed in full scale simulations and the results are compared with real crash tests;

- Chapter 8 - Conclusions and further developments for the model.

1.3   About Road Restraint Systems...

In the European Union over 300 million vehicles circulate on a road network of approximately 5 million kilometers. The societal impact of road accidents, fatalities and injuries is estimated to be around 2% of the EU GDP[1], or in other words, around 250 billion euros. Injuries and fatalities due to road accidents are a problem that can considerably be addressed if the necessary attention is given to the prevention strategies and solutions.

Road restraint systems can be considered as the most "flexible safety device" possible: they are designed to withstand a crash from different kind of vehicles in different conditions: according to their containment level, they are tested both for a small city car or a large family car; small to heavy truck or coach, with the possibility to equip it with a motorcyclist protection system (MPS) to further extend this protection to a particularly affected class of vulnerable road users.

Road safety is based on a three pillar approach, by focusing on the vehicle, the driver and last but not least, the infrastructure. In turn, infrastructure safety can be separated into active safety measures, whose role is to ensure as far as possible that the driver maintains control of his vehicle through appropriate guidance (e.g. road markings and signs) and passive safety measures, whose role is to protect drivers once they have lost control of their vehicle and, in the end, to protect drivers from their own human mistakes.
These concepts are summarized in the well known Haddon matrix:

Figure 1.1: Haddon matrix

Road Restraint Systems are one of the most efficient and cost-effective

---

[1]Gross Domestic Product

road infrastructure solutions that can reduce the impact of a road accident
and the number of fatalities and injuries for the vehicle passengers.

(a) .   (b) .
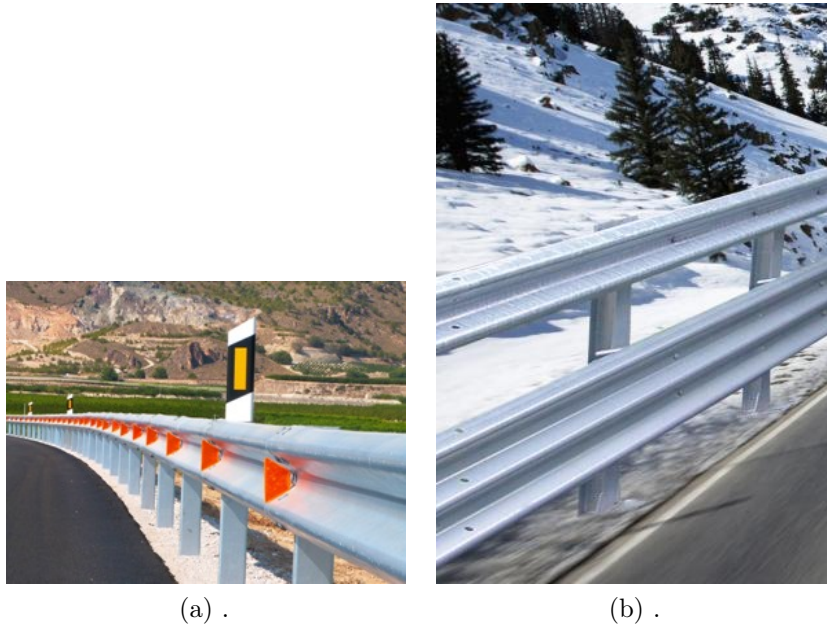
Figure 1.2: Road safety barrier

1.4   The infrastructure

In recent years the efforts in road safety have increasingly focused on the
vehicle and the driver, often neglecting the role of the infrastructure. Thus,
while significant resources have been devoted to developing new vehicle
technologies and enforcement campaigns, investments and resources for
road infrastructure have steadily dwindled over the years. According to
the International Transport Forum, investment in infrastructure for many
Western European Countries reached an all time low in 2007, a trend which
most likely has not improved since the outbreak of the economic crisis in
2008.
In addition to this overall decrease, road infrastructure has seen its per-
centage modal share decrease vis-à-vis the railways despite the fact that
road remains by far the dominant mode for both commercial freight and
passenger transport.

       While acting on the driver and on the vehicle surely has its role to
play, it is also true that investing in road infrastructure can offer fast and
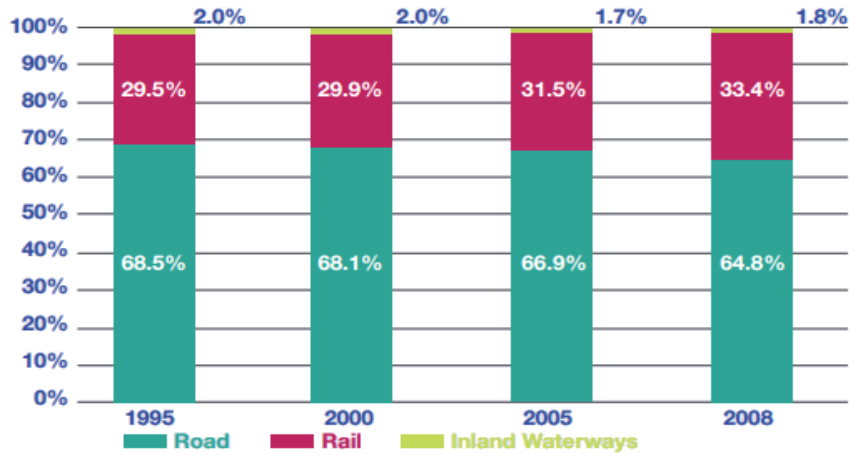
Figure 1.3: Infrastructure investment

cost-effective solutions that can reduce fatalities and related health care costs.

If investing on road infrastructure measures is a cost-effective solution for improving road safety and saving lives, then, it can be naturally assumed that failing to do so can have major consequences, not only in terms of lives, but also in terms of the cost of accidents, which are significant.

According to a study recently published in the USA by the Pacific Institute of Research and Evaluation entitled 'On a crash course: dangers and healthcare costs and deficient roadway conditions', more than half of U.S. highway fatalities are related to deficient roadway conditions, a substantially more lethal factor than drunk driving, speeding or non-use of safety belts. Furthermore, the study concluded that the cost of deficient roadway conditions was significantly higher than the costs of other safety factors. [34]
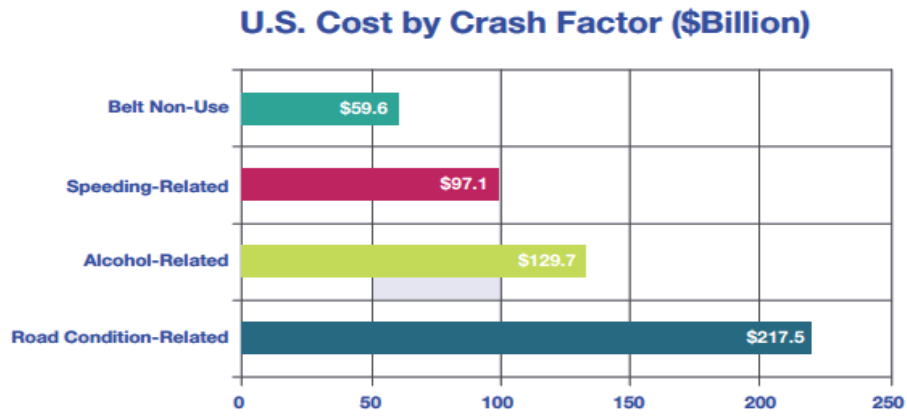
Figure 1.4: Us cost by crash factors

Figure 1.5: Distribution of global injury mortality by cause

1.5   What is a Road Restraint System

A Road Restraint System is a safety product, which aims at reducing the consequences of accidents of an errant vehicle.
Road restraint systems can be divided in:

- Road safety barriers – the road barriers are placed along the roadside or on the central reserve; their role is to prevent errant vehicles from crashing on roadside obstacles, and to retain them safely.

- Crash cushions – the crash cushions are collapsible structures that prevent vehicles (usually cars) from impacting specific hazardous sections (eg: the beginning of the central reserve). They safely stop the vehicle, avoiding worse consequences.

- Terminals for road safety barriers – Terminals are the ending part of a safety barrier; their role is to avoid those parts from becoming dangerous points for vehicles.

- Motorcycles protections systems – MPS represent an integrated system or an upgrade which, if applied on a road safety barrier, can reduce the consequence of impact for a motorcyclist after falling.

- Transition between 2 safety barriers – Transitions are products which connect two safety barriers, guaranteeing structural continuity and a correct passage from the performance of the first barrier to the following one without creating black spots in those critical points

Each of those products have to comply with several safety requirements, which take into account the safety of the occupant involved in the crash as well as the safety of incoming traffic, both on the same lane and on the opposite one, depending on their location (lateral/central).
To assess those requirements, crash tests must be performed on each of those products; they aim at recreating ideal situations representative of the worst possible real-case that may happen in real-life, considering the "state-of-the-art" of crash-testing technology, the repeatability of the tests and, of course, the need to assess reliable safety features.

1.6   Road Safety Barriers

Road barriers can be classified in 3 different groups, based on how the
device works:

- flexible barriers
- semi-rigid barriers
- rigid barriers
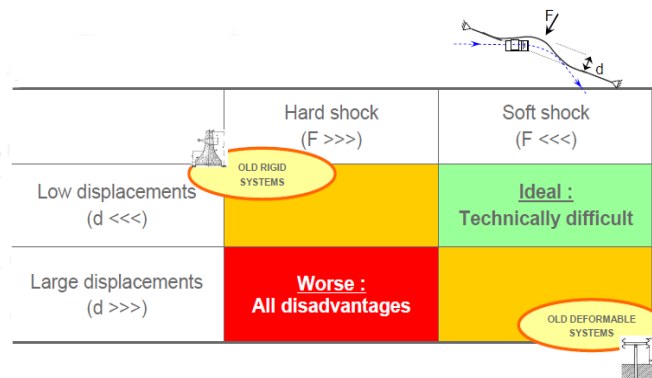
Figure 1.6: Barrier matrix

1.6.1   Flexible barriers

Typically wire systems, as shown in figure 1.7; because of the large deflec-
tions that occur in the system during the impact of the vehicle, they work
due to a yielding mechanism.

The system comprises wire ropes supported by weak posts installed pri-
marily to support them; the mechanism of flexible barriers ensure smooth
redirecting of the vehicle during the impact and the design enables the
cables to strip from the frangible posts. The separation of the post from
the wire ropes during impact makes the dissipation of the vehicle kinetic
energy through the deflection of the wire rope, minimizing the severity of
vehicle impact with the barriers.

Figure 1.7: Flexible Barrier

1.6.2 Semi-ridig barriers

Semi-rigid safety barriers mainly include systems that have a steel beam attached to wooden or steel posts.

These barriers deform permanently under impact and after the crash complete sections have to be replaced; this is possible due to the presence of bolted connections, that keep the pieces together.

In semi-rigid barrier there are 3 main components, plus a series of accessories:

- Beam
- Post
- Junctions

The beam has to absorb the energy deforming and redirect the vehicle; it is mandatory that it doesn't break nor is bypassed.

The design is quite standard, characterized by 2 or 3 waves, a thickness between 2 or 3 mm and the length of a single section typically is 4 meters. The post is responsible of absorbing a good amount of energy due to the large deformation that can sustain. Its behavior is critical because, potentially it can become a ramp for the vehicle. The sections used are several but the most common are: C, U and Σ. It is the unique component that is in contact with the soil, whose behavior affects the performances of the whole system. A too hard soil could cause the rupture of the posts meanwhile a too soft soil couldn't provide the proper resistance to the movement of the posts.

Posts are positioned each 2 or 4 meters and each 1.33 m for high containment devices; anyway the manufacturers can choose the distance to optimize the design of their products.

Figure 1.8: Example of bad soil behavior

1.6.3   Rigid barriers

Rigid safety barriers are basically a reinforced concrete wall constructed with a profile and an height that is designed to contain and redirect errant vehicles, as in figure 1.9.

Figure 1.9: Concrete barrier

They are mainly used where the conformation of the road doesn't allow enough working width to install a steel device; some administration choose them because of the low management costs, in fact in case of accident there is no need to replace any part, but, on the contrary, in case of flexible or semi-flexible devices, especially if the quality of the design is poor, the reparation needed may be huge.
Rigid barriers grant a high containment level at the price of very high ASI

values in case of small car accidents and a tendency of roll over for some heavy vehicles with particularly high center of gravity.

(a) .   (b) .

Figure 1.10: Bad performances

1.7 Norm EN 1317

In 1998 the CEN [2] created the European Norm 1317 for Road Restraint Systems laying down requirements common for everybody, in the field of testing and certification of road restraint systems.

After the 1st of January 2011, to sell a product in the European market it has to be certified with a CE Marking; this put and end to a period of three years during which the EN 1317 and similar national norms coexisted.

Due to the introduction of the EN 1317 the classification of the products is based on their performances and not on empirical experience, leading to an increase in terms of safety and quality for European drivers. New barriers installed on European roads offer a guaranteed level of safety and, in second place, the guaranteed level is the same across the whole Europe, creating a unique market for safety barriers.

The norm is divided in 8 different parts, each of which takes care of different subjects or products.

- EN 1317 Part 1: Terminology and general criteria for test methods

- EN 1317 Part 2: Performance classes, impact test acceptance criteria and test methods for safety barriers and vehicle parapets

- EN 1317 Part 3: Performance classes, impact test acceptance criteria and test methods for crash cushions

---

[2]Comité Européen de Normalisation, European Committee for Standardization

- ENV 1317 Part 4 [3]: Performance classes, impact test acceptance criteria and test methods for terminals and transitions of safety barriers

- EN 1317 Part 5: Product requirements and evaluation of conformity for vehicle restraint systems

- TR 1317 Part 6: Pedestrian parapets

- TS 1317 Part 8: Motorcycle road restraint systems which reduce the impact severity of motorcyclist collisions with safety barriers

Due to the introduction of this norm the market of road safety barriers is changing significantly: the design of the products is highly engineered, the materials used grants high performances and the numerical simulation has a huge role in the design phase, to optimize the whole process. The goal of having such a norm is retrace what has been done by the EURONCAP for automotive in the field of safety barriers.

(a) .

(b) .
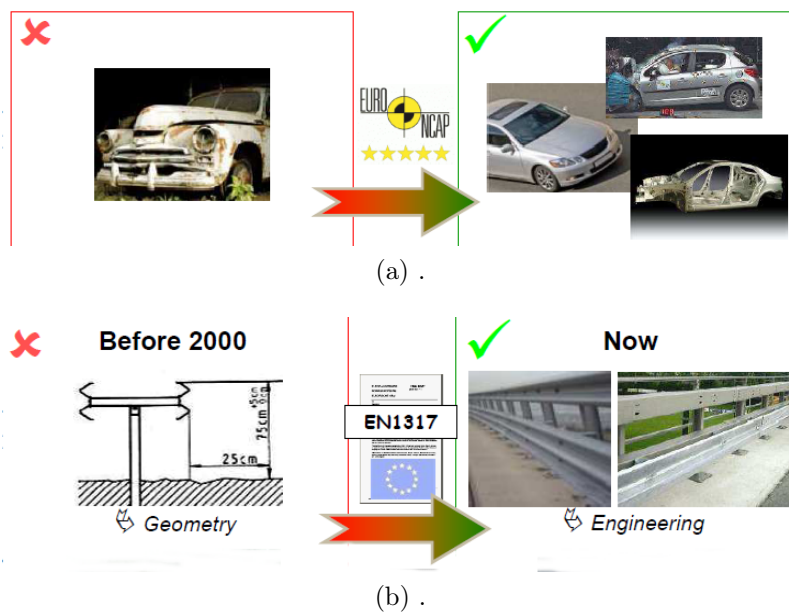
Figure 1.11: Evolution of the products

---

[3]Part 4 is going to be revised, becoming an EN and being divided into: EN1317 Part 4: Performance classes, impact test acceptance criteria and rest methods for transitions. EN 1317 Part 7: Performance classes, impact test acceptance criteria and test methods for terminals

1.7.1 Importance of Road Restraint Systems

As shown in figure 1.12 what can change depending on the country is the level of protection installed in each road, because the EN 1317 guarantees only the common procedures to test the products to achieve specific performances.

This is why on equal roads (i.e. highways, usually with almost similar speed limits and driving conditions) but of different countries the road restraint systems installed may be quite different.

Observing figure 1.12 is quite clear that in many countries, especially considering the high amount of Heavy Good Vehicles (HGV) that every day circulate on the roads, the actual containment levels chosen by the national authorities are not enough to protect against a serious accident involving such a vehicle.

Luckily this kind of events are rare, but when they happen the consequences are not negligible. The worst case happens when the vehicle is able to cross the median barrier, ending up in the opposite traffic line, or, in case of bridges, the side barrier can not redirect the vehicle, allowing it to fall down, as in figure 1.13.

(a) .   (b) .

Figure 1.13: Worst cases

Actually, research from the Road Safety Observatory in Belgium concluded that the severity of accidents involving a 'crossed' barrier on motorways is actually higher than a run-off accident against a tree and 5 times higher compared to incidents where the barrier has managed to contain the vehicle. [35]

		Side Barrier	Central Barrier	Bridge Barrier
	Austria	H2	H2	H3
	Belgium	H2	H2	H4b
	Bulgaria	H1	H2	H1
	Czech Republic	H1	H2	H1
	Denmark	H1	H2	H3
	Finland			H2
	France		H1	H2
	Germany	H1	H2	H1
	Ireland		H2	H2
	Italy	H2	H3	H4b
	Holland	H2	H2	H2
	Norway			H2
	Poland	H1	H2	H1
	Spain	N2	H1	H3
	United Kingdom			H1
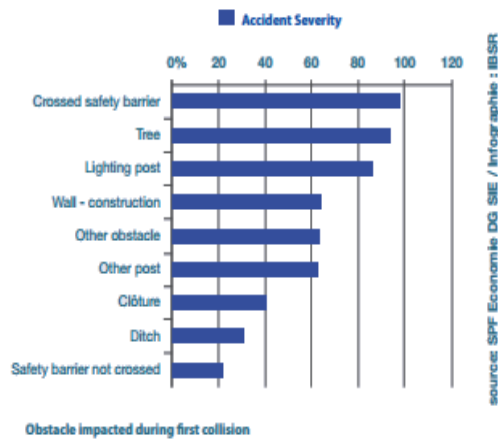
Figure 1.12

Figure 1.14: Accident severity

1.7.2 Key terminology

Concerning road safety and crash tests in general, there are certain terms that are commonly used and will be frequently used in this report:

- Containment level
- Working width
- Dynamic deflection
- Impact severity
- Redirection
- Vehicle intrusion

Containment level

The containment level of a barrier represents its capacity to contain an errant vehicle.

Define a containment level it is necessary to perform a crash test; each barrier has to be tested two times: to define its real containment level, hence using heavy vehicles, if needed; then a crash test with a small vehicle to detect the severity of the impact.

A barrier able to contain heavy vehicle but causing high accelerations on the occupants of a small car is not a desired product to have on the roads. The parameters to define a crash test, like impact speed, angle of impact, mass and type of the vehicle used are not chosen randomly nor are based on the device tested, but are specified by the norm and reported in table 1.1.

EN 1317 establishes a series of criteria that the device has to satisfy, to consider a crash test "passed":

Test	Impact Speed [Km/h]	Impact Angle [°]	Mass [Kg]	Type of Vehicle
TB11	100	20	900	Car
TB21	80	8	1300	Car
TB22	80	15	1300	Car
TB31	80	20	1500	Car
TB32	110	20	1500	Car
TB41	70	8	10000	Rigid HGV
TB42	70	15	10000	Rigid HGV
TB51	70	20	13000	Bus or Coach
TB61	80	20	16000	Rigid HGV
TB71	65	20	30000	Rigid HGV
TB81	65	20	38000	Articulated HGV

Table 1.1: Crash test parameters

- Elements of the safety barrier shall not penetrate the passenger compartment of the vehicles

- Deformations of, or intrusion into the passenger compartment that can cause serious damage are not permitted

- The center of gravity of the vehicle shall not cross the central line of the deformed system

- The safety barrier shall contain and redirect the vehicle without complete breakage of the principal longitudinal elements of the system

- The vehicle must not roll over (including rollover of the vehicle onto its side) during or after impact, although rolling pitching and yawing are acceptable

- For tests with Heavy Good Vehicles, no more than 5% of the mass of the ballast shall become detached or be split during the test, until the vehicle comes to rest.

- Following impact into the safety barrier or parapet, the vehicle when bouncing back is not permitted to cross a line parallel to the initial traffic face of the the system (see the definition of 'redirection' for more detail)

Image 1.15 illustrates all the classes actually considered, meanwhile in figure 1.16 is shown the value of the energy for each containment level, that is proportional to the impact angle and the speed of the impacting vehicle.
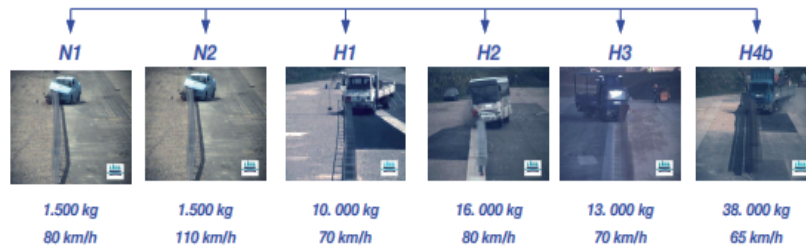
Figure 1.15: Containment level
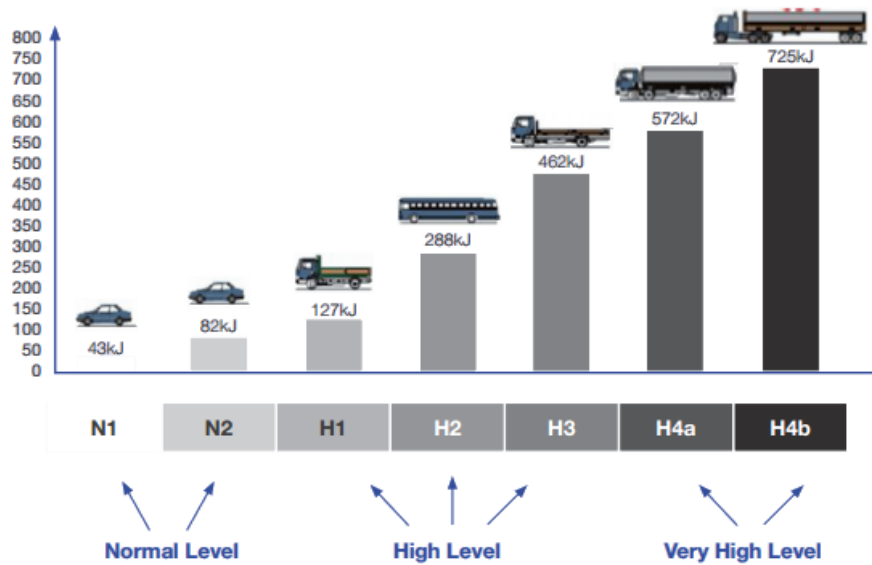
Figure 1.16: Containment level energy

Working width

Working width measures the deformation of the barrier during the impact. It is the main parameter to classify a device and one of the main requests during the initial design phase.

It is essential because it measures the space needed behind the barrier to make it work properly; it is calculated, as shown in figure 1.17, as the

distance between the traffic face of the barrier in undeformed condition
and the maximum displacement of its main components during the impact
of the vehicle.
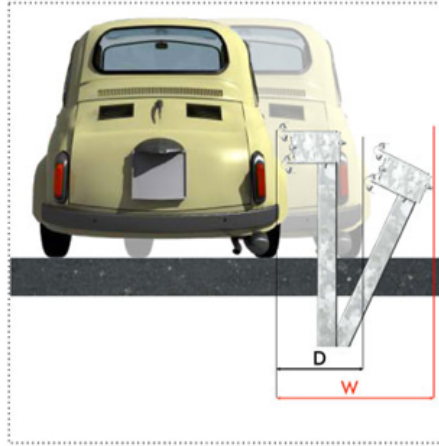
Figure 1.17: Working width and Dynamic deflection

The working with is divided in 8 levels, from 1 to 8; they are reported
in table 1.2.

Working Width Class	Working width value [m]
Wn1	Wn1 ≤ 0.6
Wn2	0.6 < Wn2 ≤ 0.8
Wn3	0.8 < Wn3 ≤ 1.0
Wn4	1.0 < Wn4 ≤ 1.3
Wn5	1.3 < Wn5 ≤ 1.7
Wn6	1.7 < Wn6 ≤ 2.1
Wn7	2.1 < Wn7 ≤ 2.5
Wn8	2.5 < Wn8 ≤ 3.5

Table 1.2: Working width levels

Dynamic deflection

Dynamic Deflection is the second parameter (after working width) to
evaluate the deformation of the system under impact and it is calculated
as the distance between the traffic face of the system in its initial condition

and it maximum displacement.
It is shown in figure 1.17.

Impact severity

Impact severity is an index used to classify the severity of an impact against the tested device; the classification is done using two different parameters:

- Acceleration Severity Index *(ASI)*
- Theoretical Head Impact Velocity *(THIV)*

The ASI is the most important of the two; it is calculated using an accelerometer positioned in the center of gravity of the vehicle. All the components are considered, as expressed in the following formula:

$$ASI = \sqrt{\left(\frac{a_x}{12}\right)^2 + \left(\frac{a_y}{9}\right)^2 + \left(\frac{a_z}{10}\right)^2} \tag{1.1}$$

A lower value indicates a soft impact, and correspond to an A level, usually desired during the design process; B level is sometimes accepted, meanwhile C class is usually not accepted nor desired by any barrier manufacturer, because the level of safety granted to the passengers of the light vehicle is not enough.
Theoretical Head Impact Velocity (THIV) has been developed for assessing the occupant impact severity for vehicles involved in collisions with road restraint systems. The occupant is considered to be a freely moving object (head) that, as the vehicle changes its speed during contact with the road restraint system, continues moving until it strikes a surface within the interior of the vehicle. The magnitude of the velocity of the theoretical head impact is considered a measure of the vehicle to road restraint system impact severity.

$$THIV = \sqrt{V_x^2(T) + V_y^2(T)} \tag{1.2}$$

The table below show the different levels/classes of impact severity as well as the maximum ASI/THIV permissible values.

Redirection

Redirection is the capacity of a restraint system to return a vehicle to the road in a controlled manner: during the exit phase the trajectory of the vehicle must be inside an "exit box".
A barrier that redirects a vehicle towards the other side of the road is not considered satisfactory.

Level	Maximum permissible values	
A	ASI $\leq$ 1.0	THIV $\leq$ 33 km/h
B	1.0 < ASI $\leq$ 1.4	THIV $\leq$ 33 km/h
C	1.4 < ASI $\leq$ 1.9	THIV $\leq$ 33 km/h

Table 1.3: Impact severity levels
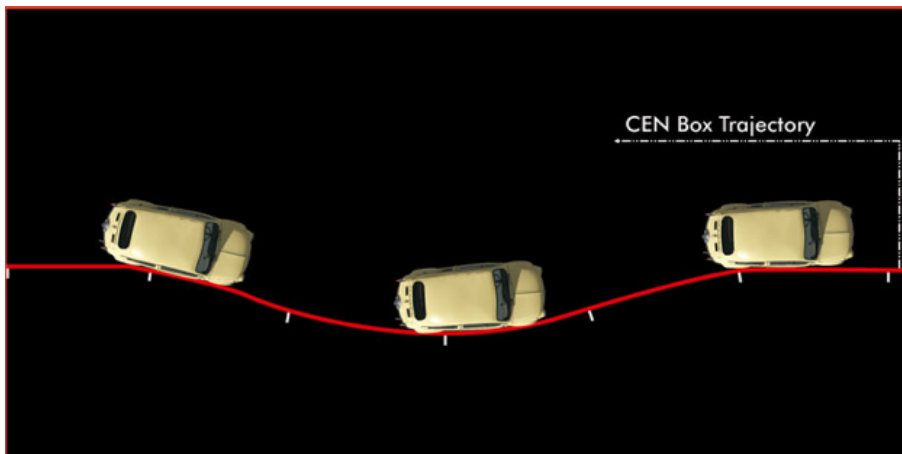
Figure 1.18: Exit box

Vehicle intrusion

This parameter applies only to Heavy Goods Vehicles *(HGV)* and it is the maximum lateral position from the undeformed traffic side of the barrier of the vehicle.

It is measured at an height of 4m and is particularly important in all those cases where the vehicle is subjected to high roll angles, causing an intrusion, much higher than the working width or the dynamic deflection, that due to the conformation of the road can not be accepted.
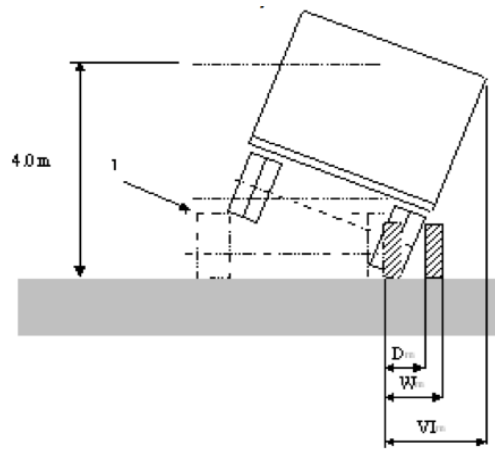
Figure 1.19: Vehicle intrusion

Chapter 2

State of the art

2.1   Importance of Bolts

During the impact between the vehicle and the restraint system the bolts
are subject to high forces and momenta that cause remarkable local stresses
and deformations; due to these loads there is the possibility of failure of
the junctions.

Typically there are two possible modes for a junction to fail: the rupture
of the bolt or the deformation of the hole on the beam, causing the bolt to
be pulled out.

In many cases, depending on the design of the product, the failure may
be desired, because it allows the vehicle to pass over the posts without
pulling down the beam; the consequences of a lowered beam are the
inability to redirect the vehicle properly or, in the worst case scenario,
the beam becomes a ramp, allowing the vehicle to pass over it invading
the opposite track line, as showed in 2.1. It is then mandatory that the
road barrier works properly, redirecting the vehicle using all the necessary
lateral displacement.

A large lateral displacement causes lower stresses on the vehicle and its
passengers: in fact, as explained in chapter 1, one of the most important
criterion the evaluate the quality of a barrier are the accelerations suffered
by the occupants of the impacting vehicle.

It is quite clear that it is not just the behavior of the bolts that will be
studied in this thesis, but how the bolts affect the whole dynamic of the
crash, interacting with the surrounding parts.

Considered what as been said, an accurate junction model able to reproduce
the behavior of the bolts during the impact dynamic is a must.

In figure 2.2 it is possible to notice the existing forces acting in a real
junction.

(a) *t = 0.0 s.*

(b) *t = 0.1 s.*

(c) *t = 0.2 s.*

(d) *t = 0.3 s.*

Figure 2.1: Junction not failing

Figure 2.2: Forces

The goal of the model is to reproduce them all, trying to achieve a perfect match between real tests and numerical simulations.

After this brief introduction it is possible to say that bolts are responsible for the local and global behavior of the road restrain system, directly affecting its deformations and the eventual failure, that, in turn, are strictly related to the safety level granted by the analyzed structure, that is a key factor for the success of the product.
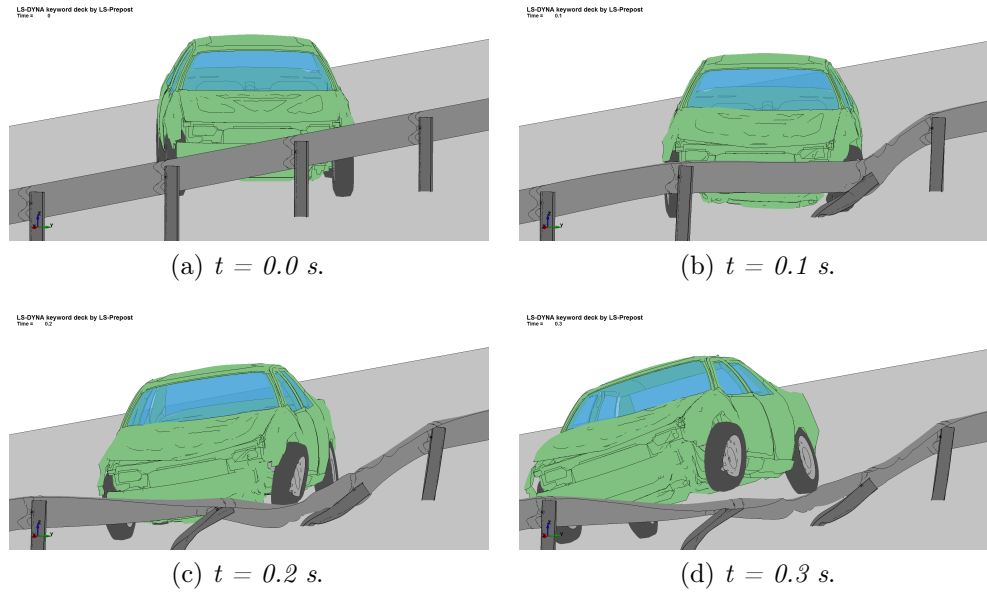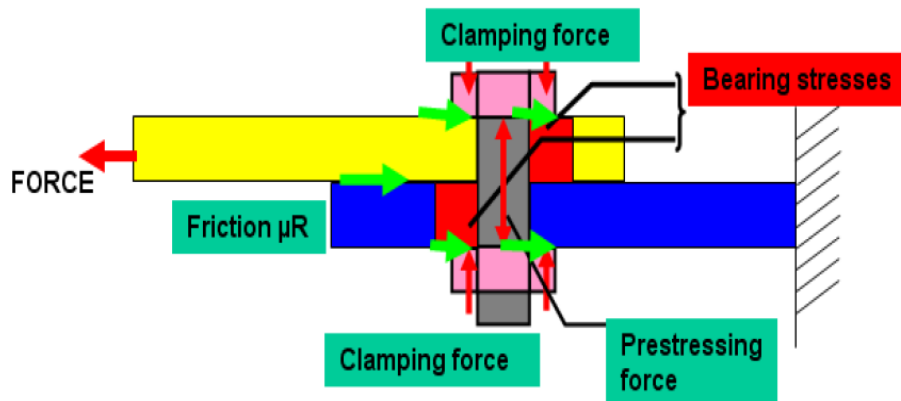
2.2 Available solutions

The easiest way to link together two parts is to use a rigid link between them; this, obviously, is not enough in the actual contest, where a detailed behavior is required: it does not even allow to introduce any kind of failure criterion, hence is excluded at the beginning of the work.

Another possible solution involves the use of springs as substitute of the shank of the bolt. As before, this solution has not been considered because of the difficulty of finding the right value for the stiffness constant of the spring; the management of the contacts would be quite complicated and, moreover, physically speaking, this solution does not represent the reality at all: there is no transmission of momenta and defining a proper failure criterion is not possible.

In figure 2.3 and 2.4 the most common solutions are shown. On the left the beam connecting the two nodes is shown, meanwhile on the right a 3D representation for the same beam is presented. This is possible due to the command *Beam Prism* offered by *LS-PrePost*.

The spotweld of figure 2.3 is the solution currently used: a simple weld point between the parts that have to be connected. It is a good practice to put the nodes of the spotweld in correspondence of the center of an element, to have a good distribution of forces on the adjacent ones.

It is easy to realize and few information have to be included in the model to make it work. The weak point of the spotweld is, clearly, the fact that it is not properly representing how a junction is made: no holes, the geometry of the bolt is not considered at all, the preload can not be introduced. To summarize, a spotweld is a numerical approximation to avoid complications; as direct consequence the results are not always correct.

As shown in figure 2.4, during the calculations the spotweld is converted into a group of solid elements. This is a source of uncertainty: studies

(a)   (b)
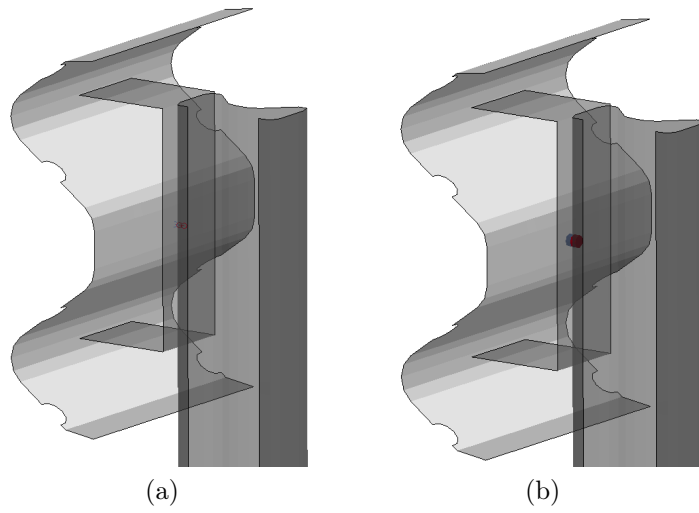
Figure 2.3: Spotweld
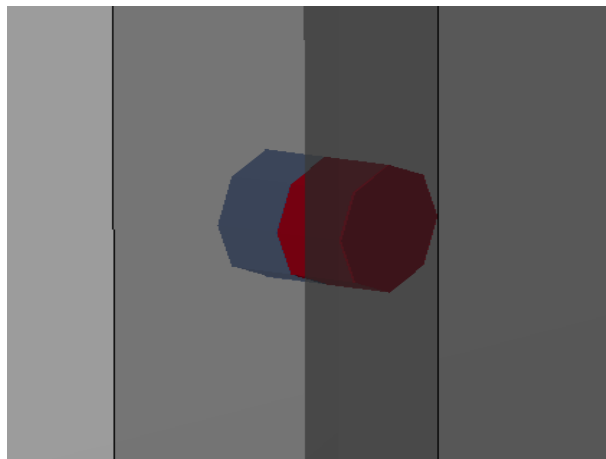
Figure 2.4: Zoom on a spotweld

show that depending on the number of elements considered the results will be significantly different. [14]

Some of the available solutions are reported in figure 2.5
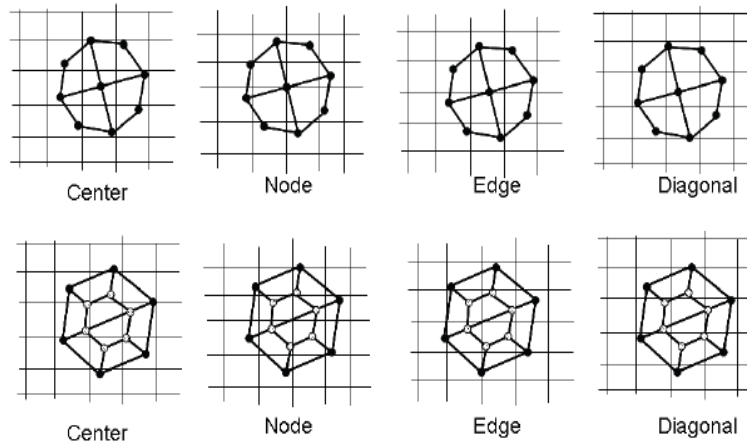
Figure 2.5: Solid spotweld with different position and number of elements

(a) *Volumic Bolts.* (b) *Contact Beams.*
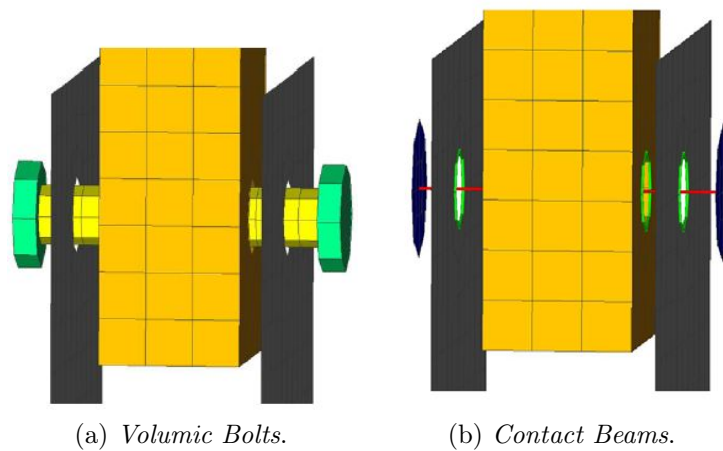
Figure 2.6: Available solutions

Modeling using volumic bolts, figure 2.6*a*, is a first step to get close to the real geometry of a junction: it requires meshing the holes of the connected parts, it uses only shell elements and, compared to the spotweld solution, does not increase the computational time required to perform the analysis.

The drawbacks of this solution are the difficulty to introduce a rupture criterion using simple material laws and the contacts between shells and

edges of the holes could lead to stability problems of numerical nature during the simulation with LS-Dyna; moreover, the model is only geometrically accurate, but the type of used elements does not reproduce the real physical configuration: the model of the bolt is hollow.

3D models, shown in figure 2.7, are a viable solution, especially for barriers with a simple geometry and a limited number of junctions: the numerical results are very accurate but the computational time not always manageable. This is, for sure, an hot topic for the further developments, because this specific modeling choice requires a sophisticated material law, that actually is not available, to properly consider rupture and failure.

Another disadvantage of this solution is the tiny mesh size required, directly linked to the increase in computational time.

Anyway, this solution will be the starting point for all the local tests, allowing a comparison between 3D model, 2D model and experimental results.

That being so, the focus of the thesis is on the contact beams solution 2.6b, compared to the old model in the next section.

(a)   (b)
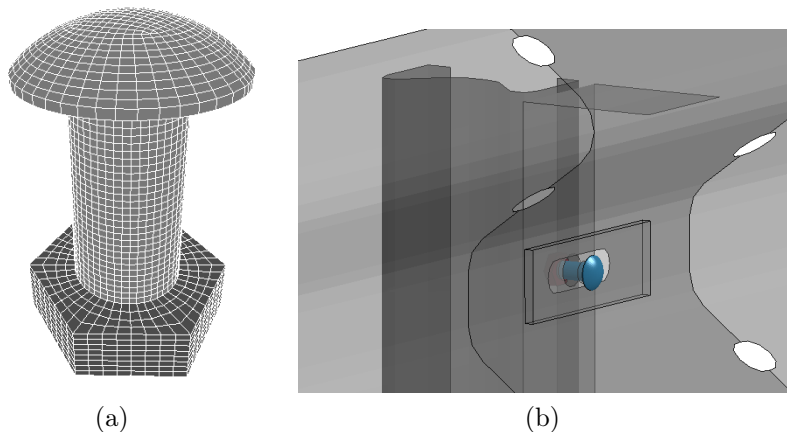
Figure 2.7: Solid Bolt

2.3   Models comparison

Before starting the work it is important to deeply analyze the features offered by the considered models, to point out pro and cons of each one.

In figure 2.8 is shown the solution using contact beams: on the right it is possible to see how it appears displaying the corresponding thickness for head, nut and the diameter of the shank.

(a)   (b)
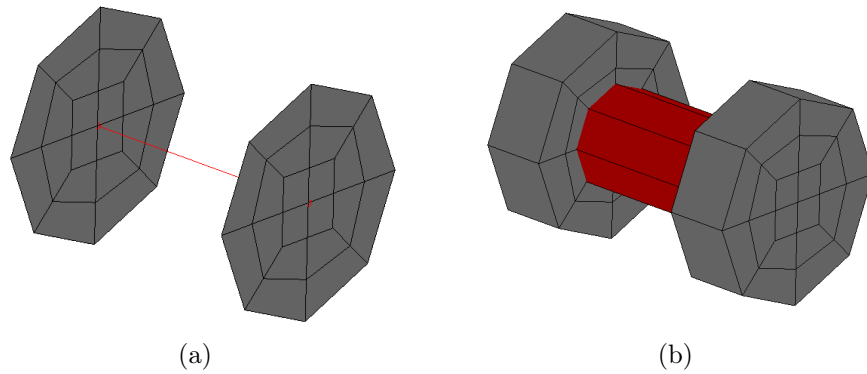
Figure 2.8: Contact beam model

The model includes:

- a beam, in red, to represent the shank of the bolt

- a reduced number of elements, in gray, for head and nut of the bolt, with and average size of the mesh of about 5 mm.
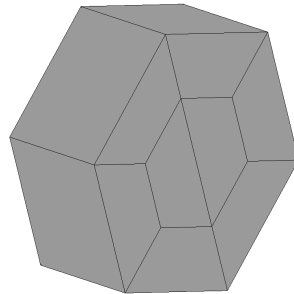
Figure 2.9: Single spotweld

In figure 2.9 the spotweld solution is shown.
In table 2.1 the features for both the choices are listed.

Let's analyze the voices one by one:

1. using a single spotweld it is possible to link just two parts; to link more then one part it is necessary to use more spotwelds, meanwhile with the new model, theoretically, unlimited parts can be connected together, simply adapting the length of the beam. With the spotweld it is not possible to simulate properly the complete disconnection of pieces like fishplate and spacer because the failure of 2 spotwelds is needed;

2. the preload used in the new model is one of the core factors. It is totally absent in the old model and it allows to reproduce numerous local effects and it affects the behavior of the connection;

3. due to the preload there are clamping forces between the two parts;

4. due to the presence of the hole the local behavior can be studied, to predict deformations and eventual pull-through of the bolt. Because the bolt is allowed to move into the hole, the decentralized configuration can be studied, significantly changing the resistance of the connection in case of pull-though;

5. the friction coefficient plays an important role and it is strictly related to the clamping forces and contributes in keeping together the two parts, allowing limited movements, as far as the bolt moves in the hole;

6. to allow the creation of the spotweld a small affinity between the two mesh is necessary; also, it is important to take into account the fact that to work optimally the spotweld must be placed in the middle on an element. With the contact beams it is necessary to model the holes, but there are not constrains on the mesh size, anyway a certain regularity and definition for the pieces are requested. This can be considered the only drawback compared to the spotweld solution;

7. with the spotweld only forces can be considered in the failure criteria, mainly because the rupture values for the momentum usually are unknown, meanwhile with the contact beams forces and momenta can be easy considered, not directly but through the use of axial and shear stress;

8. if the material of the real bolts has been properly characterized and plenty of information are available, it is possible to use them in the failure criterion, introducing the strain as rupture criterion.

Spotweld	Contact beams
One spotweld, just two parts	Unlimited number of parts are connectable
No preload	Pre-load
No real clamping	Clamping forces
No local behavior	Bearing of the slot
No Friction	Friction based on preload
No holes, mesh size is a constraint	Holes are required, no constrains on mesh
Only forces can be considered	Forces and momentum can be considered
Based only on stress and strain	Based on stress, strain and rupture

Table 2.1: Comparison

Chapter 3

Experimental tests

The experimental part of the work took entirely place in the laboratories of CRM, Centre Research Metallurgique; they consisted in a series of tests to evaluate the performances of all the components of a junction, to obtain as much as possible information about their behavior due to a pulling force. Not only the failure point is of interest, being it for the bolt or for any of the other component, but also the rupture mode.

3.1   Description of the tests

The objective of the experimental test is to evaluate the performances of bolts subject to a pure traction load.
The machine of figure 3.1 was used to carry out the tests [1].
    The test is considered concluded when the bolt is broken or if it is pulled through the hole, with or without the rupture of fishplate and beam. During the tests, force applied and displacement are measured and they will be compared to those obtained through numerical simulation; the comparison will not be just numerical, but also visual, comparing the photos taken during the tests with the numerical results.
The two principal parameters object of interest are:

- the peak load
- the trend of the curve

    The first part of the job consisted in cutting the beam, to have the desired length to perform the tests (300 mm).

---

[1]Additional information are available in Appendix

Figure 3.1: Machine for the traction test

(a) *Band saw.*
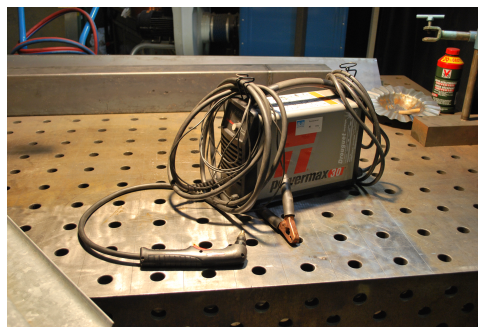
(b) *Plasma Cutter.*

Figure 3.2: Cutting system

Two different machines have been used: first a plasma cutter to reduce the initial length of the beam and allow it to fit into a band saw, that has been used afterward to obtain the exact length of the pieces.
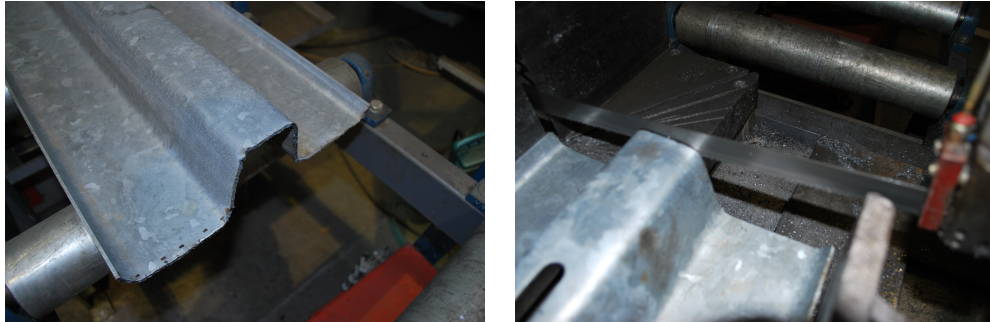
(a) *Before the band saw.*   (b) *After the band saw.*

Figure 3.3: Beam
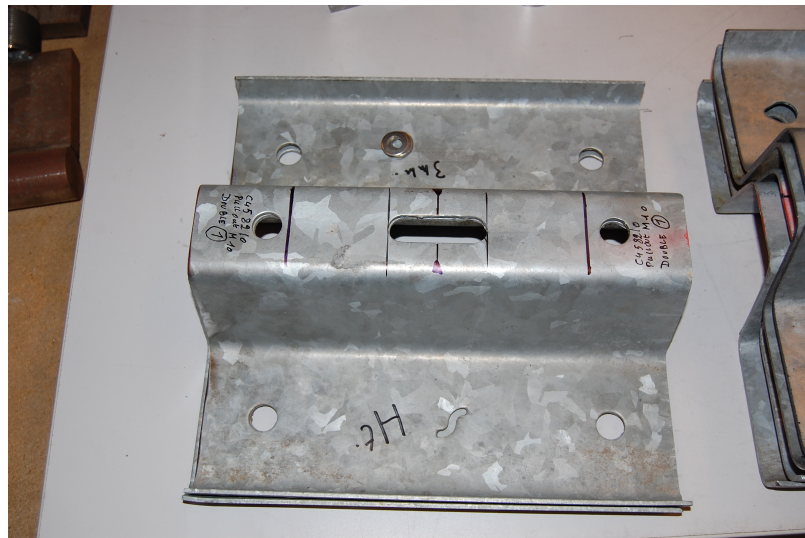
Figure 3.4: Cutted beam, ready to be used

To realize the tests, the research center provided some spare bolts, together with nuts and washers; in figure 3.5 the available components are represented and the pieces are grouped "by type". Even if the nominal specifications are the same, the bolts are not equal: some of them have a slightly bigger thread and for the nuts the inner diameter can change from a piece to another.

Figure 3.5: Spare bolts

Once the bolt is connected to the beam, the beam itself is constrained to the test machine: the configuration has been developed to grant the immobility of the beam.

As suggested by the technician of the laboratory, the torque has been applied very carefully to all the screws of the constraining system, to be sure of having a symmetric configuration for the test. The process of constraining the beam is partially illustrated in 3.6 and 3.7.
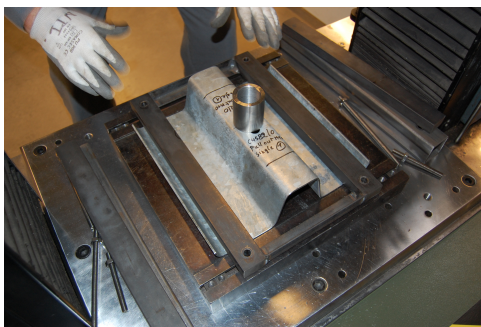
(a) *Unconstrained beam.*   (b) *Partially constrained beam.*

Figure 3.6: Constraining System

To have results with a minimum of validity, 3 trials have been performed for each configuration.

(a) *Constrained beam.* (b) *Controlling the effects of the torque.*
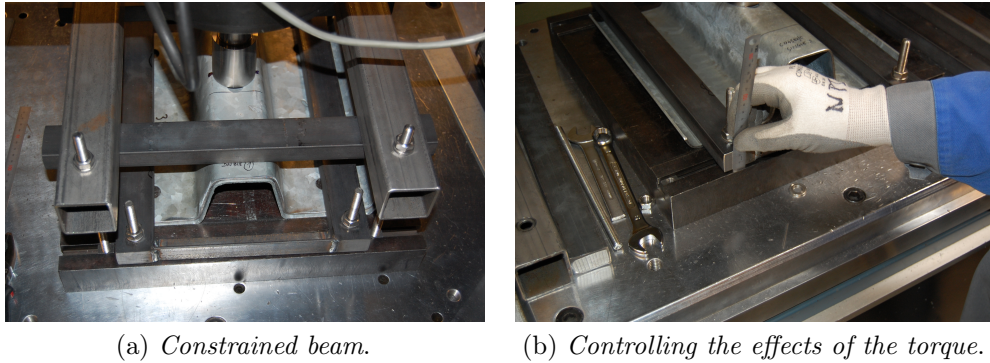
Figure 3.7: Constraining System

3.2 M10 4.6 - Results

The bolts used in all the trials are M10 4.6; some samples in 3.8 and 3.9. In table 3.1 are listed all the used pieces.

	Thickness	Hole diameter or size
Single beam	3.0 mm	60 x 18 mm
Double beam	6.0 mm	60 x 18 mm
Washer	2.3 mm	10.6 mm inner, 20 mm outer
Fishplate	5.0 mm	12 mm

Table 3.1: M10 - Used pieces

3.2.1 Single beam

The first group of trials has been performed using one beam, with the following results:

	Peak Load [N]	Displacement [mm]
Single 1	29812.9	9.550
Single 2	28796.4	13.405
Single 3	28929.2	10.424

Table 3.2: Results for single beam

(a) *M10 - Type 1.*   (b) *M10 - Type 2.*
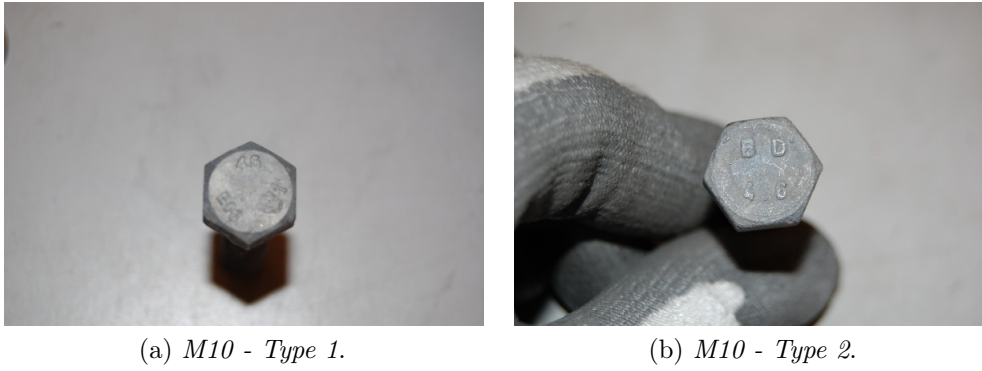
Figure 3.8: M10 - Bolts

(a) *Washers.*   (b) *Fishplate.*
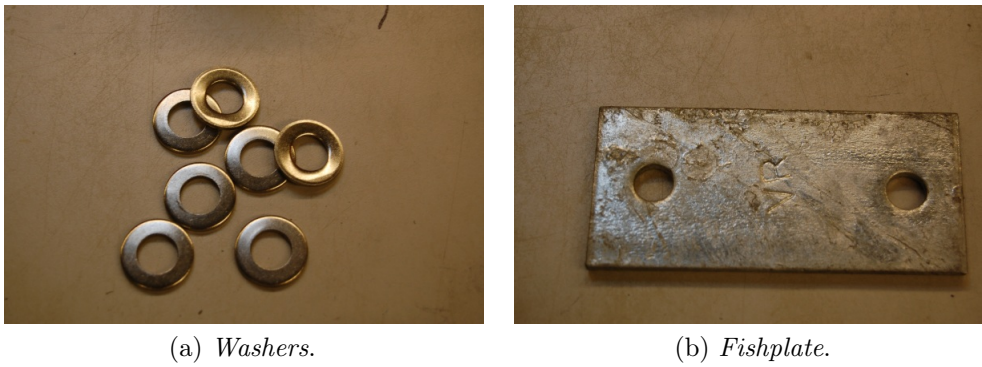
Figure 3.9: M10 - Additional pieces
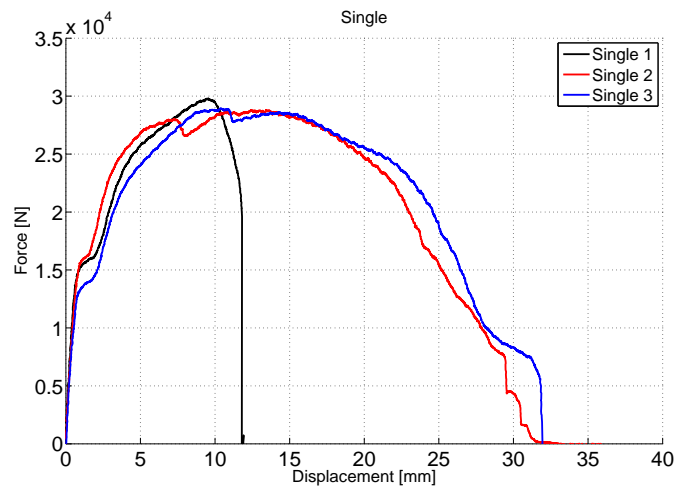
Figure 3.10: Single Beam

In the first case the bolt broke, while in case 2 and 3 the fishplate failed.

(a) *Broken bolt.*

(b) *Broken fishplate.*
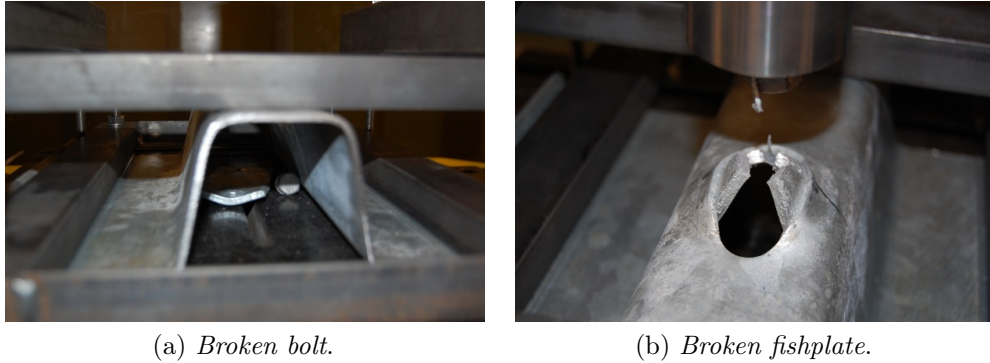
Figure 3.11: M10 - Single beam - After the test

(a) *Deformed beam.*

(b) *Bolt in case 2.*
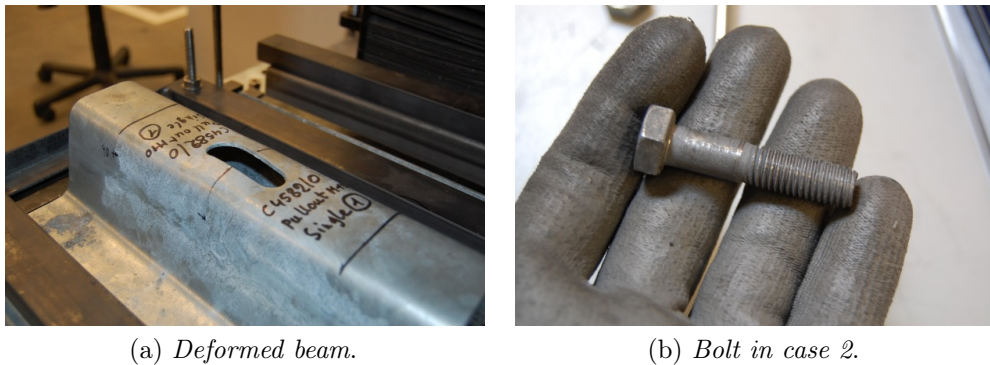
Figure 3.12: M10 - Single beam - After the test

3.2.2 Double Beam

In this case there are 2 different results, because in case 1 and 2 the proper nut has not been used, hence the thread failed. In case 3 the maximum interference (smallest nut and biggest bolt) has been used. The results are summarized in table 3.3.

In 3.14 and 3.15 it is possible to note that there is no rupture, but the failure of the thread, with consequent slip off of the nut.

	Peak Load [N]	Displacement [mm]
Double 1	31503.8	4.960
Double 2	31346.9	6.074
Double 3	34416.1	7.172

Table 3.3: Results for double beam

,
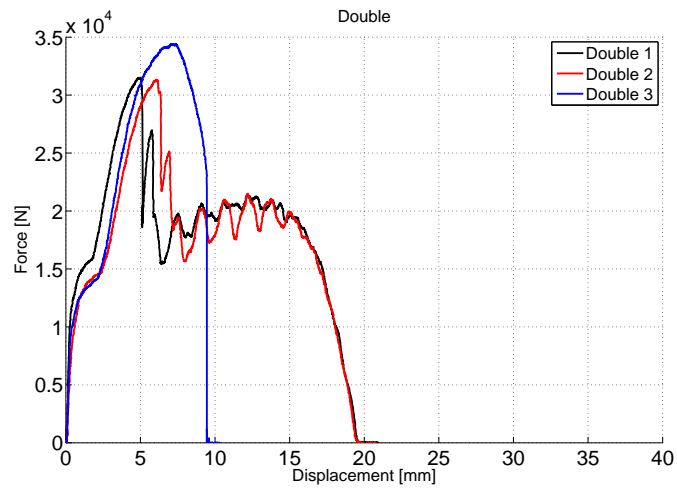
Figure 3.13: Double Beam

(a) *First stage.*   (b) *Second stage.*

Figure 3.14: During the test

(a) *Third stage.*   (b) *Final stage.*
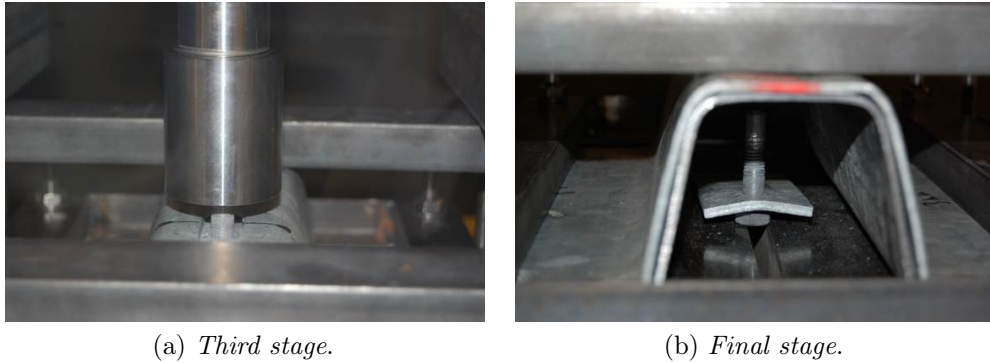
Figure 3.15: During the test

3.3 M16 5.8 - Results

The bolt considered for these tests is a M16 class 5.8.

The test configuration is the same as the one used for the M10: same constraint system, same displacement speed.

In this case only three tests are available, two in centered position and only one for the decentralized; to study at least two type of bolts, of different size and resistance, these tests are considered reliable, even without more trials to confirm the results.

In both cases 2 overlapped beams are considered.

	Thickness	Hole diameter or size
Single beam	2.5 mm	60 x 18 mm
Double beam	5.0 mm	60 x 18 mm
Fishplate	5.0 mm	18 mm

Table 3.4: M16 - Used pieces

In table 3.5 the maximum axial load for the three tests are reported, meanwhile in figure 3.18 and 3.19 the curve force - displacement is showed.

Figure 3.16: M16 and fishplate
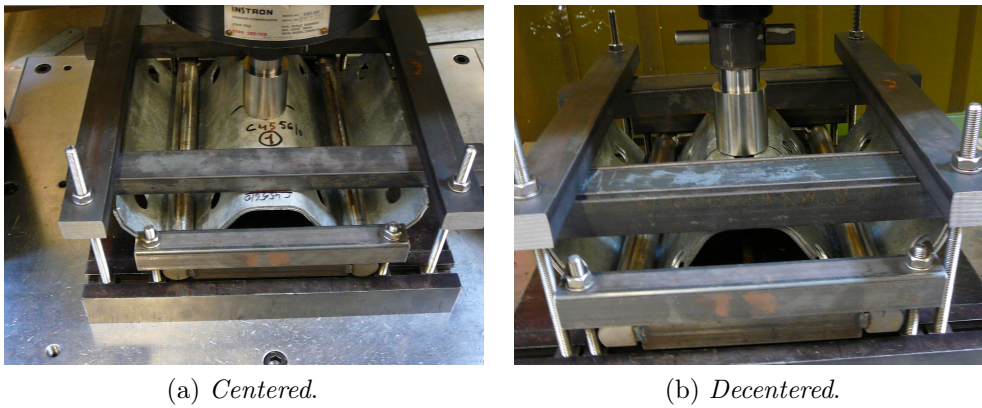
(a) *Centered.*   (b) *Decentered.*

Figure 3.17: M16 configurations

	Peak Load [N]	Displacement [mm]
Centered 1	82760	28.75
Centered 2	81203	25.02
Decentered	85489	10.75

Table 3.5: Results for M16 bolt
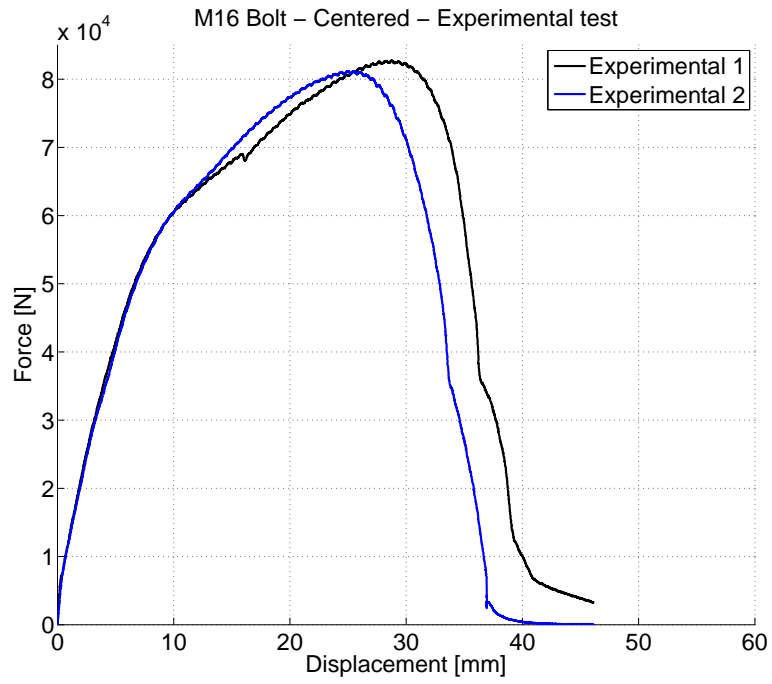
Figure 3.18: M16 - Centered configuration - Results
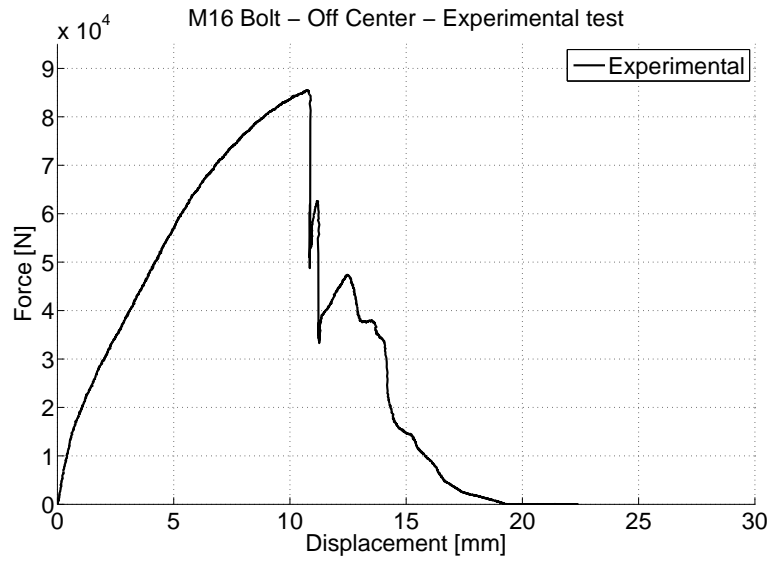
Figure 3.19: M16 - Off center configuration - Results

3.4   Analysis of the results

The analysis carried out show quite different behavior even if, on paper, the used components should be exactly the same.

This is due to the fact that the classification, for the steels used, is based on the minimum, nominal, granted level of stress. This means that for a 4.6 class bolt, the *minimum* failure stress will be, at least, 400 MPa. This affects all the other components: for instance, a steel 235 JR will have a minimum yield value of 235 MPa, but in theory, according to the actual norms it could have a yield value of 500 MPa or any value above 235 MPa.[2]
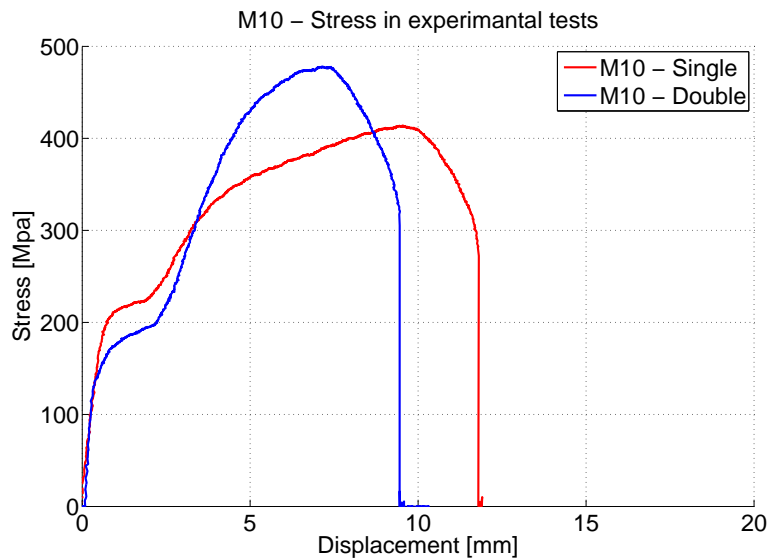
Figure 3.20: Stress in M10 bolts

As seen in figure 3.20, in both cases the real failure stress is higher than the minimum; for the second case much higher than expected.

The proposed numerical model can easily take this into account, simply modifying the failure value in the card of the material. It is then clear the importance of experimental tests, to have precise information about the pieces that will be used.

The actual model takes, as default value, the minimum granted, that without any experimental test represents the most conservative solution, but as discussed in the firsts chapters a too early rupture of the bolts may

---

[2]This is a well known issue that regards steel classification at all levels: the argument is actually discussed at European normative level by the dedicated bodies

not be conservative from the point of view of the system behavior.

Due to all these uncertainty factors, some specific tests were chosen to be reproduced during the numerical simulations, to reduce the number of variables that have to be taken into account. For the M10 only the cases with failure of the bolt: the rupture of the thread of the bolt it is impossible to simulate with the available means and, moreover, it is not object of interest for this study, while the failure of the fishplate may represent the case of a bolt more resistant than expected, hence the focus would be on the failure of the fishplate itself instead of the bolt.

Chapter 4

Description of the 3D model

The initial part of the job consists in modeling a first prototype of junction. Even if it is already known that the three-dimensional approach will not be used as final design, it is a good starting point to have an idea of how a junction works from a numerical point of view and, after a simple calibration of the model, it can be used to compare different local tests.
The advantage by using 3D models for local tests is the possibility of running implicit simulations, hence of using refined meshes with a reasonable computational cost and the displacement speed is low enough to grant a quasi - static behavior; to avoid numerical instabilities the double precision solver of ls-dyna has been used.
The choice of the design (bolt size and material, configuration of the test) is based on the available data from experimental tests.

4.1 M16 bolt: Solid model

As shown in figure 4.1, only a part of the beam is considered in experimental and numerical tests; two beams are stacked, to reproduce the overlapping zone. If the main interest of the test is the rupture of the bolt, this solution is preferred, because it considerably reduces the chances of pull through of the bolt.

In this case a bolt M16 class 5.8 is adopted and due to the dimension of the head of the bolt, slightly bigger than the hole on the beam, a fishplate has been placed, to redistribute the load on a larger area and avoid unwanted local deformations and concentration of stress.

By using solid elements there is no need to introduce any kind of simplification in the model: the geometry can be reproduced as it is in reality; only some numerical devices are needed.

Figure 4.1: Solid model
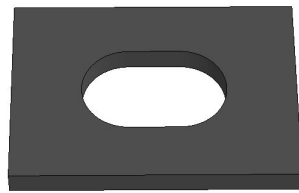
Figure 4.2: Fishplate - Solid elements
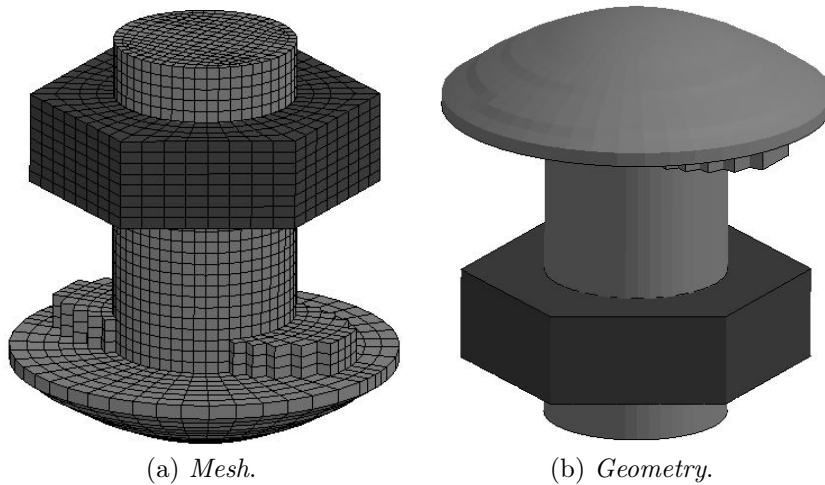
(a) *Mesh.*   (b) *Geometry.*

Figure 4.3: Bolt M16

In all the trials *MAT_24 has been used, with the curves of figure 4.4, provided by *Arcelor Mittal*.
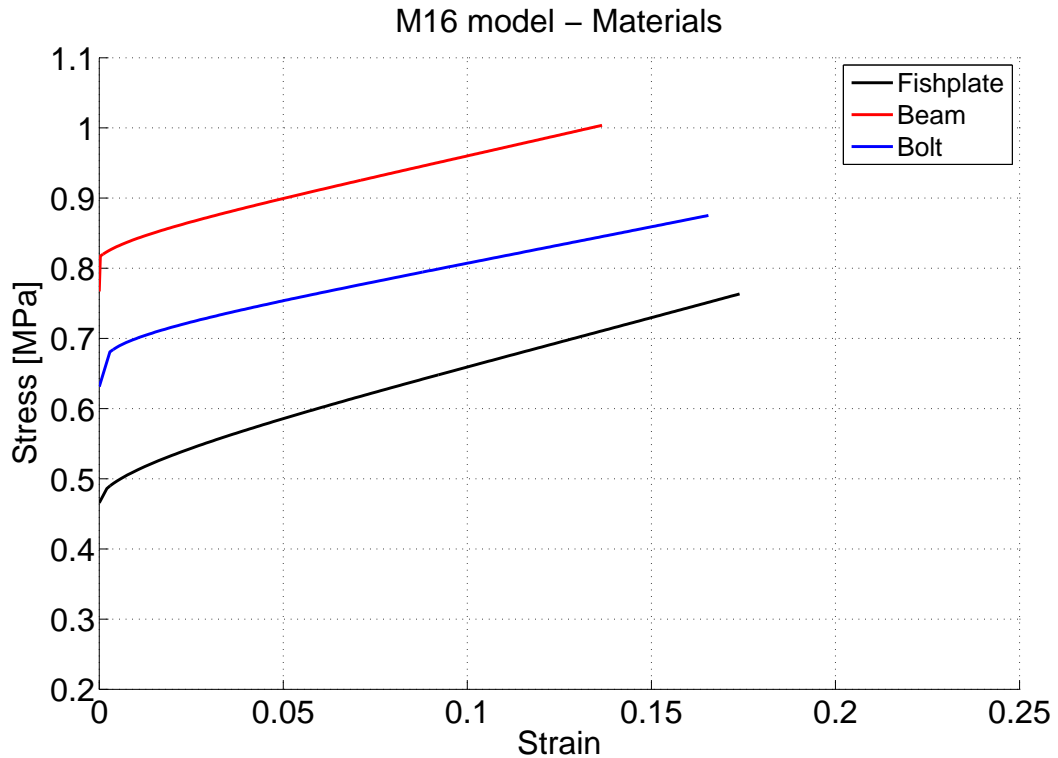
Figure 4.4: M16 - Materials

Due to confidentiality reasons the values have been normalized to 1. This very same material laws have been used also for the shell models. *Mat 24* lacks the possibility of introducing a sophisticate rupture criterion: the only one available is based on the level of plastic strain reached in each element; when the plastic strain exceeds a prescribed value the elements are deleted from the model.

This approach is dependent from the mesh size, meaning that the failure criterion is triggered by the deformation of each element: the failure and consequent deletion is done element by element, hence the piece is not considered in its entirety; this type of approach is local and not global.

For this specific model, after some numerical trials, the value of plastic strain giving results comparable to those obtained in real tests is 0.18 for the bolt and 0.6 for the fishplate; for the beam the failure of elements is not considered.

Obviously it is very important that the dimension of the elements is as

homogeneous as possible; such criterion could not be use for different parts with different mesh sizes; in this case the average element length is 1 mm. In case of a new mesh, the calibration procedure has to be done again: the values adopted work only for this specific model.

Even if none of the curves shown in figure 4.4 reach the prescribes value of failure, Ls-Dyna automatically extrapolates the curves using an horizontal slope: it means that the last point of the curve represents also the maximum reachable stress. This is the biggest numerical limit of the model: the strain can increase indefinitely but with a constant stress.

The rupture criterion has some other limits: first of all the deletion of elements with the consequent loss of mass in the model is not physical at all; in second place, plastic strain can only increase during the whole simulation, hence compression phenomena increase the level of plastic strain of each element as well: with *Mat 24* traction and compression have the same effects.

Anyway, for the purposes of these analysis, with the listed hypothesis and with the proper calibration, it suits the needs of this work.

The model, showed in figure 4.5, consists of:

- 349578 nodes
- 294708 elements

(a) *Upper view.*   (b) *Bottom view.*
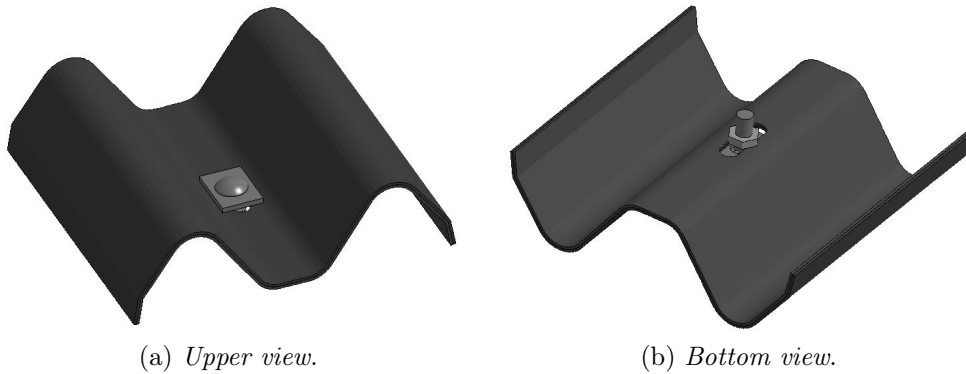
Figure 4.5: 3D model

All elements have assigned the basic formulation: *ELFORM=1*, constant stress solid element (default). The choice of this sub-integrated formulation has been done on purpose; fully integrated elements sometimes are victim of numerical errors and instabilities: negative volumes, bad convergence that cause a stiffer behavior and, moreover, they require at

least twice the computational time.

To take into account the limits of the choice, during the modeling phase 3 elements has been placed along the thickness of beam and fishplate, to be able to evaluate the stress distribution.

To avoid instabilities an hourglass control has been imposed, using type 6, mandatory for implicit analysis.

To properly reproduce the experimental tests the models have been constrained as shown in 4.6:

Figure 4.6: M16 - Constrained nodes

The constrained nodes can not move along the three direction, but rotations are permitted.

Since the test consists in pulling the bolt to evaluate its resistance, a displacement is applied to a rigid disk (in red in figure 4.7) that reproduces the machine used in the experimental tests; always to try to have a numerical model as similar as possible to the experimental tests, the disk can only move in the vertical direction.

The movement law is described by the curve in figure 4.8

Obviously, the real experimental tests are done in a quasi static condition, with a very low displacement speed to completely neglect inertial forces; for numerical needs it is not possible to simulate the exact amount of time of the tests. Anyway, since for the materials dynamic the effects of hardening are not introduced, a speed of 10 mm/s has been considered reasonable and a good compromise; in chapter 6 this hypothesis will be verified comparing internal and kinetic energy.

The preload has not been applied: the nut has been positioned close enough to the beam to avoid any possible movement in the direction of the axis of the bolt: the coincident nodes of the shank of the bolt and the nut were
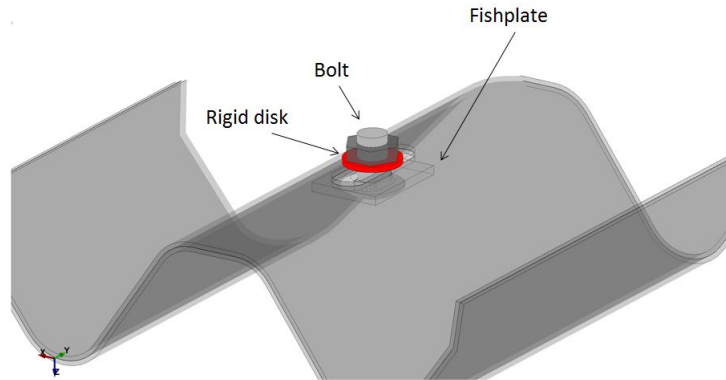
Figure 4.7: Pull system
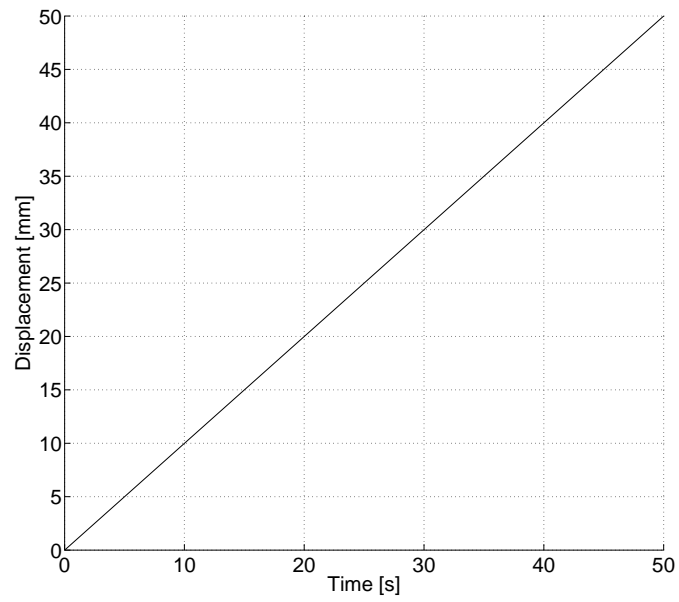
Figure 4.8: Displacement trend

merged to grant the union of the two pieces; the use of specific contacts or any other numerical artifice would have only sophisticated the model without introducing any significant improvement to the final result.

To optimize the computational cost *Automatic surface to surface* contacts have been defined between each part; this solution resulted more stable, from a numerical point of view, than using the *Single* option.

The decentralized model is exactly the same as the centered version; bolt, nut, rigid disk and fishplate were simply moved to the edge of the beam's hole.

(a) *Upper view.*   (b) *Bottom view.*
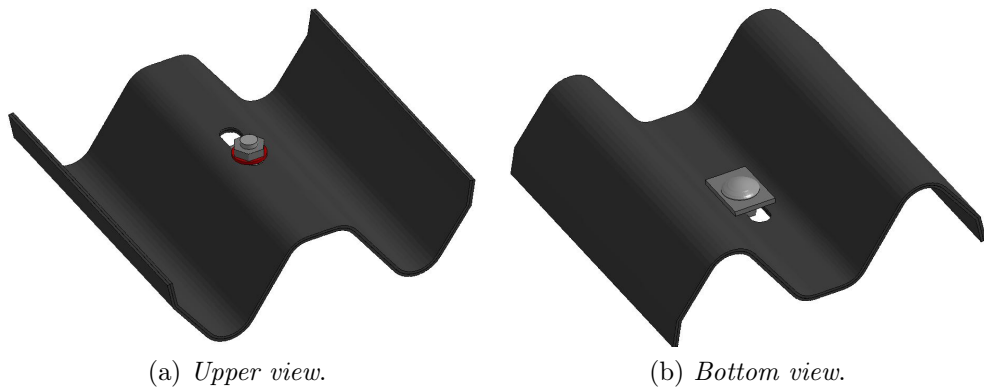
Figure 4.9: M16 - Decentralized configuration

4.2   M10 bolt: solid model

All the numerical devices adopted for the M16 model have been used in
the model of the M10, since, as presented later on, the results and the
global behavior of the model were satisfactory.

(a) *Upper view.*   (b) *Bottom view.*

(c) *Bolt M10.*   (d) *Fishplate.*
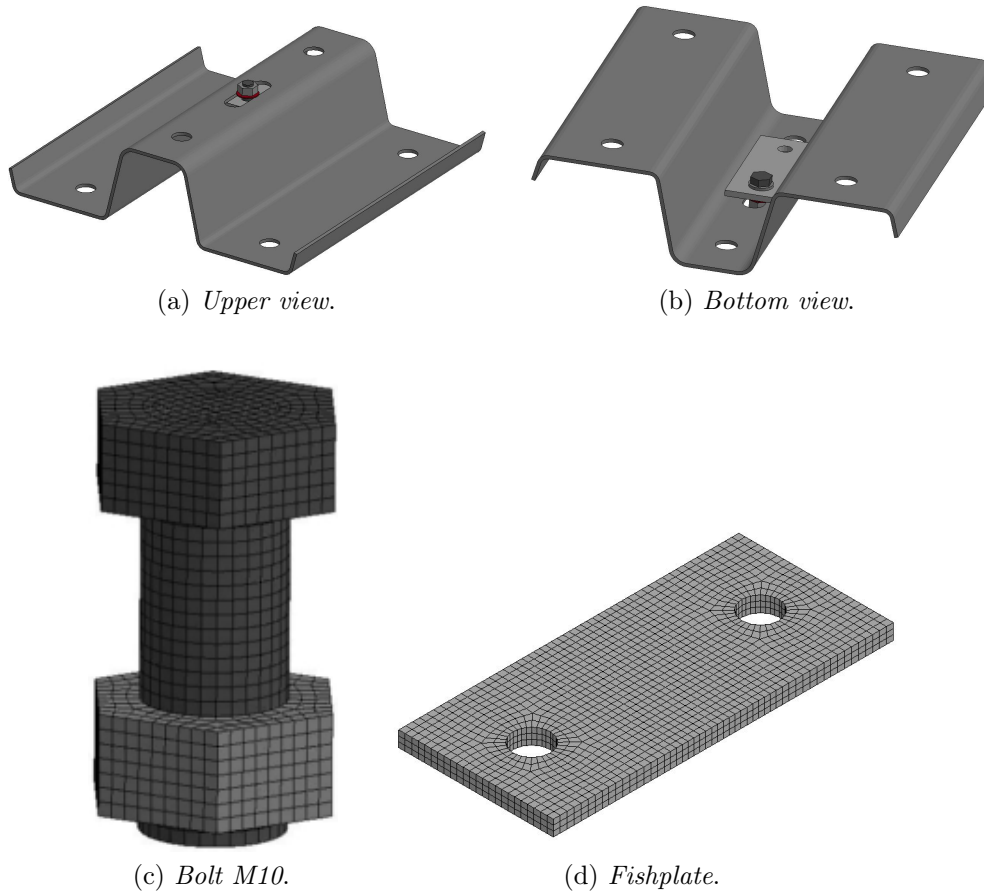
Figure 4.10: M10 - Single beam - Components

In this case the model consists of:

- 140044 nodes
- 103287 elements

In figure 4.11 the constrained nodes, to have the same configuration of
the experimental tests.

As before, *Mat 24* was used; the failure of elements was taken into
account only for the bolt, with a plastic strain value of 0.21.
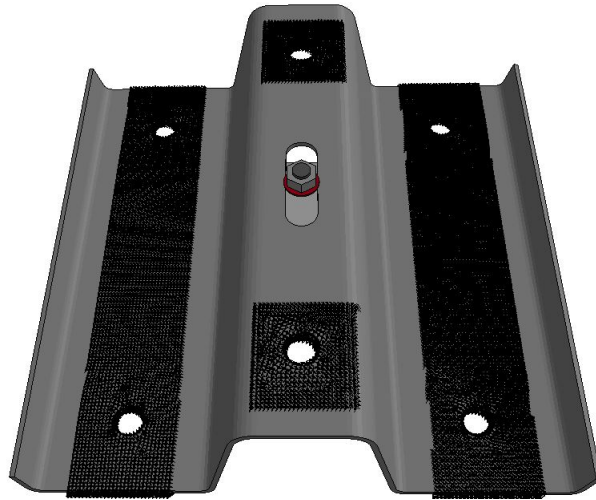
Figure 4.11: M10 Constrained nodes
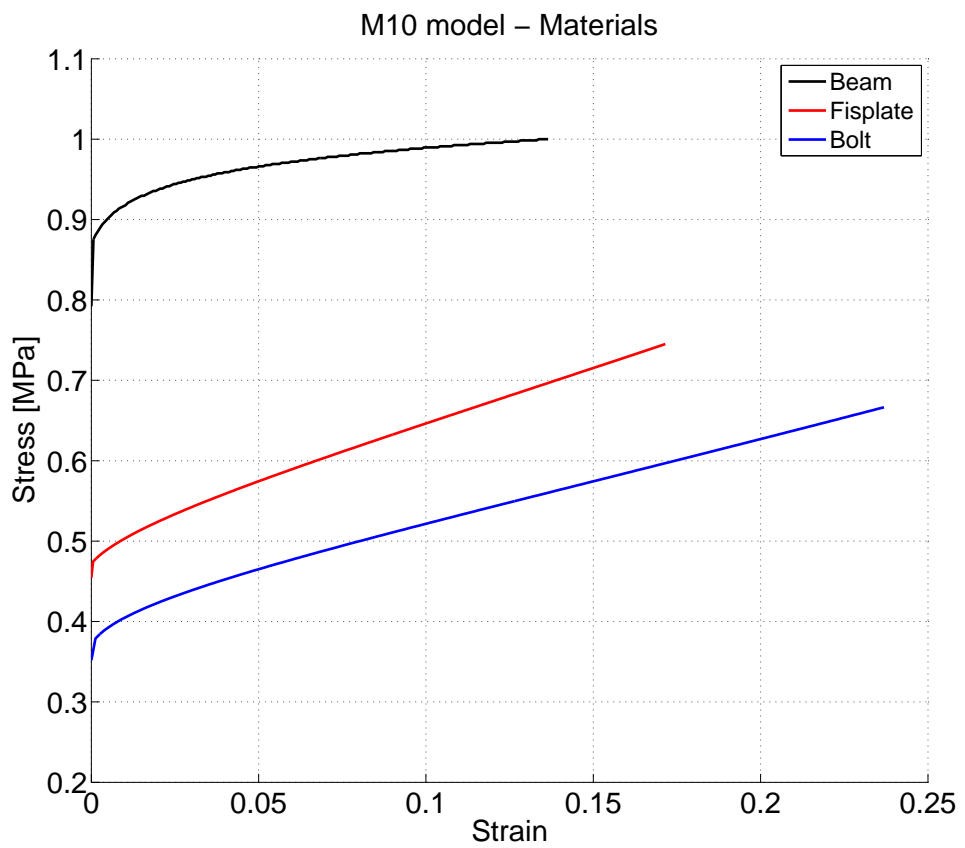
Figure 4.12: M10 - Materials

Chapter 5

Description of the 2D model

5.1 General description

In this chapter there is no distinction between M10 and M16: the model is general and it can be used for all the bolts configurations, just adapting mesh and geometry of the parts.
In contrast to the solid model, the bi-dimensional one was solved using the explicit solver of Ls-Dyna; this has been a natural choice, due to the fact that full scale simulations are performed in explicit, hence the main interest is to understand and evaluate the behavior of the model as it will be used in its final version.
This choice forced to use a not-so-static displacement speed with a reasonable coarse mesh for the beam.
The model consists of a beam, to reproduce the shank of the bolt, that links together a group of shells simulating head and nut of the bolt, as showed in 5.1.
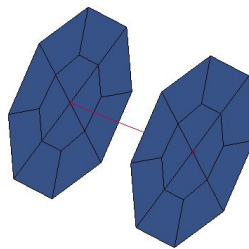
Figure 5.1: Bidimensional Model

The simplicity of use and modeling, together with good numerical results and high computational efficiency, are the strong assets of this

solution and favored its use.

Just using these elements it is possible to create a model able to reproduce everything that exists in the reality, except the thread of the bolt: to consider this and obtain a realistic representation of the pull out of the nut form the bolt, an extremely detailed model is required, using solid elements and a refined material law. Anyway, this is not the goal of the study, which is focused on the rupture of the junction.

The key factors of this choice are:

- detailed characterization of the local geometry of the junction
- failure criteria
- preload
- null beams to realize the contacts

5.2   Local geometry

One of the first problems that occurred during the introduction of the new model is related to the mesh of the parts of the barrier actually used: in none of them are available the holes to allow the insertion of the bolt.

The numerical models currently relay on spotwelds to link together the different parts of the barrier, hence the hole to connect each part together is not required, as in figure 5.2.
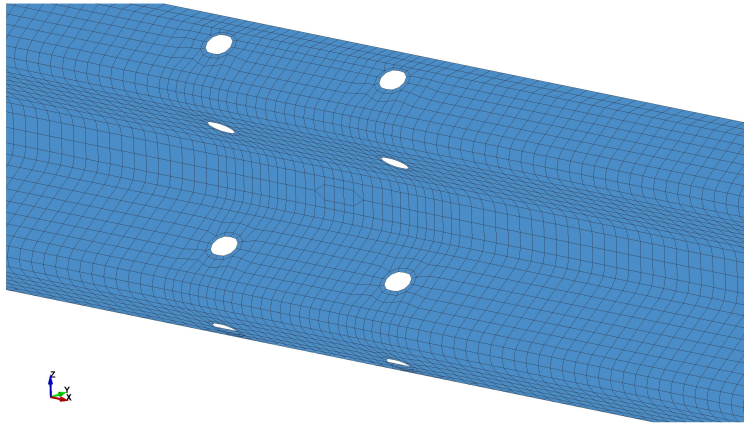
Figure 5.2: Proper mesh to use a spotweld

That being so, the first part of the job consisted in the modification of the local meshes, avoiding the use of too small elements, but trying to make it very regular around the holes. For circular holes, good results are obtained using a total of 8 or 12 elements on the perimeter; to have an even more regular and symmetric mesh, usually only a quarter of the discretization was created, to be subsequently reflected.
These details are required to avoid any kind of asymmetric behavior, that due to the high local stresses could lead to a wrong failure of the junction, mostly due to bearing of the hole.

(a) *Fishplate.*   (b) *Spacer.*

(c) *Beam.*   (d) *Post.*
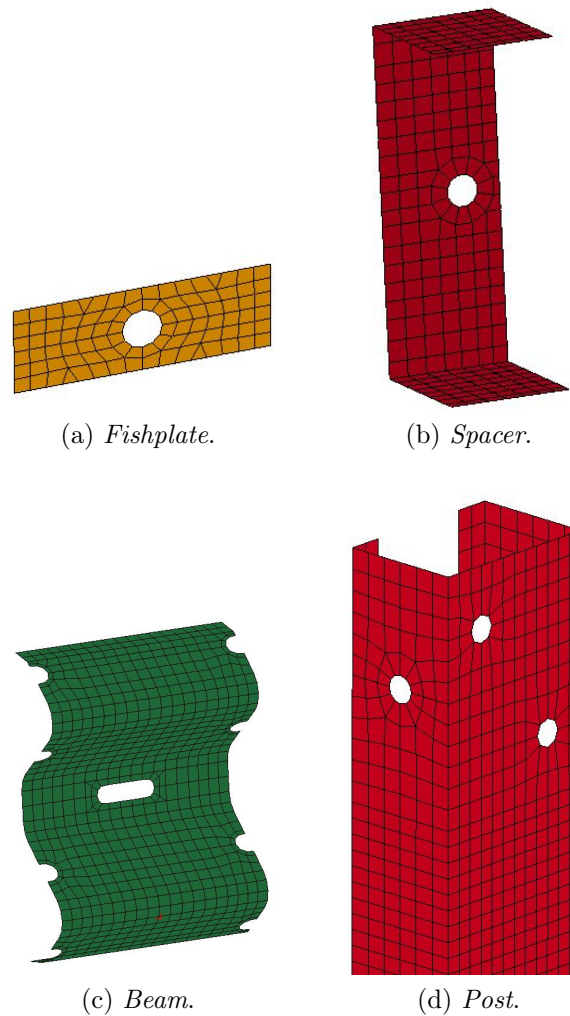
Figure 5.3: Re-meshed parts
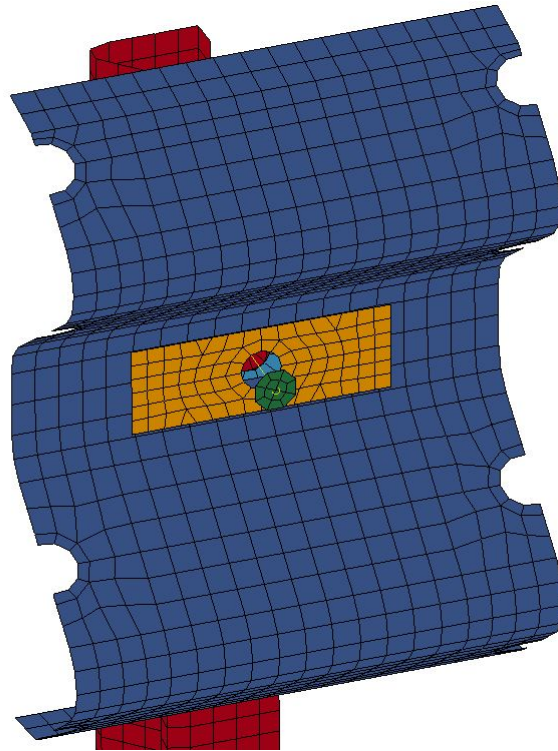
Figure 5.4: Assembly

5.2.1   Timestep and mass scaling

The most important thing to consider while meshing is to avoid very small elements that could significantly affect the time-step of the analysis, since the simulations launched are solved using the explicit scheme, the time-step is based on the highest natural frequency of the system:

$$\Delta t < \frac{2}{\omega_{max}} \tag{5.1}$$

where

$$\omega_{max} = \frac{2c}{l} \tag{5.2}$$

l is the edge or diagonal length of the element considered; c is the speed of sound in each element, calculated as

$$c_{beam} = \sqrt{\frac{E}{\rho}} \qquad c_{shell} = \sqrt{\frac{E}{(1-\nu^2)\rho}} \qquad c_{solid} = \sqrt{\frac{E(1-\nu)}{(1+\nu)(1-2\nu)\rho}}$$

Since the full scale analysis, final objective of the work, are well suited for the explicit solver, due to their numerical characteristics, like the high number of elements and the need of results with high frequency, the implicit counterpart has been completely ignored for the bi-dimensional model, even for the local tests: the focus is on the explicit only. [1]
LS-Dyna, to try to not use a too small time-step, has the possibility, for each element, to artificially modify the density of the material; the added mass is non physical, but anyway it affects the results [2]. In many cases the effect is negligible, especially if the mass is added in non critical parts of the model or where the velocities are small, nonetheless this should always be verified.
Mass scaling is introduced in LS-Dyna via the time-step: based on its sign the effect will be different, as shown in figure 5.5. Using a positive time-step the global mass is kept constant, some elements have their mass increase and some others have it decrease; usually this approach is not used, but a negative time-step is preferred: this option enables the addition

---

[1]For the sake of completeness, it has to be said that many available commands in LS-Dyna work only with the explicit solver, such as the one used to introduce the preload

[2]think to the product $F = m \cdot a$

of mass only to those elements whose time-step is less than the critical one.
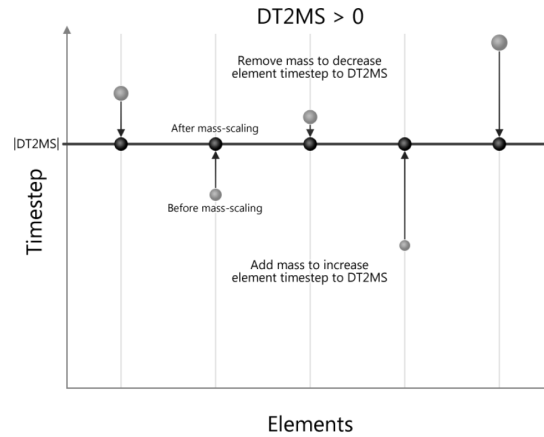
(a) *Positive time step.*
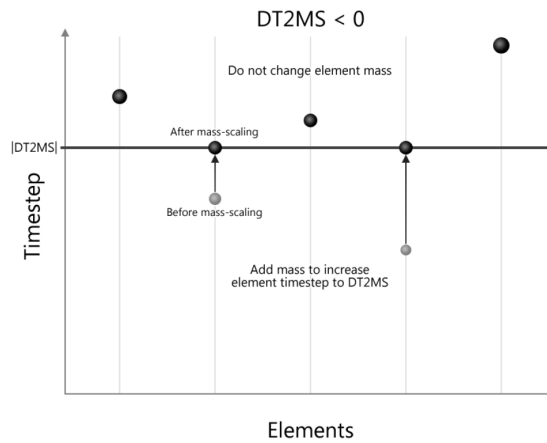
(b) *Negative time step.*

Figure 5.5: Mass scaling

Another possible solution to increase the time-step is to change the elastic stiffness, E, to decrease the sound speed thereby increasing the resulting time-step; this last approach has never been used.

As prescribed by the norm EN-1317, the added mass must not be more than the 3% of the total mass of the model and for each piece the amount of added mass have to be less than 10% of its initial value; where possible an analysis without mass scaling should be performed, to gauge the sensitivity of the results to the amount of mass added.

5.3 Failure criteria

The choice of the failure criterion is the most important one, because it will regulate the functioning of the whole model; it should use all the available information, be simple to modify, with just a couple of mouse clicks and, of course, predict the failure of the bolt in the most possible accurate way, because, as already remarked before, the behavior of the whole restraint system will depend on it.

Evaluated all the possibilities offered by LS-Dyna, a stress based failure, computed from the resultants is chosen; this option has been adopted because it allows to consider all the three components for both, forces and momenta, and to work it requires only the maximum axial and shear stress at failure, usually known, because they are part of the initial design specifications.

The value for the shear stress is calculated as:

$$\tau = \frac{\sigma}{\sqrt{2}} \tag{5.3}$$

this is a modification of the Von Mises theory, whereby to obtain the shear stress the division should be done using $\sqrt{3}$.

After the first numerical simulations where the theory was respected but the rupture of the bolt always occurred too soon, the value for τ has been calculated according to equation 5.3.

The material that satisfies these requirements is *MAT 100: Spotweld damage failure* and it has been assigned to the beam that represents the shank of the bolt; its LS-dyna card is reported in table 5.1. It has to be used with a specific element formulation: *ELFORM = 9* in the card *SECTION*.

In the material card the failure criterion is activated through the parameter *OPT*, seting it equal to 1.

The rupture criterion is only for the beam, in its entirety; it is not possible to predict which part of the shank will fail, nor which side of the bolt. To work properly it requires two parameters:

- σ_{rr}^F - Maximum axial stress at failure;
- τ^F - Maximum shear stress at failure

used in the following equation:

$$\left(\frac{\sigma_{rr}}{\sigma_{rr}^F}\right)^2 + \left(\frac{\tau}{\tau^F}\right)^2 = 1 \tag{5.4}$$

MID	ρ [Ton/mm]	E [MPa]	μ	SIGY [MPa]	ET	DT	TFAIL
1	$7.85e^-9$	$2.1e^5$	0.3	395			

EFAIL	LCAX [MPa]	LCTAU [MPa]
	500	354

RS	OPT	FVAL	TRUE T	BETA
	1.0			

Table 5.1: Card Mat 100 for a 5.8 class bolt

If the left term of the equation 5.4 exceed 1, the spotweld fails, causing the rupture of the junction.
σ_{rr} and τ are calculated as follow

$$\sigma_{rr} = \frac{N_{rr}}{A} + \frac{\sqrt{M_{ss}^2 + M_{tt}^2}}{Z} \tag{5.5}$$

$$\tau = \frac{M_{rr}}{2Z} + \frac{\sqrt{N_{rs}^2 + N_{rt}^2}}{A} \tag{5.6}$$

where:

- N_{rr} - Axial force resultant
- N_{rs} - Shear stress along S
- N_{rt} - Shear stress along T

- M_{ss} - Moment resultant S
- M_{tt} - Moment resultant T
- M_{rr} - Torsional resultant

and:

$$A = \pi \cdot \frac{d^2}{4} \tag{5.7}$$

$$Z = \pi \cdot \frac{d^3}{32} \tag{5.8}$$

where d indicates the diameter of the bolt.

In figure 5.6 it is clearly notable how the curve goes to zero after the rupture index exceeds 1, synonymous of no more stresses present in the beam, due to the failure of the junction and the consequent deletion of the element.
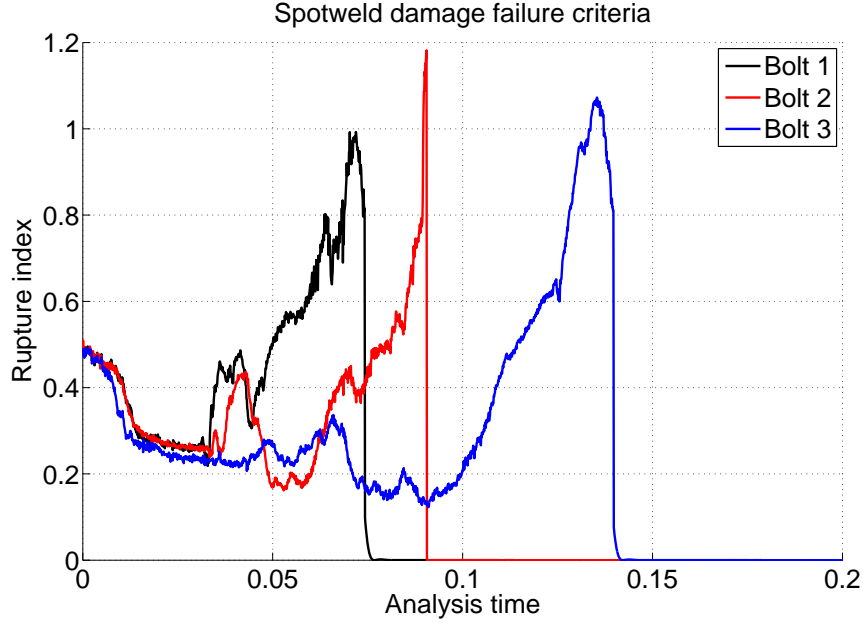

Figure 5.6: Failure of the bolt

The rupture criterion used for the spotweld is a resultant-based failure criterion that fails the weld if the resultants are outside of the failure surface defined by equation 5.9:

$$\left(\frac{N_{rr}}{N_{rr}^F}\right)^2 + \left(\frac{N_{rs}}{N_{rs}^F}\right)^2 + \left(\frac{N_{rt}}{N_{rt}^F}\right)^2 + \left(\frac{M_{rr}}{M_{rr}^F}\right)^2 + \left(\frac{M_{ss}}{M_{ss}^F}\right)^2 + \left(\frac{M_{tt}}{M_{tt}^F}\right)^2 - 1 = 0$$

(5.9)

used without considering the values for the momenta.

5.4 Preload

An axial force is applied to the beam to simulate the preload existing in the reality due to the torque used to tighten the nut; based on the size of the bolt different values are applied. In all the cases a ramp is used to describe

the path of application, to avoid impulsive and unrealistic behavior.

The axial load is applied during the dynamic relaxation, a part of the analysis specifically created to introduce particular loads, like the gravity, into the model.

One of the main advantages of this solution is the intrinsic damping introduced, that makes possible to apply the load in a very short amount of time, 5 ms, reaching the desired value of 21875 N, corresponding to 70 Nm of torque, appropriate for an M16 bolt; in case of a smaller bolt the value has to be proportionally reduced.

This specific value has been chosen because commonly used in safety barrier applications. For a pure tension test the influence of preload is minimal; its impact is different for the full scale simulations, where with a low preload the bolt can easily slide to the edge of the hole, significantly changing the behavior of the whole junction.

Since the assembly of the road restraint system sometimes is done by not qualified people, especially on secondary and small roads, can be interesting to study the effects of the position of the bolt in hole on the global behavior of the barrier. Of course, such a study can not be done using the spotweld model.
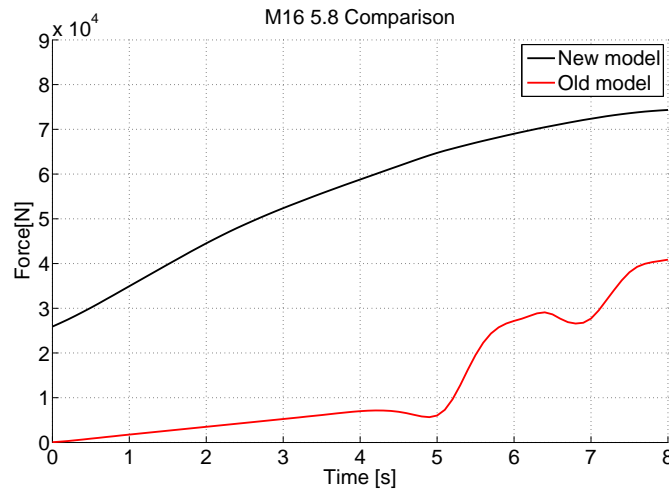

Figure 5.7: Different approaches to introduce the axial load

In figure 5.7 the two lines represent the axial load acting on the bolt; the red one has been obtained applying the preload during the transient analysis, in fact at the beginning of the load path (time = 0) the force acting on the bolt is null. Instead, using the dynamic relaxation (black

line) at time = 0 the bolt is already preloaded.

This is even more important if the model is a full scale analysis, because the simulated time would be 0.5 seconds longer just to apply the load, considerably increasing the computational time: around 50% more time for a TB11 and 20% for a TB51.

To summarize, several advantages of the dynamic relaxation are:

- saves computational time: the simulated time is around 0.01 seconds and the process is done at the same time of the initialization of the gravity. The global increase of computational time due to the preload is almost zero;

- introduces damping, avoiding unwanted vibrations and peaks of forces that could hinder the reaching of the desired value of axial force;

- allows to restart the simulation. If the model remains the same it can be initialized only the first time and re-used in future.

(a) *First stage.*

(b) *Second stage.*
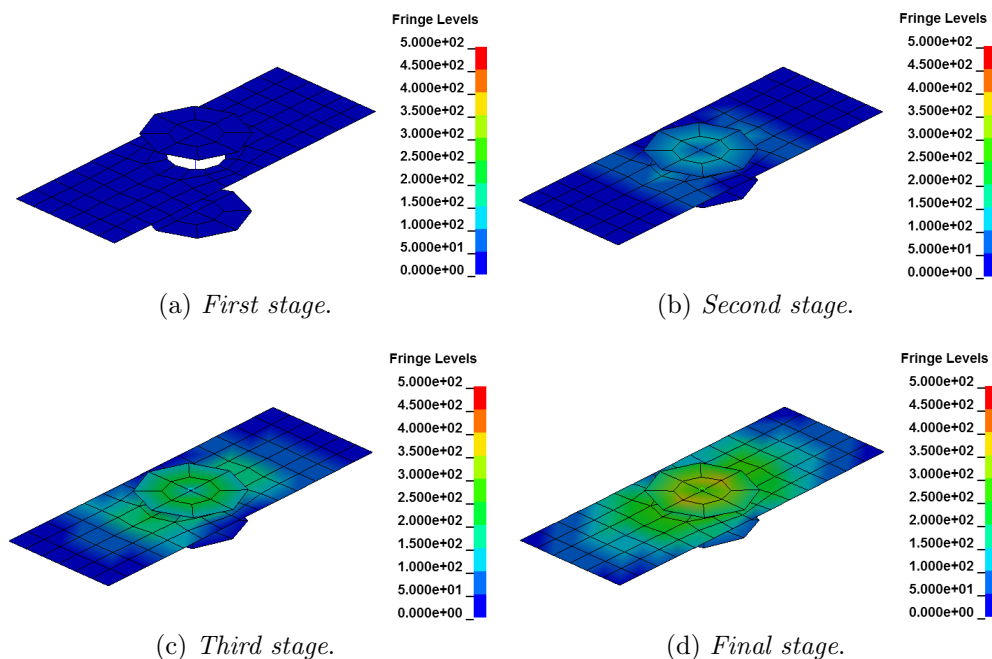

(c) *Third stage.*

(d) *Final stage.*

Figure 5.8: Introduction of the preload

Thanks to the preload there is a significant difference with the old model: now the parts of the model are really kept together due the frictional forces

introduced. It is possible to perform sensitivity studies on the frictional coefficient or on the value of preload, to simulate an improper assembling of the barrier and the effects that it has on the global behavior of the structure.

5.5   SIGY - Initial yield stress

In the card of the material *MAT 100 Spotweld Damage Failure* (fig. 5.1)is possible to find the field corresponding to the initial yield stress for the beam.
Introducing the real yield value in this card causes some numerical issues, because once the value is reached it is not exceeded.
LS-Dyna considers this value as the maximum limit in terms of stress; higher stresses can not be accounted in the beam, causing an anomalous behavior: the beam, in case of an applied traction at extremity, lengthen indefinitely (fig. 5.10), without any physical justification, and the load is kept constant, never reaching the rupture point, as shown in figure 5.9.
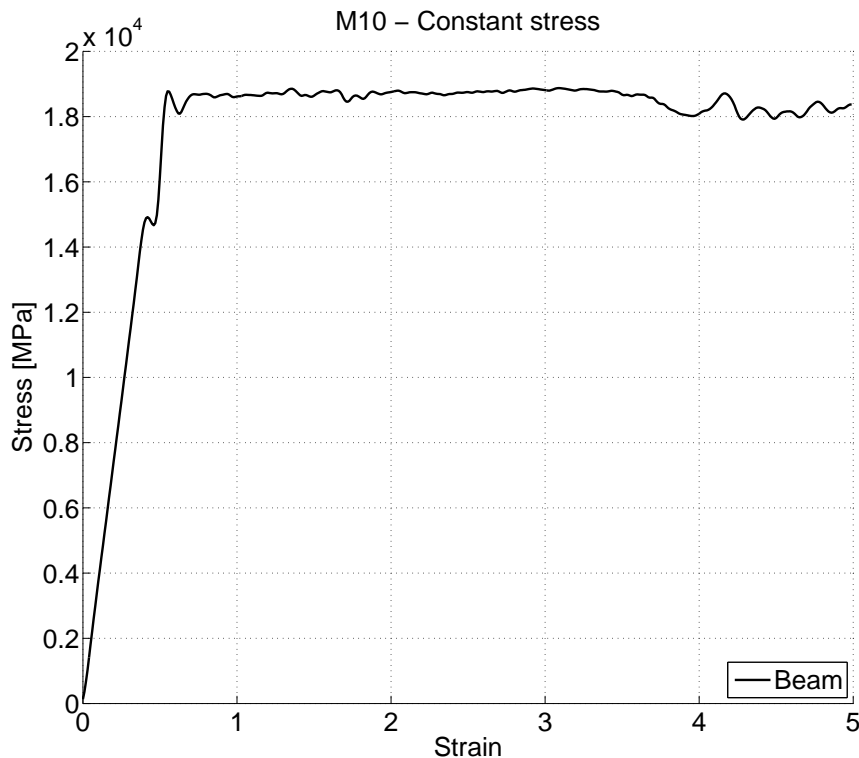

Figure 5.9: Unrealistic constant force

(a) *First stage.*

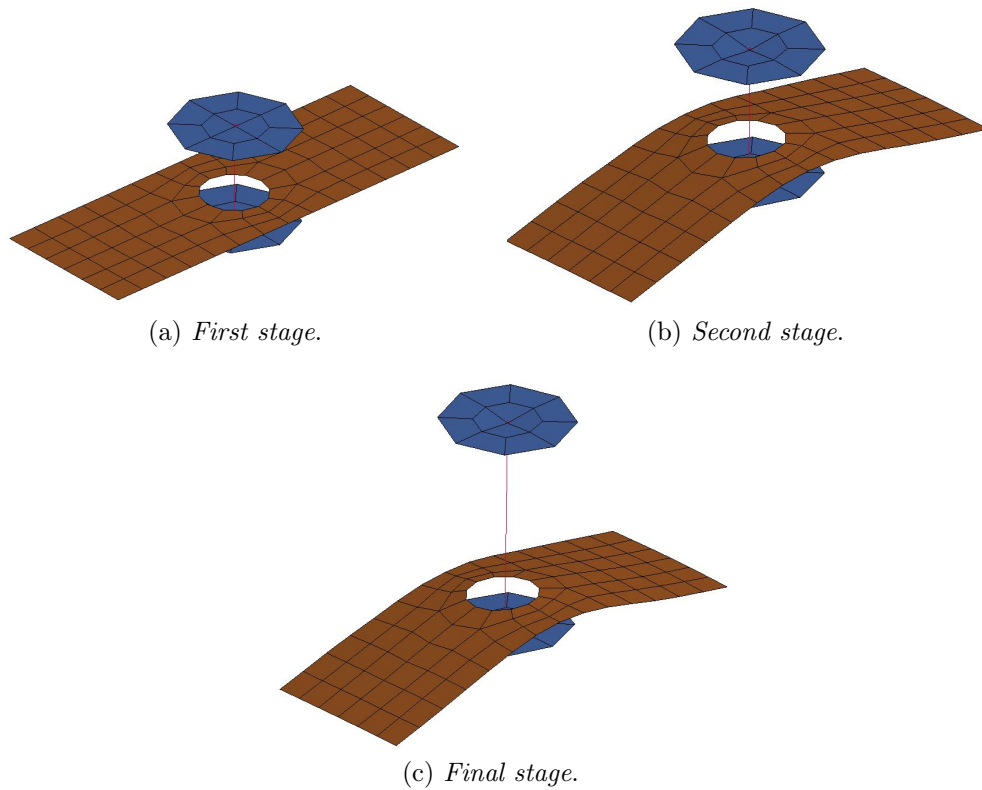(b) *Second stage.*

(c) *Final stage.*

Figure 5.10: Effect of Yield stress

A partial solution is to impose a null value in this card, forcing LS-Dyna to use 1% of the young modulus as the yield stress: doing the math, a value of 2100 MPa is obtained. The beam has a perfect elastic behavior, with a very steep slope, thus it can be considered almost rigid, going directly to the rupture point, avoiding to plastic phase.

The $SigY$ parameter is supposed to be used together with ET, in the same material card, to define a curve characterized by two segments with different slope.

Observing figure 5.9 it is possible to note that the force is around $19.000N$. The graph refers to an M10, which section is around 78.54 mm^2; hence:

$$\sigma = \frac{F}{A} = \frac{19000}{78.54} = 240 MPa \tag{5.10}$$

That is exactly the value chosen for $SigY$ in this specific test.

5.6   Head and Nut

Head and nut of the junction are modeled with *MAT 24: Piecewise linear plasticity*, without implementing any criterion to define the failure, since, according to the available experimental tests, the rupture of head or nut never occurred. Of course, the use a more sophisticated material, like *MAT 224: Tabulated Johnson Cook* should provide more accurate results, especially if the junction is subject to bearing or high deformations around the hole. It requires a wide range of numerical and experimental tests to be properly used and calibrated, hence, since it is not needed to develop the content of this thesis, it is not considered
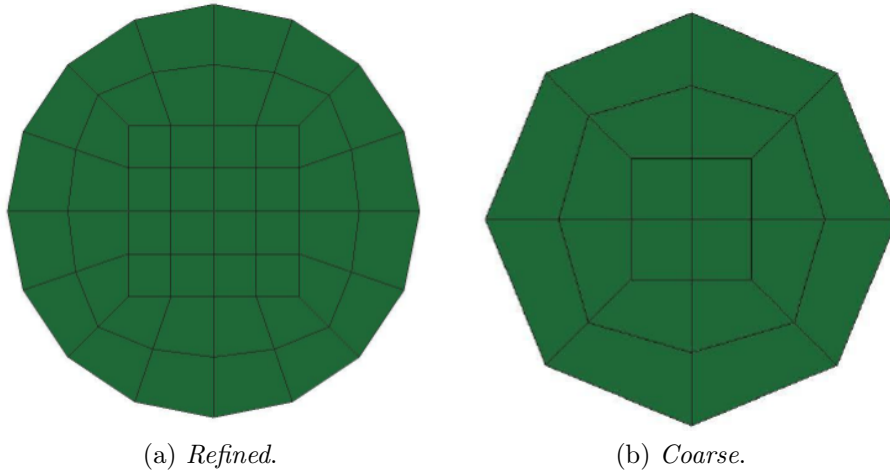

(a) *Refined.*   (b) *Coarse.*

Figure 5.11: Mesh for head and nut

Figure 5.11 shows a good technique to model head and nut: the so called butterfly scheme is adopted; it is not necessary to have an extremely refined mesh, 8 or 16 elements on the perimeter are enough.
The thickness assigned to the elements should be equal to the one of the real pieces; eventually can be increased slightly to avoid numerical errors similar to those caused by the parameter $SigY$ for the beam.[3]
Considered the critical role played by head and nut a fully integrated formulation is adopted, coupled with the dedicated hourglass formulation, *to activate the full projection warping stiffness for accurate solutions.*

---

[3]This problematic is deeply analyzed in chapter 6

5.7 Contacts

One of the key aspects of this kind of simulations is the management of contacts between all the involved parts, due to the impact they have, not only on the global behavior of vehicle and road restrain system but on the computational time too, since it is estimated that around 30% of the time spent calculating is due to the contact algorithm.

For the junctions a dedicated set is required.

The adopted way to represent the contacts between the barrier and the junction model makes use of null beams: a null beam is a beam with a defined shape, whose material is null, then it does not sustain any kind of stress.

It is necessary to define null beams along all the edges involved in the contact, typically:

1. the hole of the barrier;
2. the hole of the spacer;
3. the hole of the fishplate or washer;
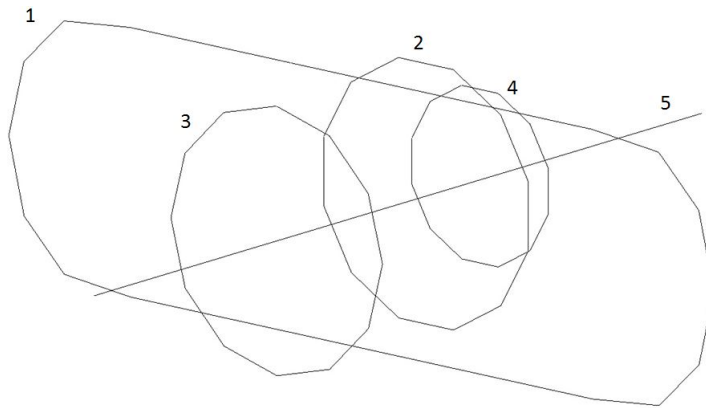4. the hole of the post;
5. the shank of the bolt.

Figure 5.12: Null beams

Once a *set part* containing all the null beams is defined, a specific contact card must be created: **Contact Automatic General.*

To manage all the other contacts of the model the command **Contact Automatic single surface* is used. [4]

---

[4]The strong hold of the automatic contacts is the detection of penetrations on both sides of the elements, regardless of the chosen normal. More info on the Ls-Dyna user manual.

5.8   5 Beams model

After the first round of numerical simulations using the presented model some issues emerged, two in particular: one for weak and small bolts like the M10 and another one for the stronger M16.

These become evident after the first full scale tests, where for the M10 an early rupture happened quite often, while for the M16 an unphysical deformation for head and nut occurred. These results are presented in the dedicated chapter.

To solve these problems the model was modified, trying to be even more representative of a real bolt.

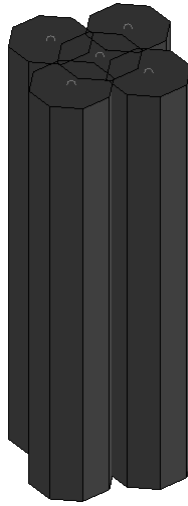There are now five beams instead of one, keeping the total section constant.

Figure 5.13: 5 Beams Model for the M10

Another improvement regards the material used for the spotweld. As shown in figure 5.1 three parameters were not used, to have the simplest possible working model: E_T, E_{FAIL} and RS.

Through these values it is possible to define a more sophisticated behavior that is able to simulate the evolution of damage for the beam, introducing the necking point and a third segment for the material law; actually, once the maximum stress value is reached the beam fails and it is deleted from the model.

This improvement can be much more significant for big and strong bolts, like the ones used to anchor the posts to the concrete in case of road restraint systems installed on bridges. In these cases the shear stresses are

much more significant and the deformation of the bolt before failure can not be neglected.

Due to the lack of experimental data only a numerical calibration was performed, and the most reasonable values are:

E_T	E_{FAIL}	RS
2100	0.05	0.5

Table 5.2: Spoweld parameters

ET represents the slope of the segment between the yield point and the necking point.

E_{FAIL} is the value obtained by equation 5.11 corresponding to the stress failure level imposed, while RS refers also to equation 5.11 but in this case the value for l is taken at rupture, the last point of the curve.

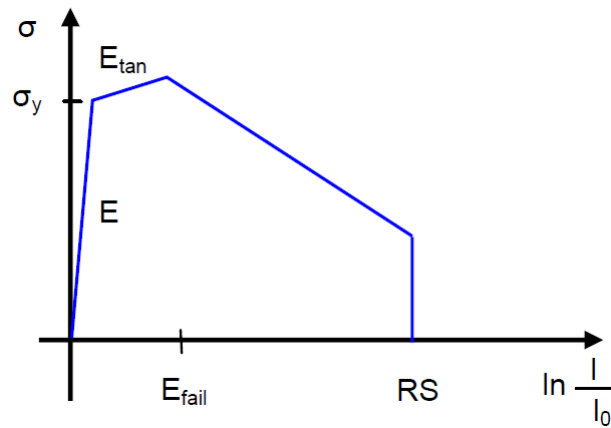$$E_{FAIL} = ln\frac{l}{l_0} \tag{5.11}$$

Figure 5.14: Stress - strain relationship

Due to the lack of time this aspect was not deeply analyzed, but for sure it can be a starting point for further developments to have a general bolt model that can be used in all the contexts.

Chapter 6

Numerical - experimental correlation

In this chapter the results of local numerical tests are presented and compared with the data obtained by the experimental ones. A parallel with the photos of the tests and of the numerical results will be carried out, together with graphs representing the force - displacement curve.

Further on in the work, the best local models will be used in full scale simulation to have a definitive proof of their reliability.

The solid solution worked quite well since the first trials, only tuning the parameter for the deletion of elements due to plastic strain has been needed.

Instead, for the bi-dimensional solution several modification to optimize it were needed: due to some problems that emerged from the tests the model has been updated, increasing the number of beams used to simulate the shank of the bolt.

Both the cases presented in the experimental chapter have been considered:

- M10 4.6
- M16 5.8

Due to computational limits and needs, it wasn't possible to reproduce the numerical experiments using the same speed for the displacement of the bolt, even for the solid approach solved with the implicit solver: it would have taken too much time without bringing significant improvements.

For the solid case a speed of 1 mm/s was adopted, considered slow enough to have a quasi static condition.

The other case, instead, due to the explicit scheme, required a much faster displacement, to have a total simulated time of about 1 second: the chosen

speed is 100 mm/s. To evaluate this choice a comparison between the internal and the kinetic energy has been done.
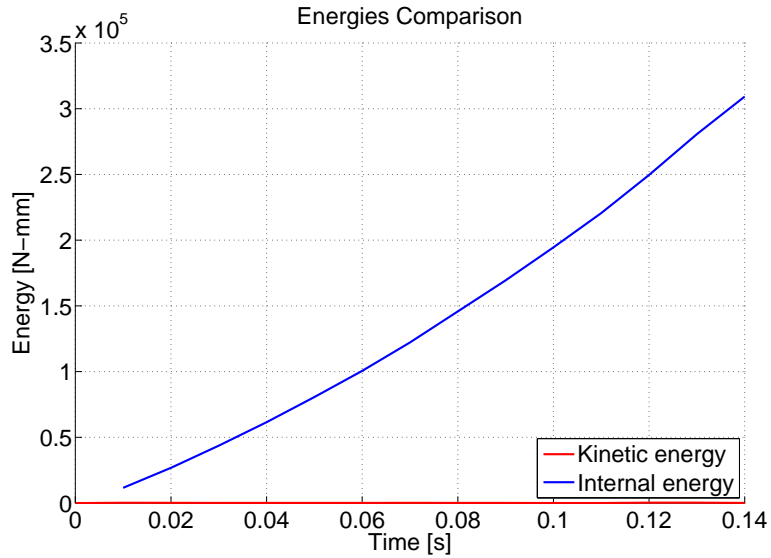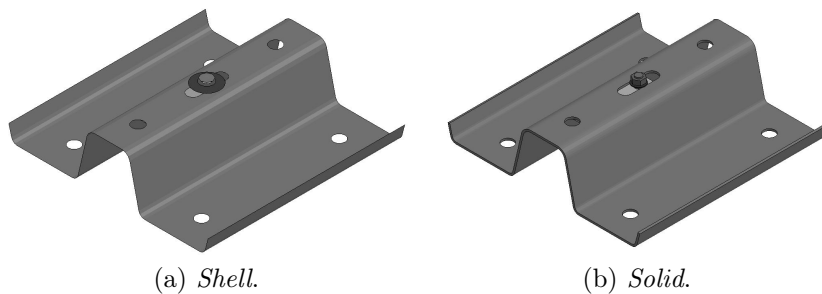

Figure 6.1: Energy comparison

As shown in figure 6.1 the difference of order of magnitude between the two energies is 3, that satisfy the requirement to have a static behavior. Since the adopted speed is the same for both cases, M10 and M16, the result is considered valid for all the tests.

6.1   M10 4.6

6.1.1   Single Beam

(a) *Shell.*   (b) *Solid.*

Figure 6.2: M10 - Single beam

In figure 6.3 the obtained results are shown and in table 6.1 the numerical values for the peak force are reported.
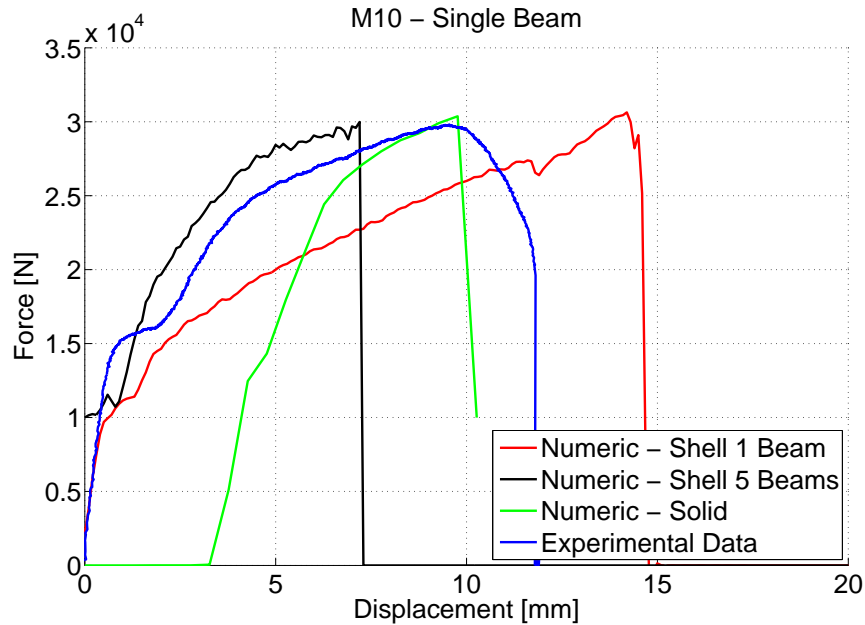

Figure 6.3: M10 - Single Beam - Results

Case	Numerical [N]	Exp test [N]	Delta	Error [%]
Shell 1-beam	30635	29813	822	2.7
Shell 5-beams	29986	29813	173	0.6
Solid	30368	29813	555	1.9

Table 6.1: M10 peak force - single beam

Considering table 6.1 and the graph 6.3 it is clear that the solution with the 5 beams is the best one, even better than the solid approach, that due to an approximate material law has some limitations. If during the simulation an element reach a strain value higher than the latest point of the provided material curve, showed in 4.4, LS-Dyna performs a linear extrapolation: the post necking behavior is neglected due to its complexity.

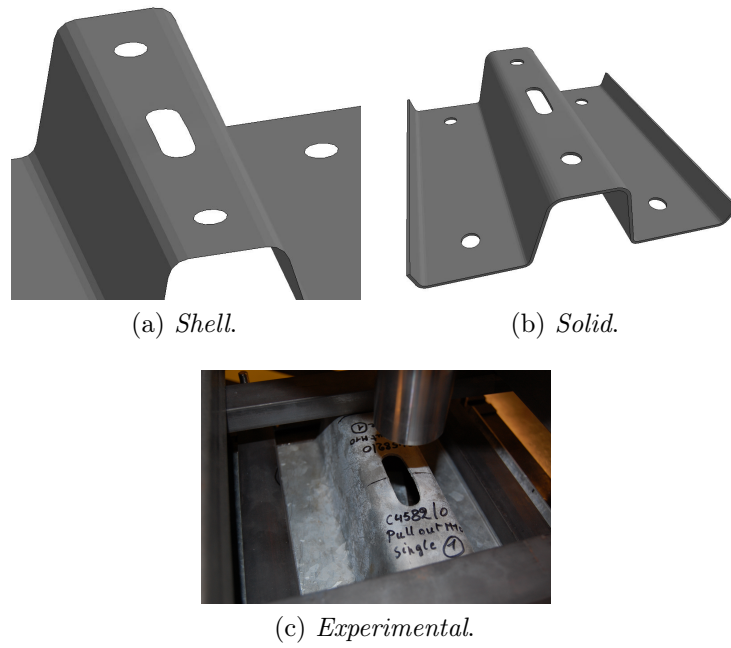Some images showing displacement, deformations and Von-Mises stresses are presented in 6.6.

(a) *Shell.*

(b) *Solid.*

(c) *Experimental.*

Figure 6.4: M10 - Single -Final deformation

(a) *Shell.*

(b) *Solid.*

(c) *Experimental.*

Figure 6.5: M10 - Single -Failed Bolt

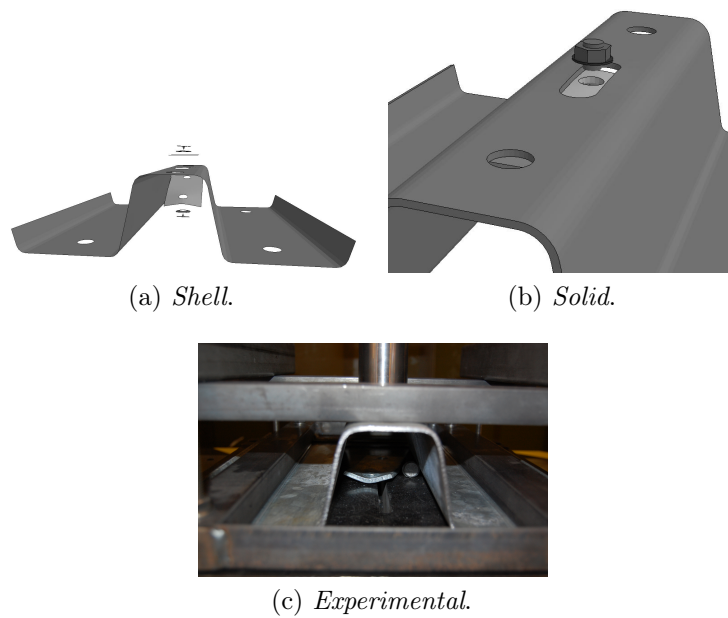(a) *Shell 1-beam.*   (b) *Solid.*
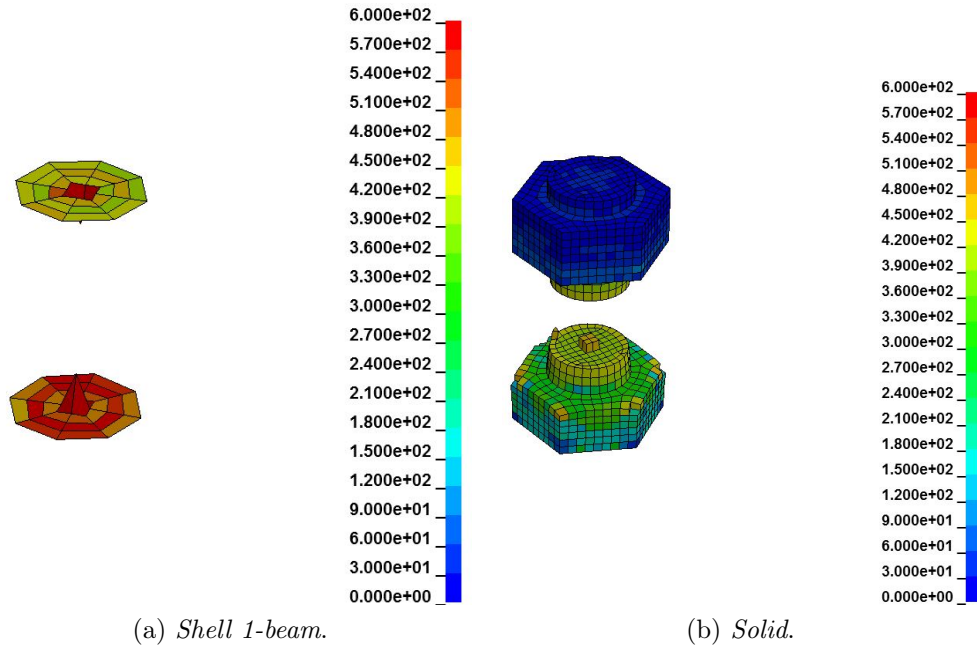
Figure 6.6: Broken M10 - Single beam

Observing the shells it is possible to remark a significant issue: the central elements suffer a big and unrealistic deformation. Obviously it is a numerical problem, caused by the combination of an approximate material law and, especially, by the fact that the forces, to be transferred to the head and nut of the bolt, are obliged to go though a single node, common to all the adjacent shells.

Another limit of this solution then emerged, particularly with small diameter bolts, like the M10: even if, for the computation of the stresses in the spotweld the considered section is, to all intents and purposes the chosen one, the model is not able to contrast the momenta present in the junction, because the group of shells representing head and nut are free to rotate around the central node in charge of the connection. Instead, in reality, the shank itself contrasts these momenta, simply due to its dimensions respect to the head of the bolt.

The relevance of this problem is minimal in a pure traction test like this, but in a full scale simulation, where the load condition is not only axial, but a combination of all the components, this could give yield to quite high momenta, that in some cases could lead to an early failure of the junction. A first solution consisted in constraining the rotations for the nodes of the elements of head and nut of the bolt and it worked quite well; anyway it was not completely generalizable, hence the model with the 5 beams was

introduced.

Some differences in the level of stress after the breaking of the bolt were remarked comparing the results of shell and solid elements, as shown in 6.7; the different discretization may be responsible for this.
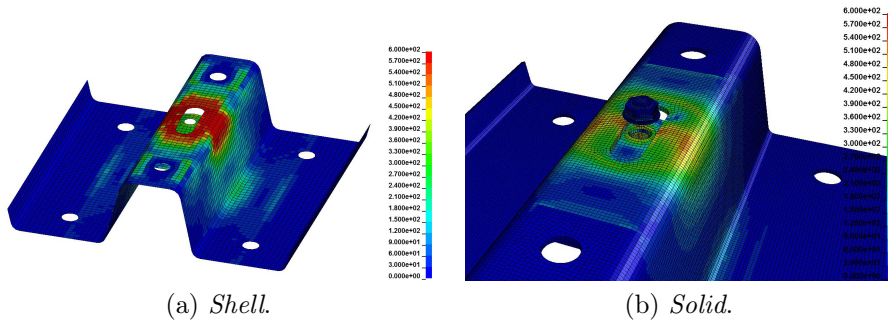

(a) *Shell.*   (b) *Solid.*

Figure 6.7: Final stress level - after bolt failure

(a) *First stage.*   (b) *Second stage.*

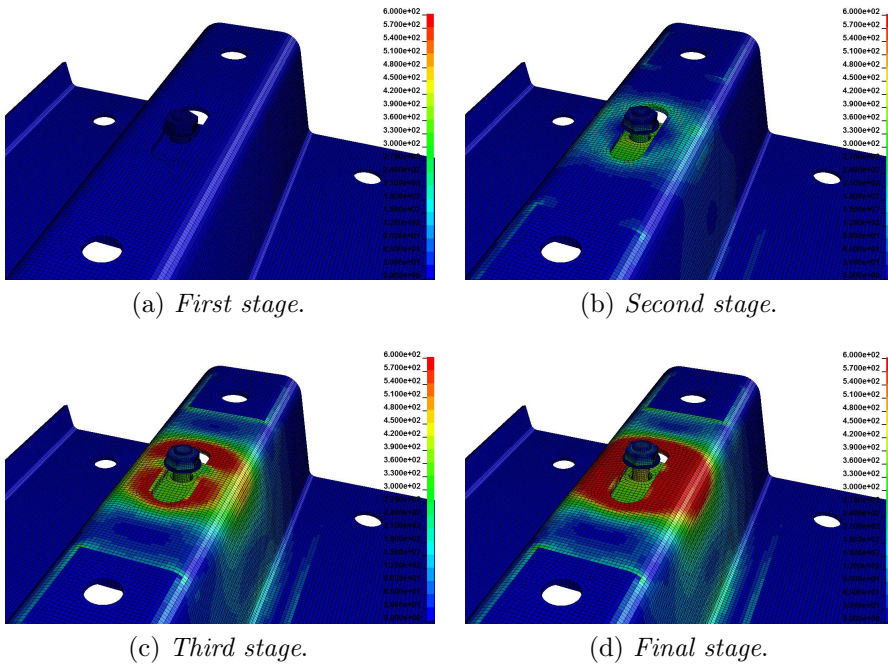(c) *Third stage.*   (d) *Final stage.*

Figure 6.8: M10 - Single - Stresses

6.1.2 Double Beam

The test is exactly as before, the model is the same; for the shell case the thickness has been increased, meanwhile for the solid discretization 3 elements, each one 1 mm thick, have been added.
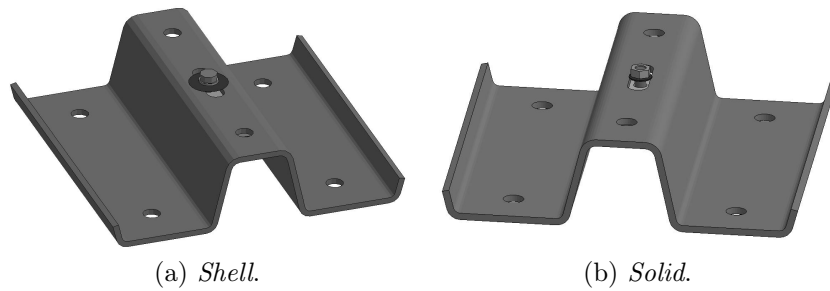The left image of 6.9 was taken visualizing the real thickness for the pieces.

(a) *Shell.* (b) *Solid.*

Figure 6.9: M10 - Double beam

In figure 6.10 the obtained results are shown and in 6.2 the numerical values for the peak force are listed.
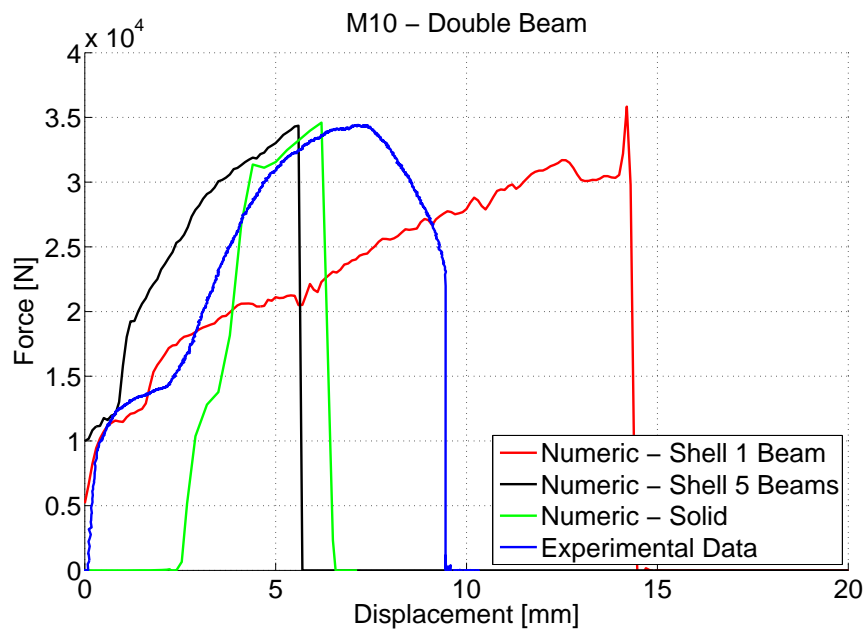

Figure 6.10: M10 - Double Beam - Results

Like before, the best results are achieved using the solid model or the 5 beams; this last case will be now deeply analyzed.

Case	Axial force [N]	Exp test [N]	Δ	Error [%]
Shell 1-beam	35840	34417	1423	4.1
Shell 5-beams	34361	34417	56	0.2
Solid	34601	34417	184	0.5

Table 6.2: M10 peak force - double beam

As expected, the peak of the axial force in the five beams reaches the breaking value in the same instant, as showed in 6.11. A direct comparison between the 2 solutions is available in 6.12.
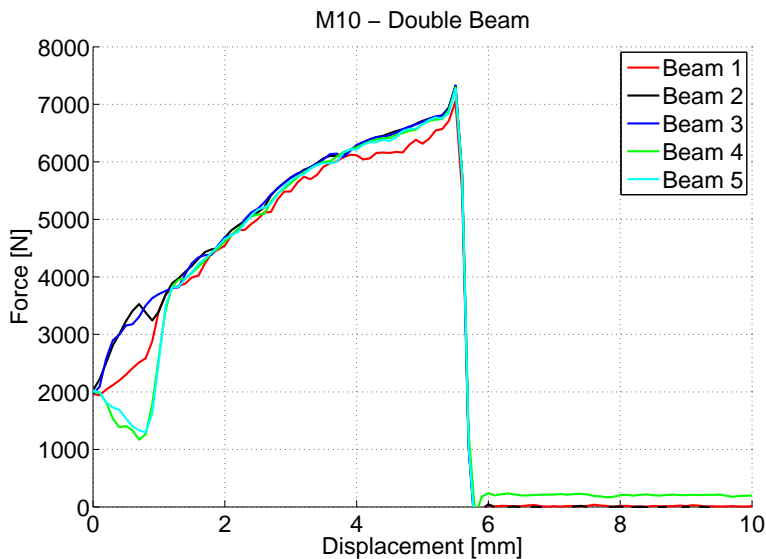

Figure 6.11: M10 - Double - 5 beams axial forces

The load distribution in the 5 beams model is homogeneous, the stress level in the shell elements representing head and nut of the bolt is more reasonable and proportioned to the one in the beams: the unrealistic deformation of the elements is avoided.

The study now focuses on the 6 components that act on the spotweld: axial force, shear, momentum and torque. In figure 6.13 the 6 components are plotted and the two cases of 1 and 5 beams are compared; the contribute of each beam, for the 5-beams case, has been summed to easily compare the results.
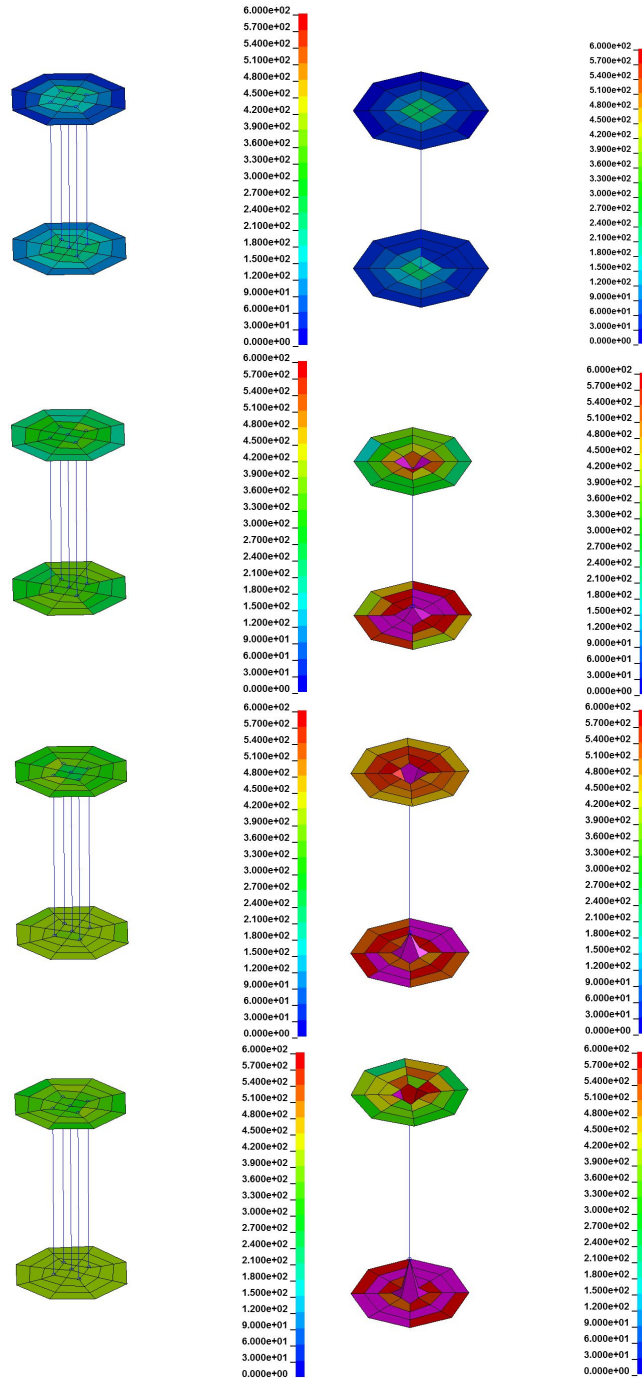
Figure 6.12: 1 and 5 beams comparison
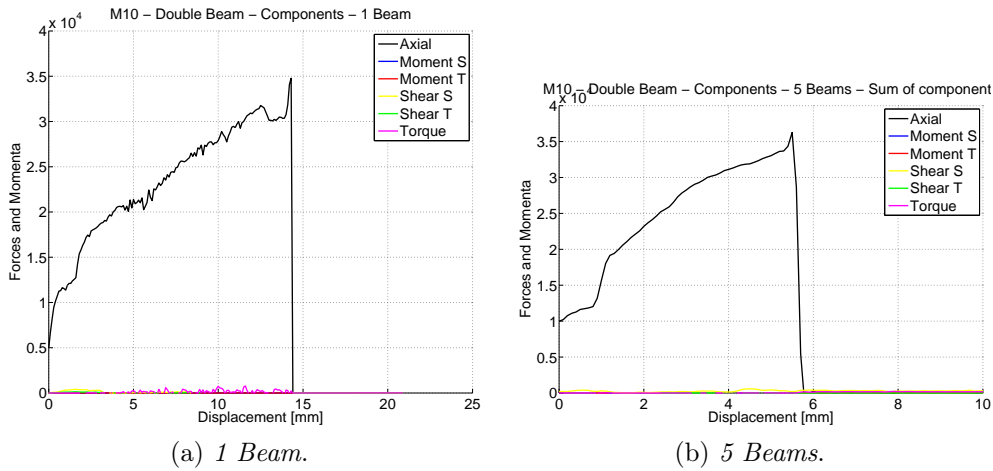
(a) *1 Beam.*
(b) *5 Beams.*

Figure 6.13: M10 - Double - Components comparison

To conclude the section concerning the M10 bolt, in figure 6.14 and 6.15 it is verified that the rupture criterion works as expected and presented before.
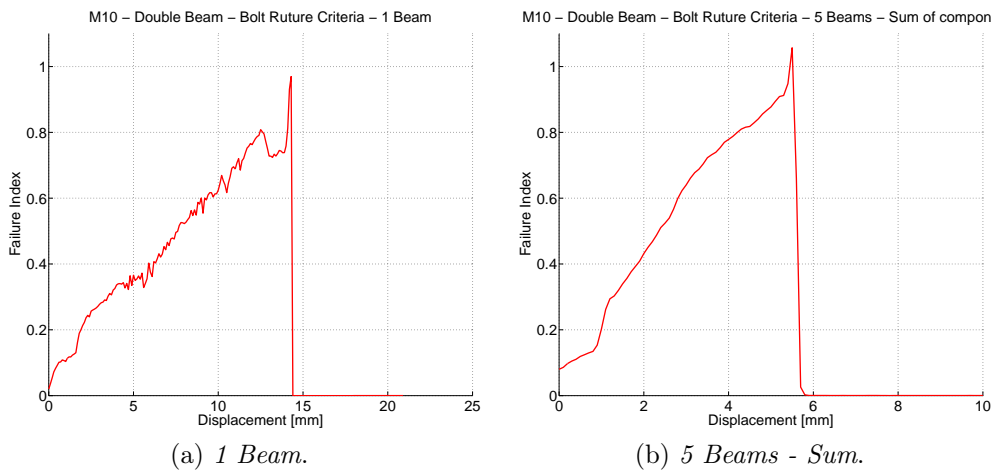

(a) *1 Beam.*
(b) *5 Beams - Sum.*

Figure 6.14: M10 - Rupture criterion

In 6.16 and 6.17 deformation and Von Mises stress for the various components are showed.

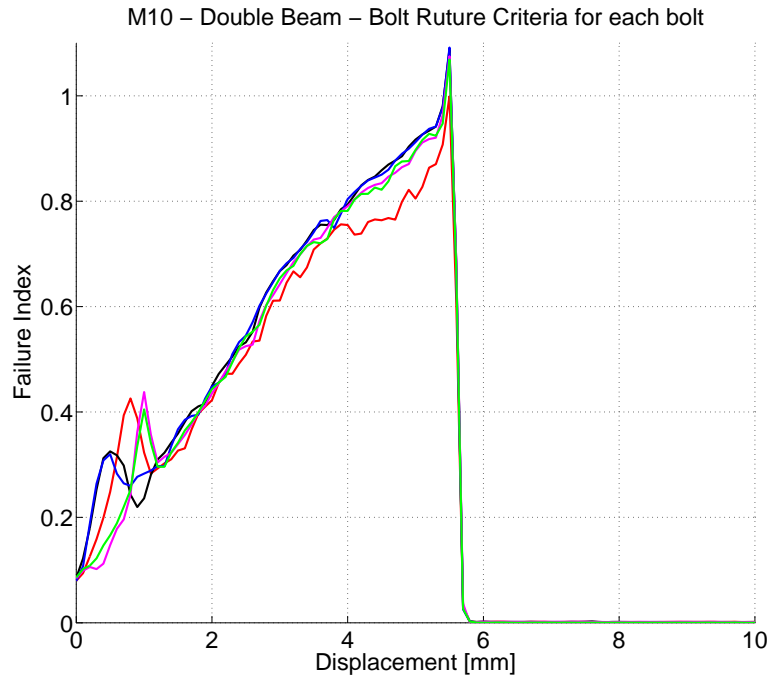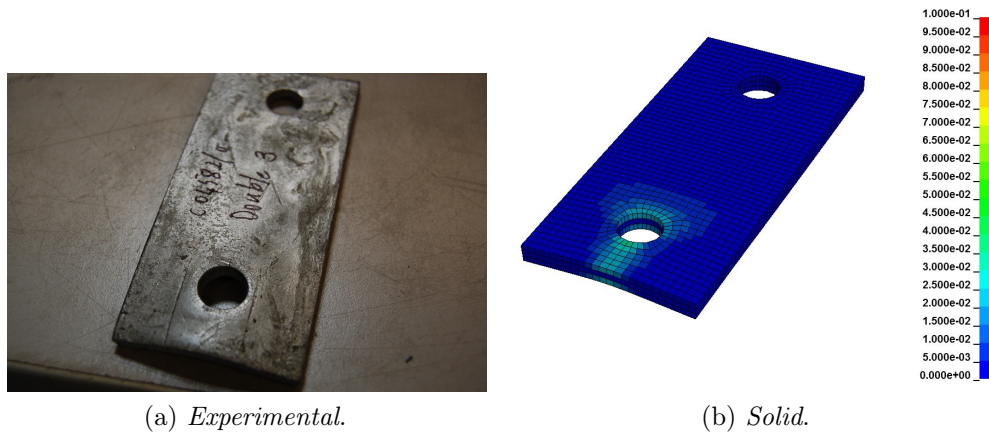Figure 6.15: M10 - 5 beams - Rupture criterion

(a) *Experimental.*   (b) *Solid.*

Figure 6.16: M10 - Double - Fishplate

(a) *First stage.*

(b) *Second stage.*

(c) *Third stage.*
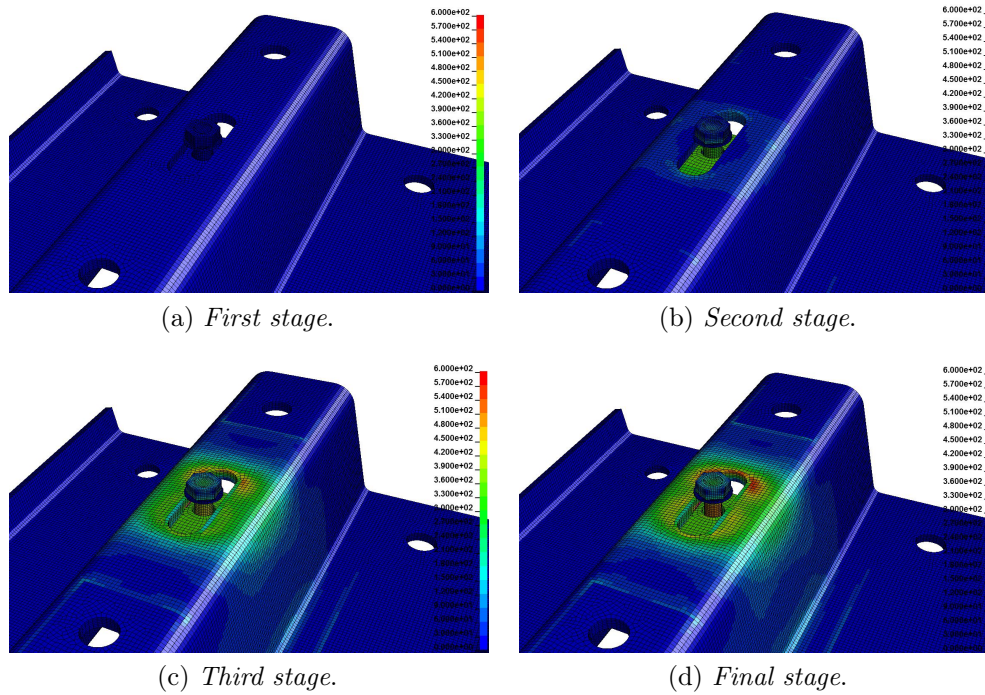
(d) *Final stage.*

Figure 6.17: M10 - Double - Stresses

6.2   M16 5.8

### 6.2.1   Centered Bolt

In figure 6.19 and table 6.3 the obtained results are shown.

Case	Axial force [N]	Exp test [N]	Δ	Error [%]
Shell	81553	81981	428	0.5
Solid	81434	81981	547	0.7

Table 6.3: M16 peak force - Centered

Except for some oscillations the behavior of the solid model represents quite well the experimental tests. The shell model catches the value of the peak force, while the trend could be improved; anyway, in order to perform a full scale simulation, the result can be successfully used. Since there is no failure for the connection, it is clear that the behavior of the curves is mainly dominated by the material laws of the beams.
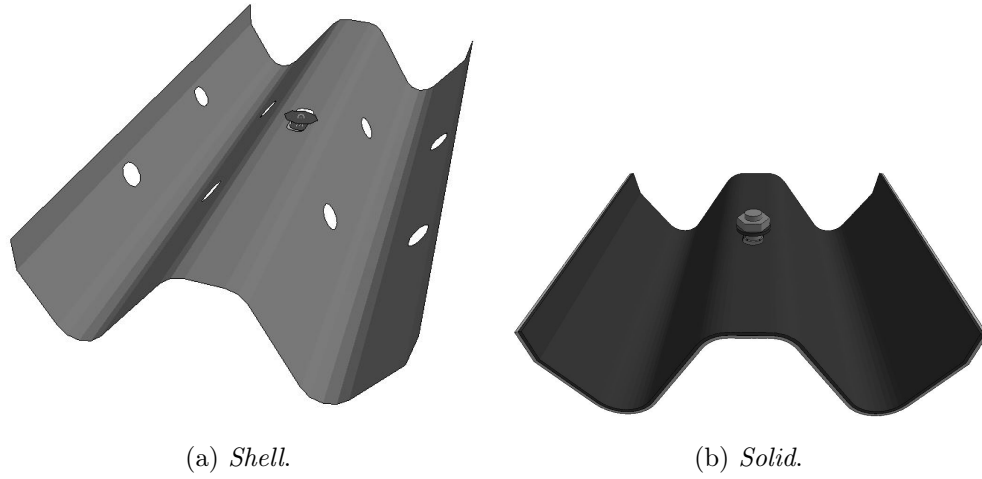
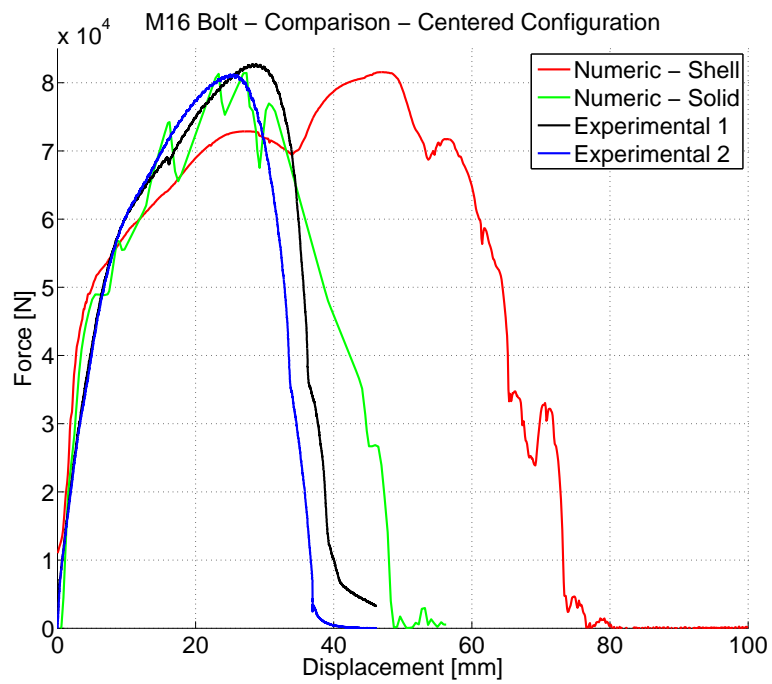(a) *Shell.*   (b) *Solid.*

Figure 6.18: M16 - Centered

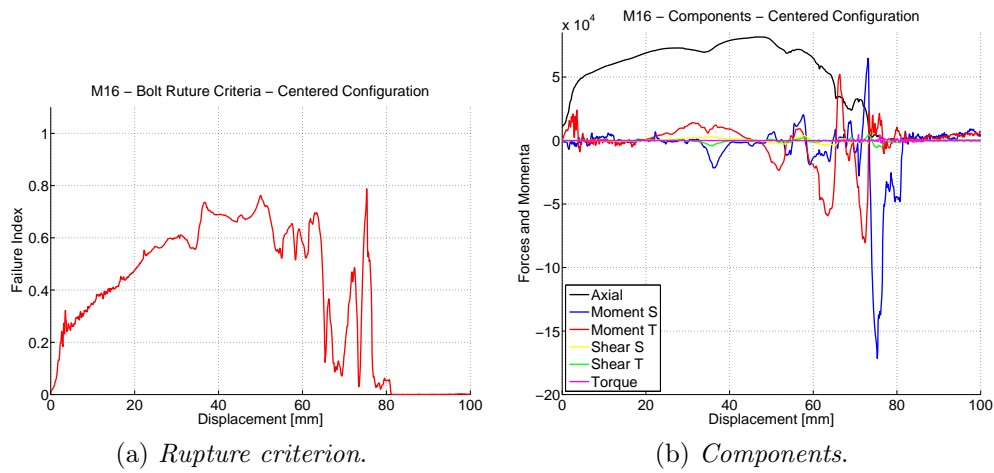Figure 6.19: M16 - Centered - Results

(a) *Rupture criterion.*

(b) *Components.*

Figure 6.20: M16 - Centered - Rupture

It is now interesting to investigate witch forces act in the bolt and how the failure criterion behaves.

From figure 6.20, it is possible to note that as the momentum increase there is also a peak in the failure index. Since the bolt used is quite big and resistant those momenta are not a significant source of issues, as they can be for the M10.

Later on a visual comparison of the 3 configurations (6.21), the final stage of the test with the bolt completely pulled through the beam (6.22) and the Von Mises stress (6.23).

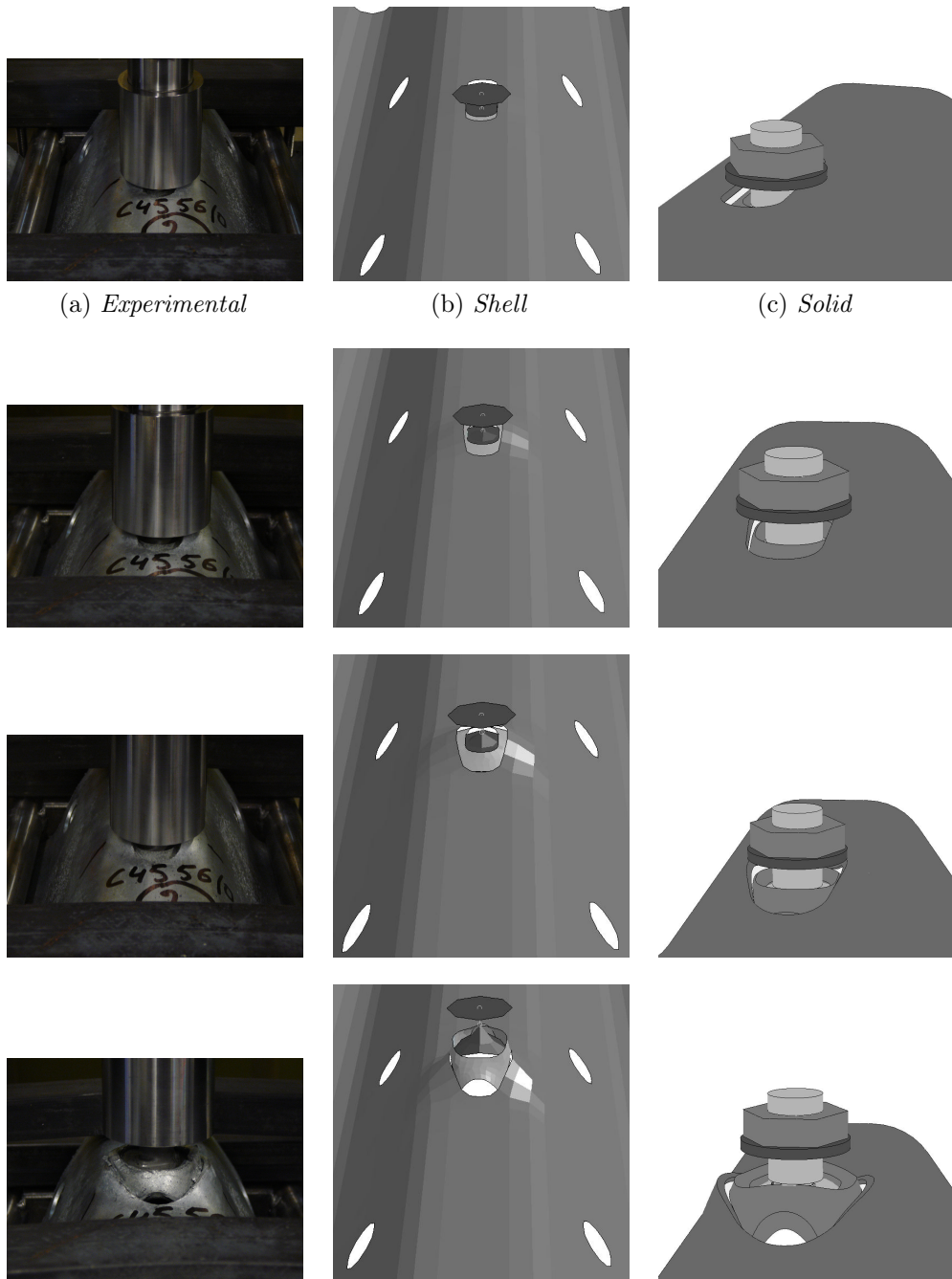(a) *Experimental*   (b) *Shell*   (c) *Solid*
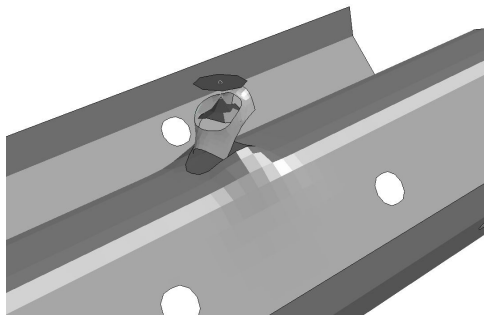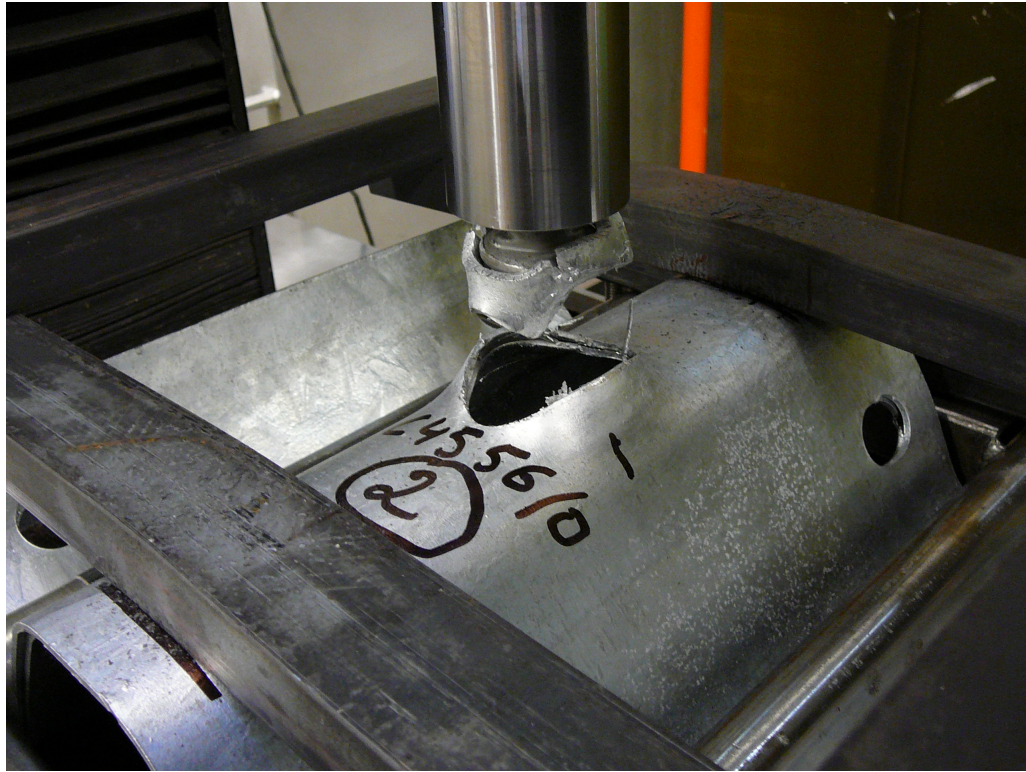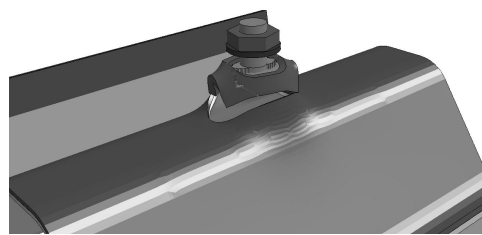
Figure 6.21: M16 - Centered - Displacement

(a) *Shell.*   (b) *Solid.*

Figure 6.22: M16 - Centered - final stage

(a) *First stage.*

(b) *Second stage.*

(c) *Third stage.*
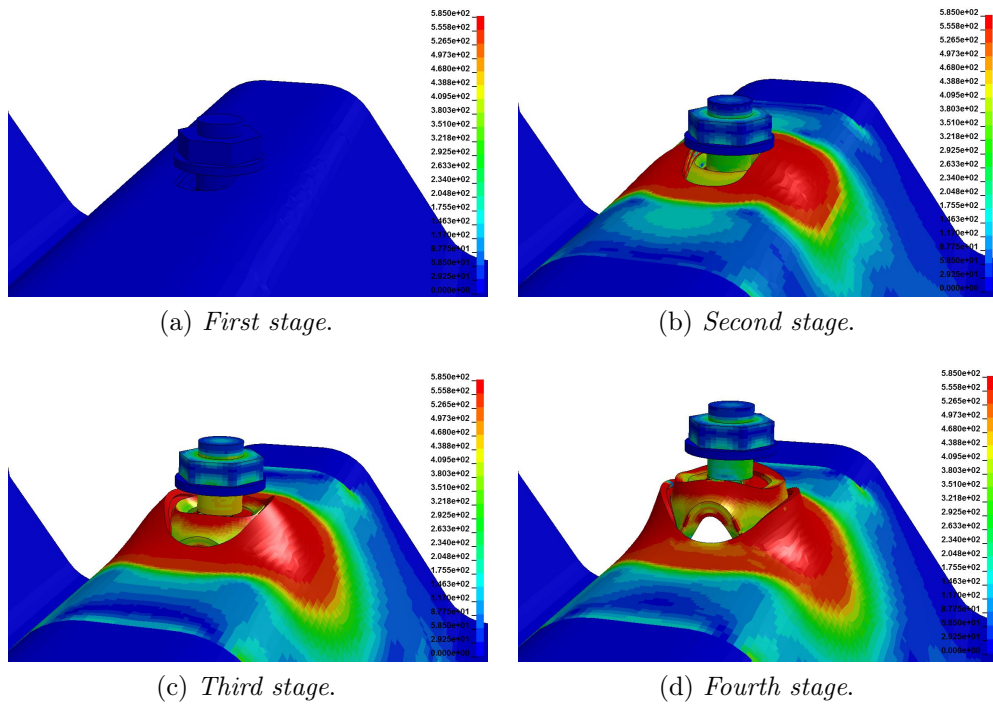
(d) *Fourth stage.*

Figure 6.23: M16 - Centered - Von Mises

6.2.2 Off-center Bolt

Contrary to what happened in the centered configuration, now the bolt breaks: the off-center position grants more contact area between the fishplate and the beam, hence the pull-through requires much more force. Since the shell model is considered more interesting and useful for the final goal of the work, the rupture criterion, the forces and momenta in the beam are reported in the following table and figures.

Both models, solid and shell elements, achieve a very good correlation with the experimental results, being the error < 1%.

Case	Axial force [N]	Exp test [N]	Δ	Error [%]
Shell	85233	85489	256	0.3
Solid	86139	85489	650	0.8

Table 6.4: M16 peak force - Off-center

(a) *Back view.*
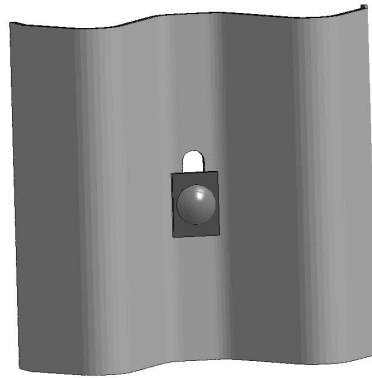
(c) *Front view.*
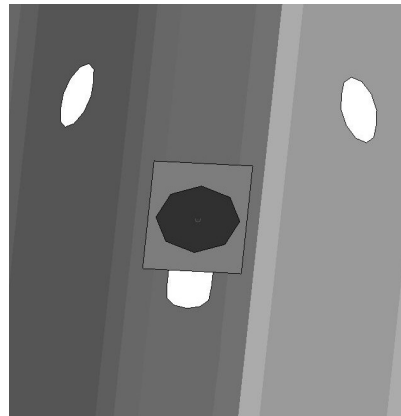
Figure 6.24: M16 - Off-center
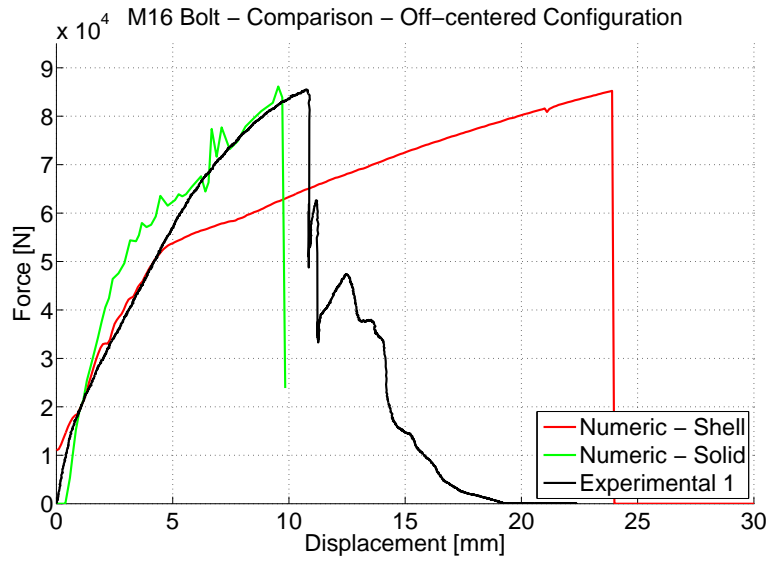
Figure 6.25: M16 - Results - Off-center
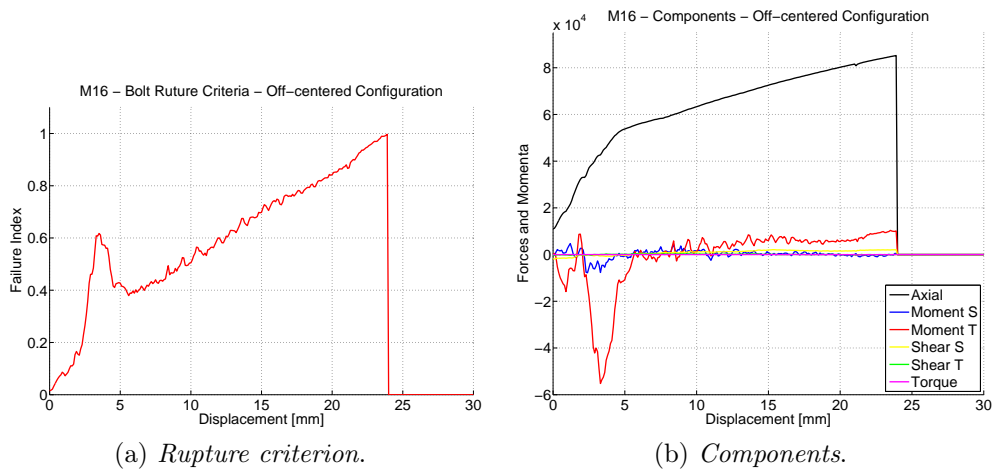
(a) *Rupture criterion.*

(b) *Components.*

Figure 6.26: M16 - Off-center - Rupture

Also from a visual point of view, numerical and experimental results show the same results.

(a) *Experimental.* (b) *Solid.*
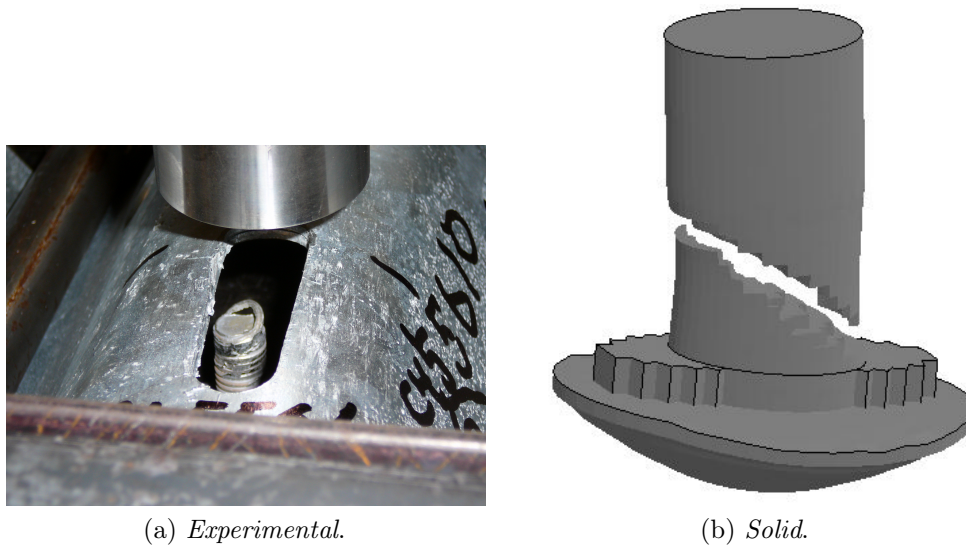
Figure 6.27: M16 - Off-center - Broken bolt

(a) *Experimental.* (b) *Solid.*
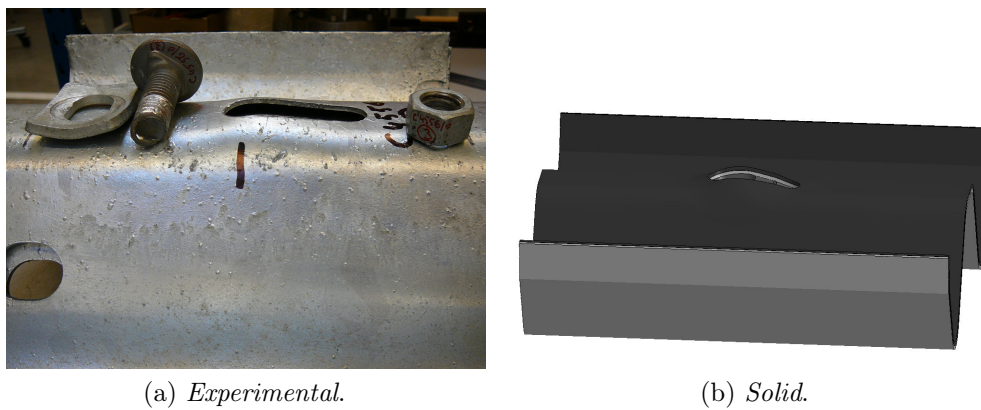
Figure 6.28: M16 - Off-center - Beam final deformation

(a) *Experimental.*   (b) *Shell.*
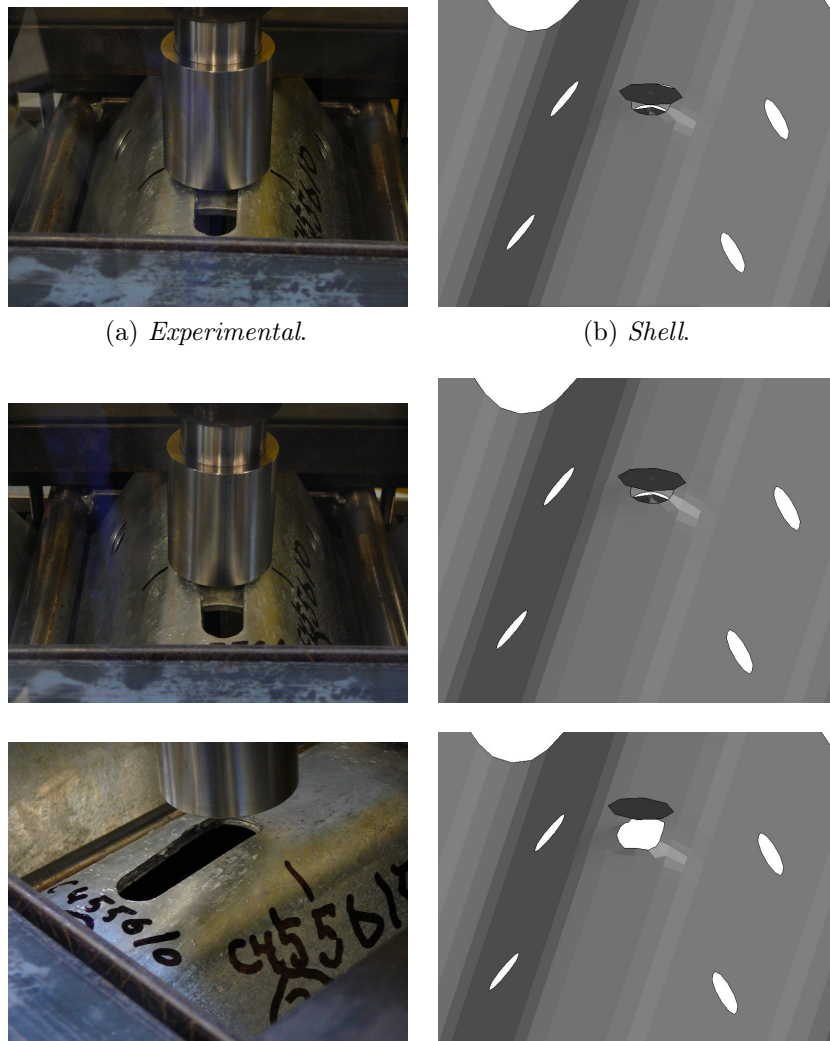
Figure 6.29: M16 - Off-center - Displacement

6.3 Computational time

To conclude the chapter, the computational time required by some analysis is reported, to highlight the high efficiency of the bi-dimensional model compared to the solid one.

Model	Time
M10 - Single beam - 1 Beam	11m31s
M10 - Single beam - 5 Beams	11m57s
M10 - Single beam - Solid	24m21s
M16 - Centered - 1 Beam	11m29s
M16 - Centered - Solid	8h13m

Table 6.5: Computational time

Chapter 7

Full scale crash test simulations

In the following pages the results of the full scale simulations are presented. The key factors to evaluate the quality of a model are:

- computational time;

- accuracy of results, in terms of number of disconnections, working width and dynamic deflection of the barrier.

A remark concerning the computational time: since at GDTech are available several machines dedicated to calculations, the performances of each one can change, due to different hardware configuration and general optimization of the computer itself.
Where possible the same version of Ls-Dyna was used, focusing the attention on 2 most reliable and available at the time of the stage:

- 5.1.1
- 6.1.1

In both cases the Massive parallel processing (*MPP*), that grants better contacts management and optimize the performances with multiple CPU, was used.
Version 6.1.1 at the beginning of the work was not yet available, hence local tests were performed with version 5.1.1; as soon as the newer became available it has been adopted as the standard for all the analysis. For full scale simulations, instead, there were some restrictions due to the model of the vehicle or soil used. Anyway, after some tests it has been estimated that the impact of the version on the final computational time is around 10%.
To evaluate the speed-up or speed-down due to the junction model, compared to the spotweld solution, an *index* has been created; this was needed

because the models are all different from each other (in terms of elements, simulated time, etc...).

Since doubling the number of CPU doesn't comport halving the computational time, a brief study was conducted, with the following results: the simulation object of the test is the full scale of *Barrier B*.

Image 7.1 and table 7.1 report the speed up increasing the number of CPU, from 4 to 40:
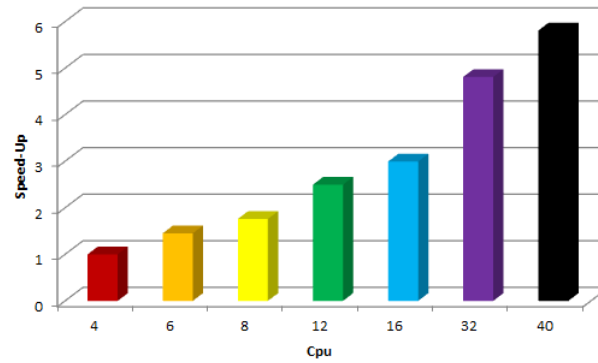
Figure 7.1: Speed - up

Number of CPU	4	6	8	12	16	32	40
Speed-up	1	1.45	1.76	2.50	2.99	4.81	5.81

Table 7.1: Speed up - Coefficients

After these consideration the formula to calculate the index is:

$$Index = \frac{CPUTime/Coeff./SimulatedTime}{Nodes} \cdot 10000 \qquad (7.1)$$

The computational time is divided by the simulated time, that varies for an analysis to another; in many cases the simulations were stopped just after the point of interest was reached; to consider the different sizes of the models the number of nodes is a very significant parameter.

The product for 10000 is just to have the result in a comfortable way.

7.1 Description of the barriers

For confidentiality reasons the real names of the barriers used are not reported; a brief description of the models is anyway reported.

7.1.1 Reference Barrier A

The first model, barrier A, is an H1, designed to redirect a 10 tons truck: the shape is quite standard, with a two wave beam, a U-section spacer and C-section post.

The installation length is 76m plus 32m of terminals, whose nodes below the soil level are constrained; the soil model is discrete and it consists in non linear springs working in the X and Y directions.

For all the shell elements an under-integrated formulation has been adopted, together with a proper hourglass control: they are the best compromise between computational efficiency and accuracy of results. For such application, considering that the average element length is between 10 and 15 mm, a fully integrated solution is not needed: the improvement would be negligible.
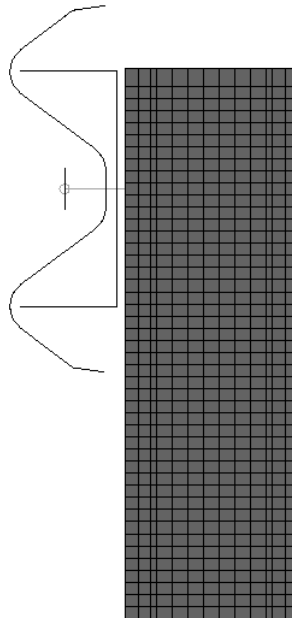
Figure 7.2: Barrier A - Back view
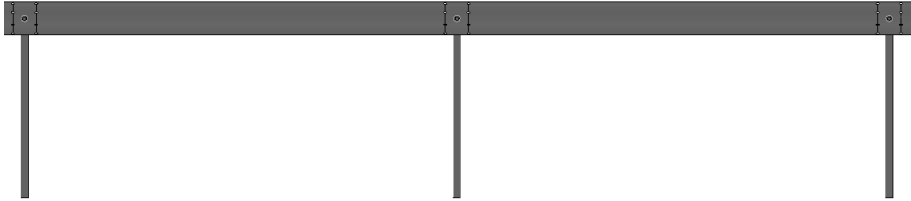
Figure 7.3: Barrier A - Side view

Containment Level	H1
ASI Level	A
Working Width	1.2 m - W4
Dynamic Deflection	1.1 m
Vehicle Intrusion	2.9 m - VI8
Height	0.76 m
Width	0.24 m
Beam Thickness	2.5 mm
Posts Distance	4000 mm
Post sizes	150 x 75 x 25 x 3.5 - H = 1755
Spacer size	200 x 70 x 5
Bolts	M16 5.8

Table 7.2: Barrier B - Specifications

7.1.2 Reference Barrier B

(a) *Iso view.*   (b) *top view.*
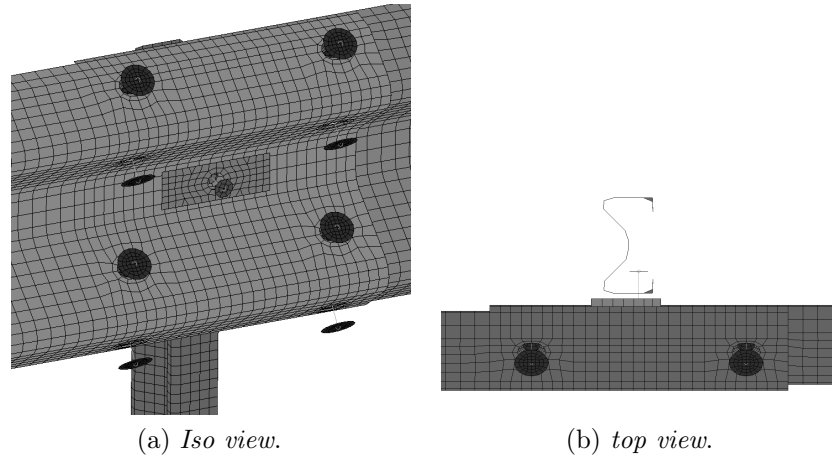
Figure 7.4: Barrier B - Top and Iso view

The second model, Barrier B, is similar to the first one, except the section of the post is a sigma (Σ). The material used is S235 JR. The impact point is located at 1/3 of the total length of the device, in accordance to the crash test report. The installation length is 60 m plus 32 meters of terminals.

Containment Level	N2
ASI Level	A
Working Width	0.8 m - W2
Dynamic Deflection	0.7 m
Height	0.76 m
Width	0.193 m
Beam Thickness	3 mm
Posts Distance	2000 mm
Post sizes	100 x 55 x 4.2 mm
Spacer size	200 x 82 x 5.0 mm
Fishplate	115 x 40 x 5.0 mm
Bolts	M10 4.6

Table 7.3: Barrier B - Specifications

7.1.3   Vehicles
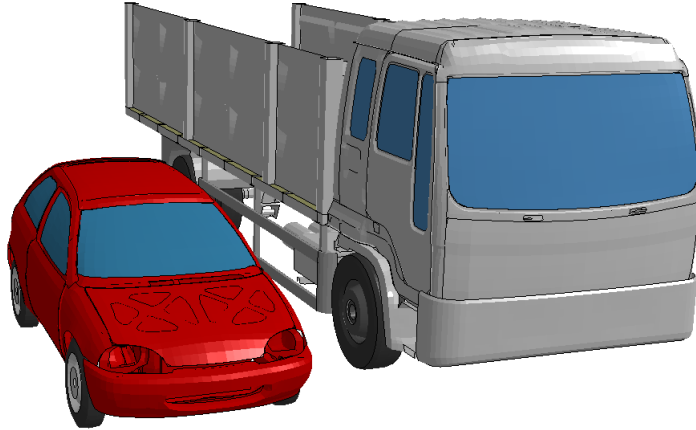
Vehicle	Number of elements
Car	25040
Truck	81998

Table 7.4: Vehicles - Number of elements

Both the two numerical models of the vehicles are calibrated and validated according to the norm EN-1317: this means that their specifics are within the imposed limits and the global quality of the model is satisfactory, hence their behavior is considered reliable.
A vehicle model, to be validated has to pass a series of test specifically designed to evaluate the performances of the critical components as suspensions and steering system.

7.2   Barrier A - TB 11

For this case, in the real crash test the fishplate was not used, highly increasing the chances of pull-though for the bolt. Such behavior can be reproduced, but, as already explained, there are some limits due to the material law used.
The test involves a 900 kg small car, at 100 km/h with an impact angle of 20 degrees.

Name	Elements	Time	Discs.	WW	DD	ASI	Index
Spotweld	473.138	33h38m	4	0.85	0.79	0.75	1.30
1-Beam	482.013	13h47m	2	0.86	0.65	0.93	0.32
Real Test	-	-	2	0.76	0.68	0.80	-

Table 7.5: Results of barrier A - TB11

For this configuration the improvement due to the bolt model is relevant: the number of disconnections matches between numerical and real test. The dynamic deflection is much closer to the real one and the working width does not change much, because it depends from the displacement of the post, that is mostly influenced by the soil.

Figure 7.5: Barrier A - TB11

In this case the vehicle shows a good behavior too, because, as it can be seen, the detachment of the wheel was reproduced.
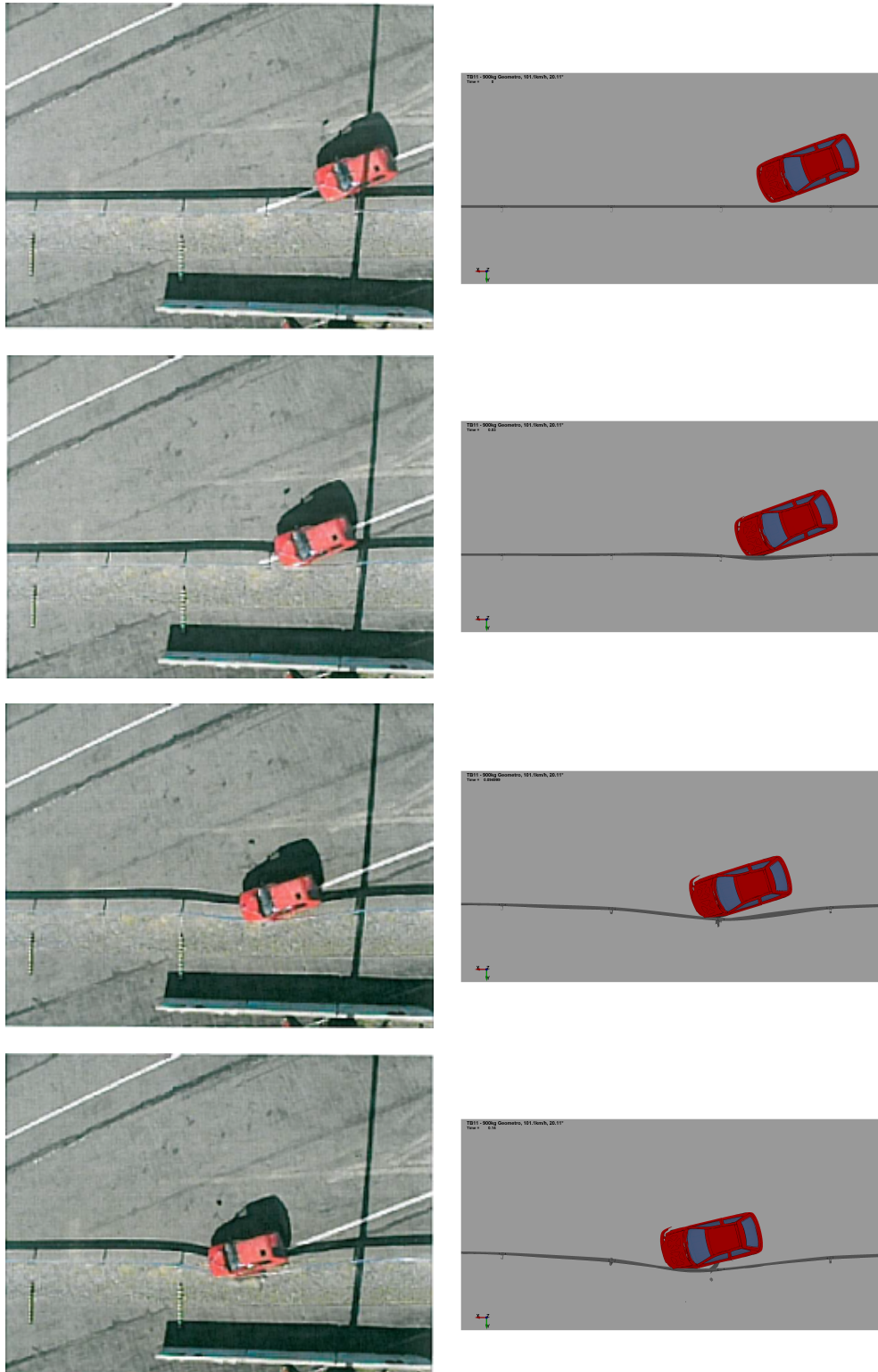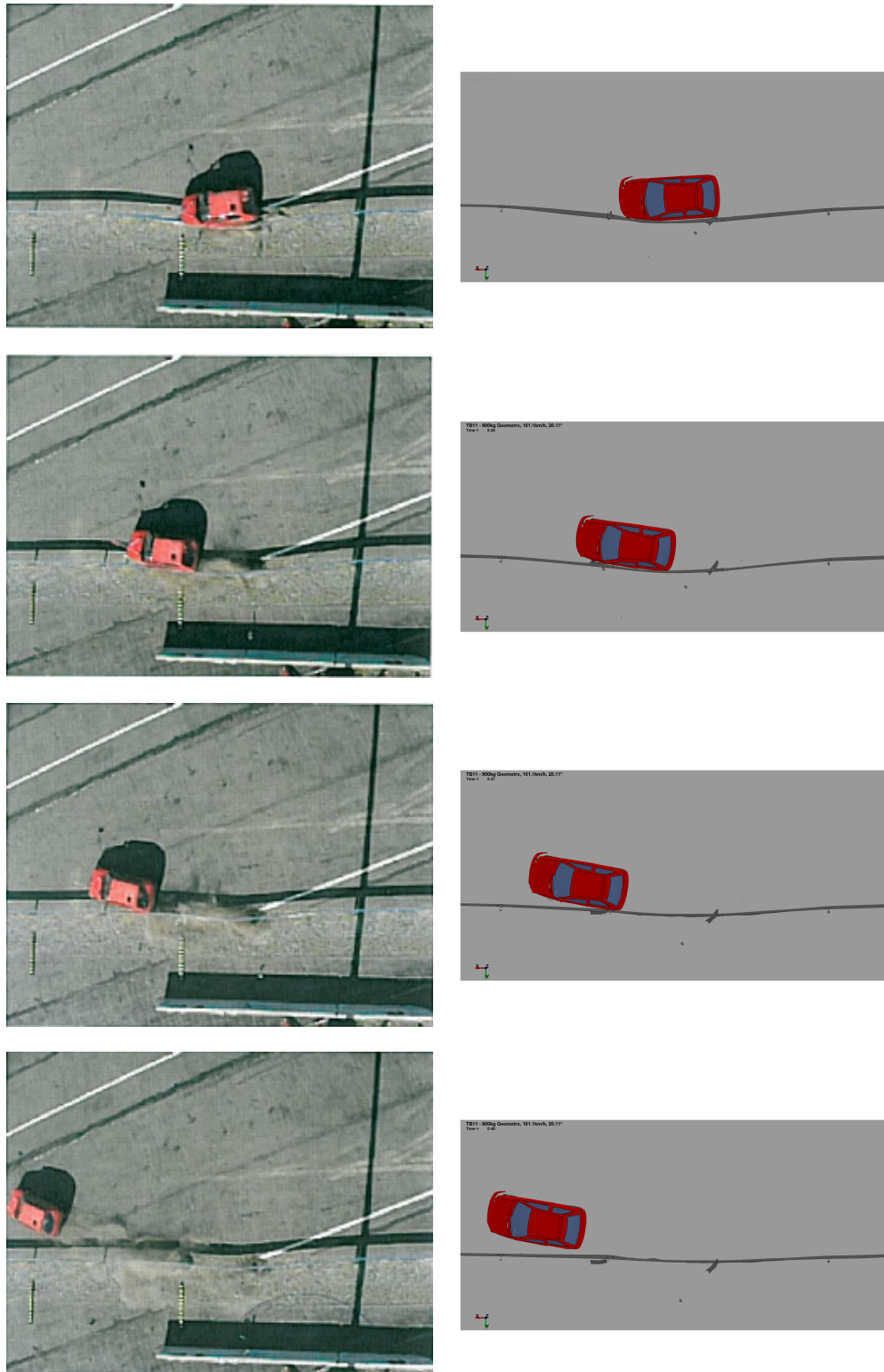
Figure 7.6: Crash Test A - TB11

Figure 7.7: Crash Test A - TB11
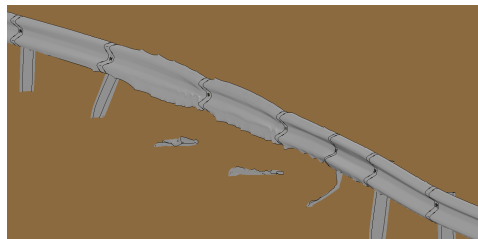
7.3   Barrier A - TB 42

The barrier is the same, the vehicle changed. It is now a 10 tons truck, with a speed of 71.9 km/h and an impact angle of 14.5 degrees.

Name	Elements	Time	Discs.	WW	DD	VI	Index
Spotweld	473138	36h27m	3	1.22	1.13	3.04	1.63
1-Beam	482013	37h24m	2	1.22	1.15	1.60	0.19
Real Test			2	1.19	1.11	2.90	

Table 7.6: Results of barrier A - TB42

(a) .   (b) .

Figure 7.8: Barrier A - TB42

The number of disconnections of the numerical simulation matches the real one; between spotweld and bolt model there are not many differences in terms of working width and dynamic deflection. Remarkable, instead, is the difference comparing the values of vehicle intrusion.

This aspect was investigated and other simulations were performed; the results are in figure 7.11: on the left the simulation with the new version of the 10Ton truck performed with version 6.1.1 of Ls-Dyna. On the right, instead, the results were obtained with and older truck model, unable to run with the latest version of the solver; due to this reason the version used was 4.2.1.

This is just a simple example to demonstrate the complexity to calibrate a barrier and obtain results comparable to the real ones; the factors that play a key role are multiple and the role of the engineer is determinant to understand the limits of the numerical model to adapt it to each case.
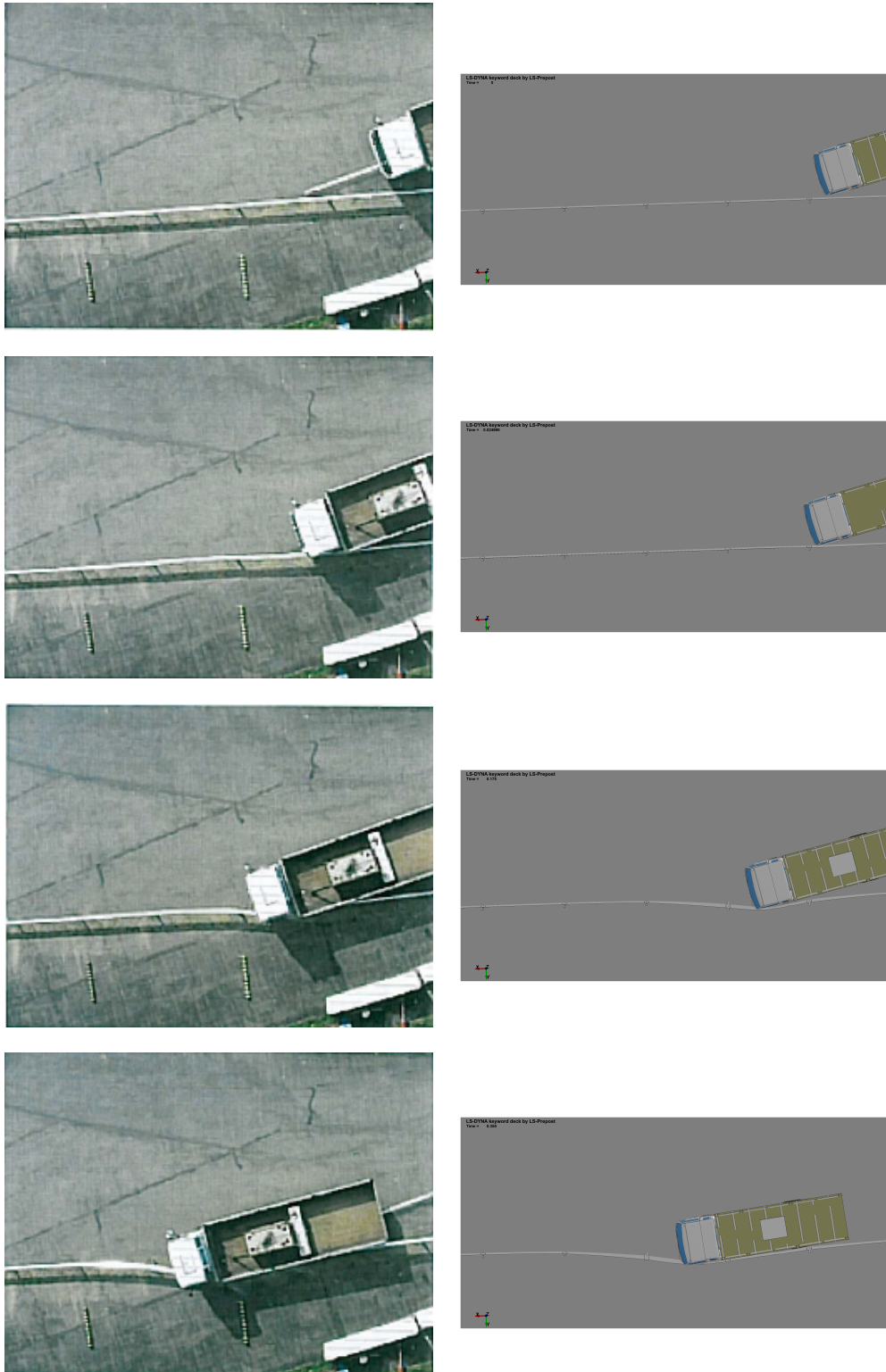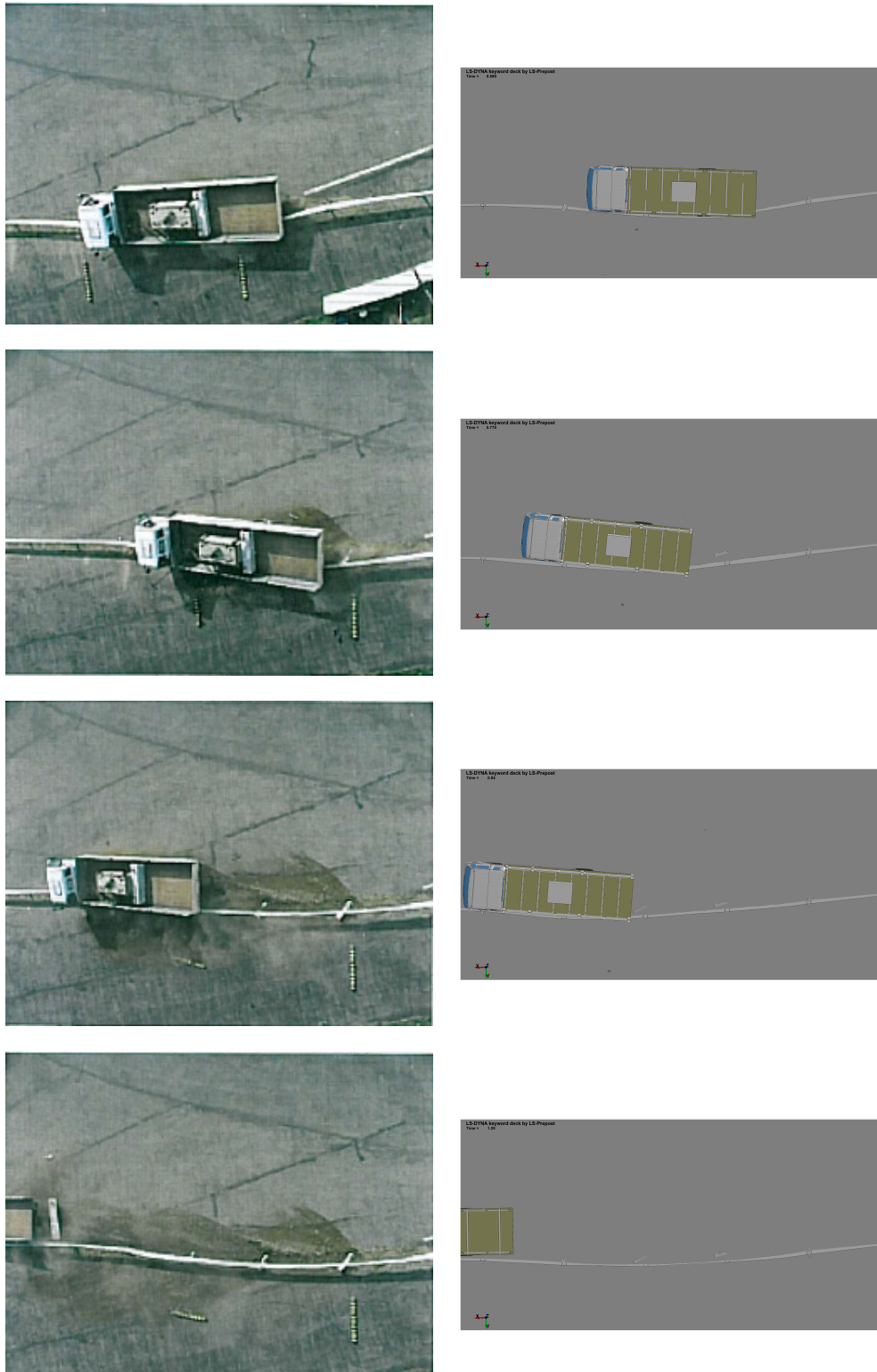
Figure 7.9: Crash Test A - TB42
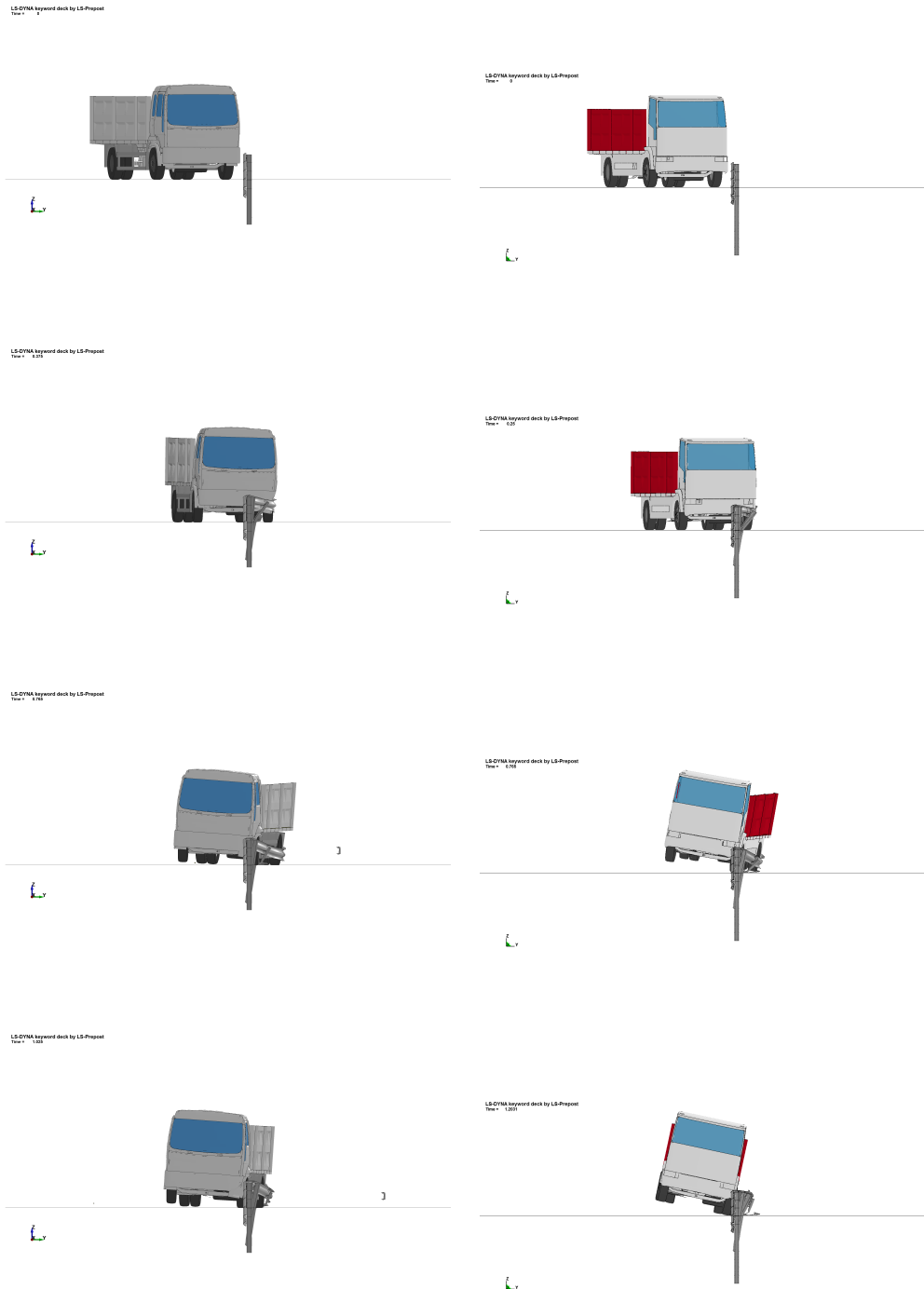
Figure 7.10: Crash Test A - TB42

Figure 7.11: Crash Test A - TB42 - VI Comparison

7.4   Barrier B - TB 11

A different barrier, the test is again a TB11.
In this case all the possible way to model a junction were considered:

- Spotweld
- 1-Beam
- 5-Beams
- Solid elements
- Double beam

The last term of the list deserves an in-depth analysis: due to the use of the spotwelds, the connection between two beams usually is not modeled. To represent the overlapping area a double thickness is the assigned to the corresponding elements, yielding a working model but with some limits. Thanks to the junction model it is now possible to simulate this feature of the barrier too; in this case, the real improvement does not regard the junction itself, that due to the strong bolts usually present it never breaks, but the behavior of the barrier, in terms of stresses distribution, dynamic deflection of the system and consequently the trajectory assumed by the vehicle after the contact with the road restraint system.

Name	Elements	Discs.	WW	DD	Exit Angle	ASI
Spotweld	585.310	5	0.75	0.54	8	0.75
1-Beam	567.407	4	0.83	0.62	8	0.75
5-Beams	568.648	4	0.83	0.60	9	0.78
Solid	670.937	3	0.82	0.61	9	0.69
Double	582.004	3	0.80	0.68	9	0.71
Real Test	-	4	0.8	0.7	9	0.7

Table 7.7: Results of barrier B - TB11

The results confirm the quality of the model: the number of disconnections is matched by the beam solution.
Since this analysis, once calibrated, was used as benchmark to evaluate the effects on the results of changing the version of LS-Dyna the temporal results are reported in table 7.8; the above parameters were more or less constant. Significant is the improvement in terms of disconnections, in fact the real results is matched only using version 6.1.1 of dyna.

Name	Hours	CPU	LS-Dyna Version
Spotweld	31h18m	8	4.2.1
1-Beam	32h49m	4	6.1.1
5-Beams	33h12m	4	6.1.1
Solid	34h20m	4	5.1.1
Double	33h44m	4	6.1.1

Table 7.8: Results of barrier B - Computational time

The difference is remarkable comparing spotweld and the others, but it can also be because of the different version of the solver.
Using the junction model the computational time doesn't change significantly and, more important, it does not increase if compared to the spotweld solution.
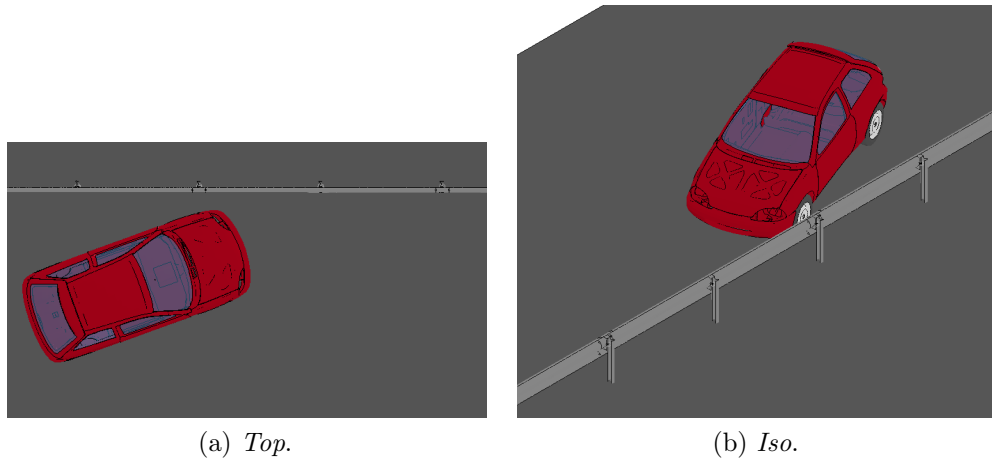

(a) *Top.*   (b) *Iso.*

Figure 7.12: Barrier B - Impact point

It is now shown a parallel between the real crash test and the simulation using junctions to connect the beams with each other.
To avoid having a model with too many elements, the area with the overlapping beams modeled is limited to impact zone.

Figure 7.15 shows the differences, in terms on Von Mises stress, between the models with single and double beam. the peak values are almost the same, around 590 MPa but the distribution is completely different; for the case with single beam, in correspondence of the part with double thickness, there is a discontinuity for the stress. Meanwhile, the use of two overlapping beams grants the continuity of the stresses.
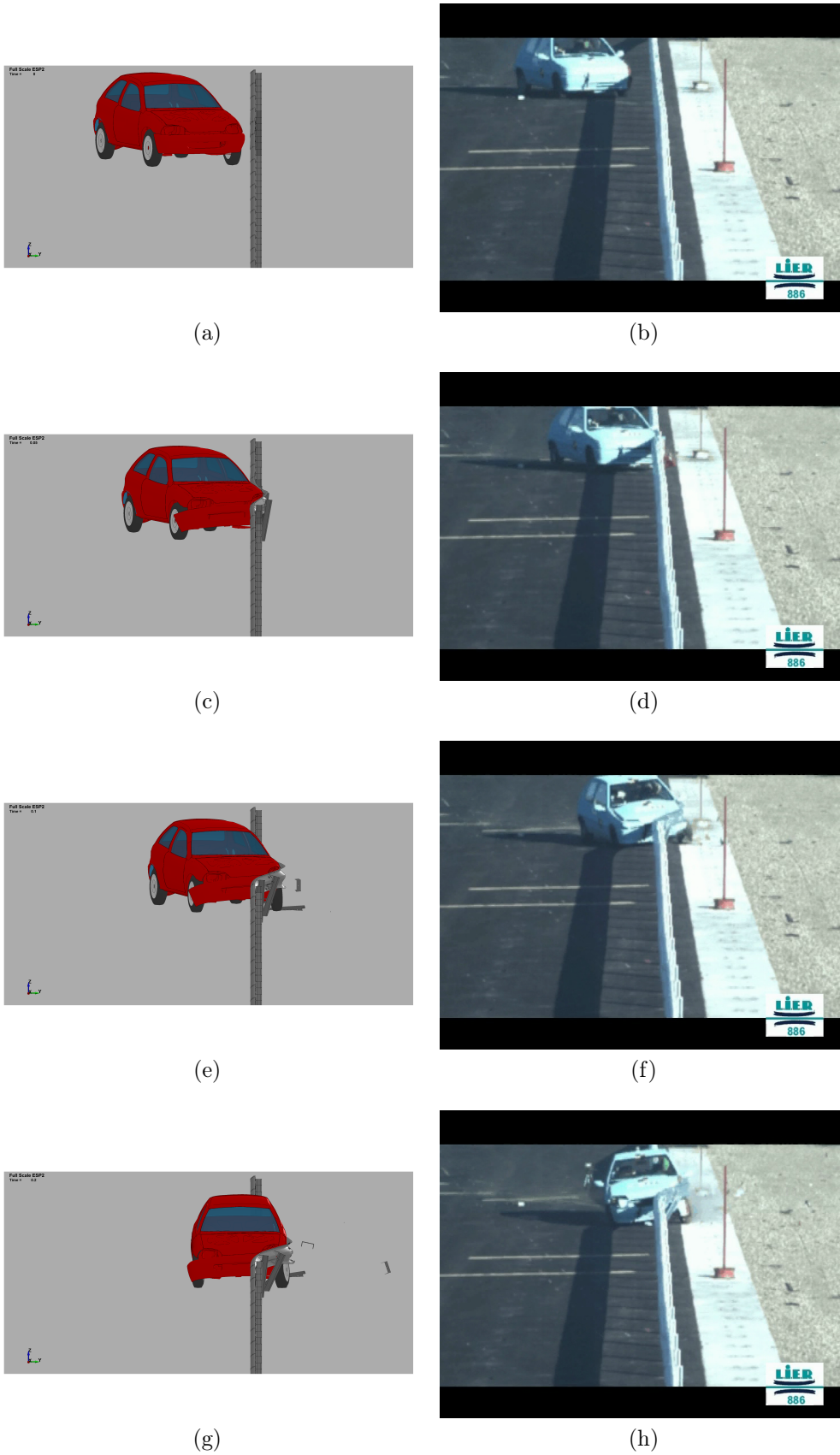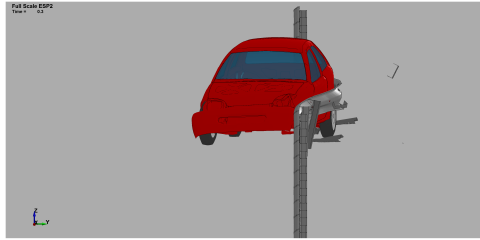
(a)

(b)

(c)

(d)

(e)

(f)

(g)

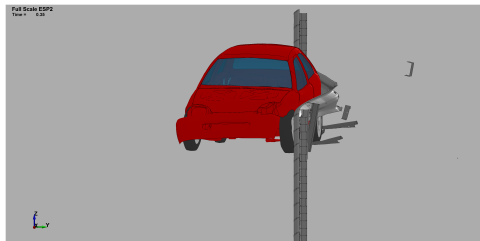

(h)

Figure 7.13: Crash Test B - TB11

(a)

(b)

(c)

(d)
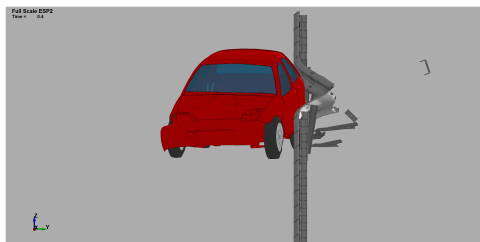
(e)

(f)
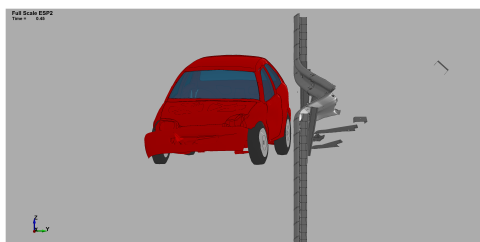
(g)

(h)

Figure 7.14: Crash Test B - TB11

(a) *Single.*

(b) *Double.*
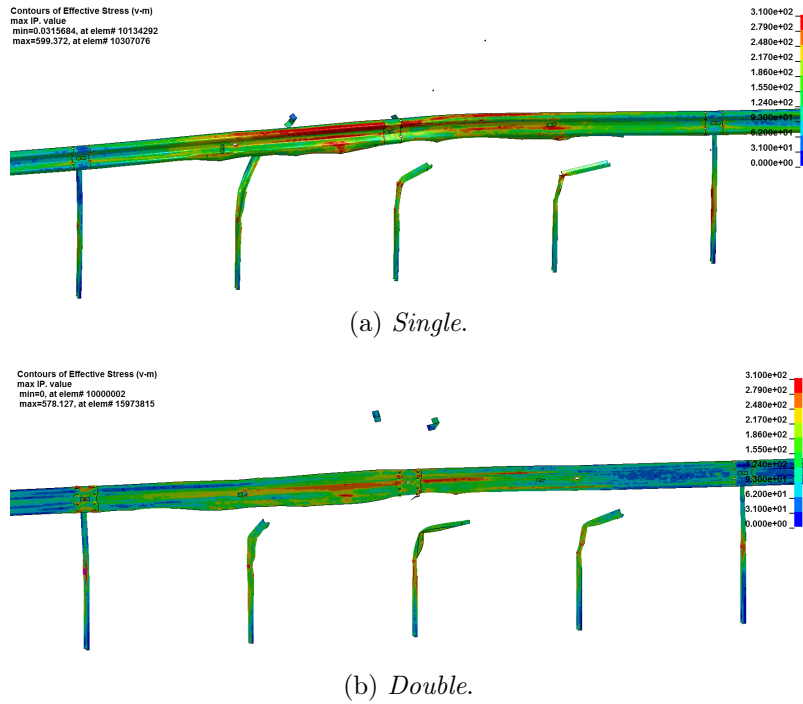
Figure 7.15: Von Mises comparison

The case of 1-beam to model the junction is now analyzed. To confirm the numerical stability of the simulation, the graph with the energies is reported in 7.16: the hourglass energy is negligible, the total energy is constant.

To verify the reliability of the numerical model the failure index for each bolt is presented in 7.17, together with the components and stress for each beam, 7.18.

From figure 7.19 emerges that the failure is not only due the axial stress, but also to the presence of momenta, whose contributes are significant.

Figure 7.16: Barrier B - Energies

Figure 7.17: Barrier B - Bolts failure

Figure 7.18: Barrier B - Bolts stresses

Figure 7.19: Crash Test B - Bolts components

Chapter 8

Conclusions and further developments

This thesis presents the development of a numerical model of a bolted connection using finite elements, to be used with numerical simulations in 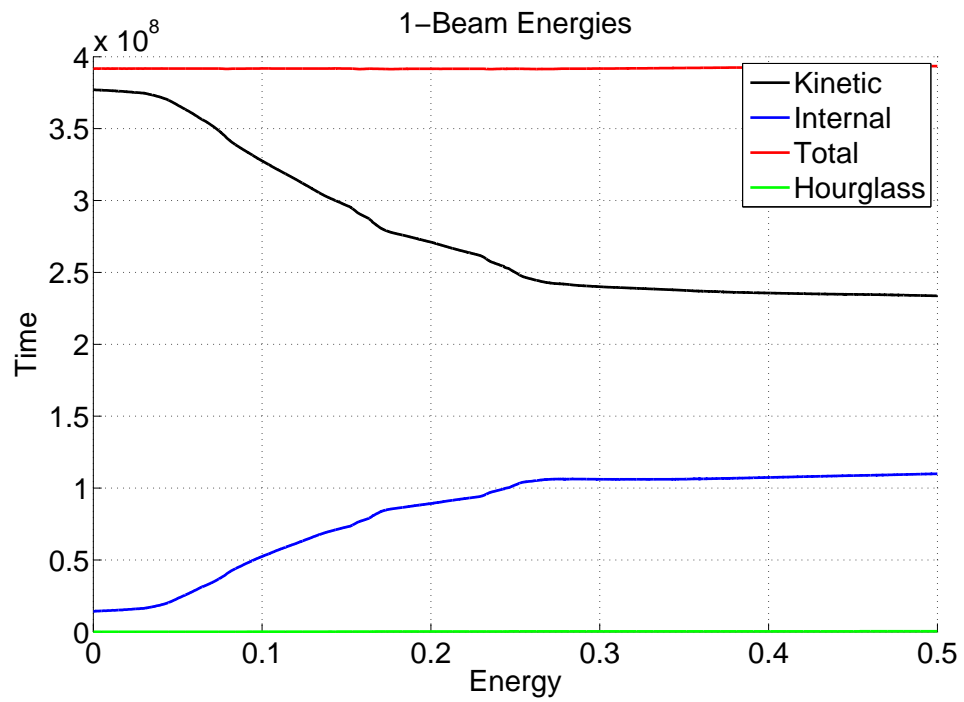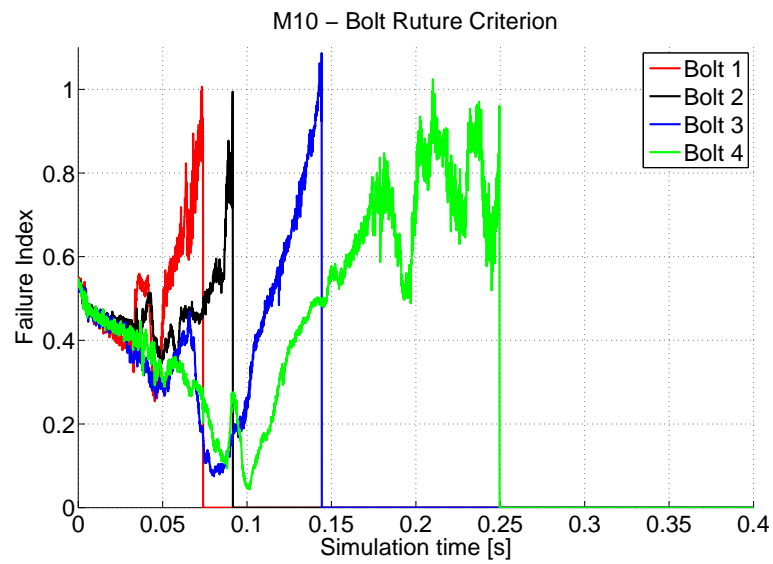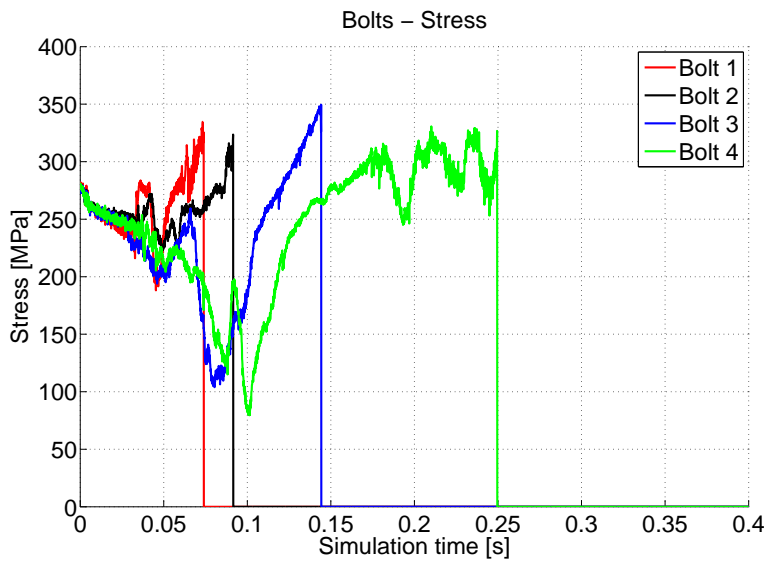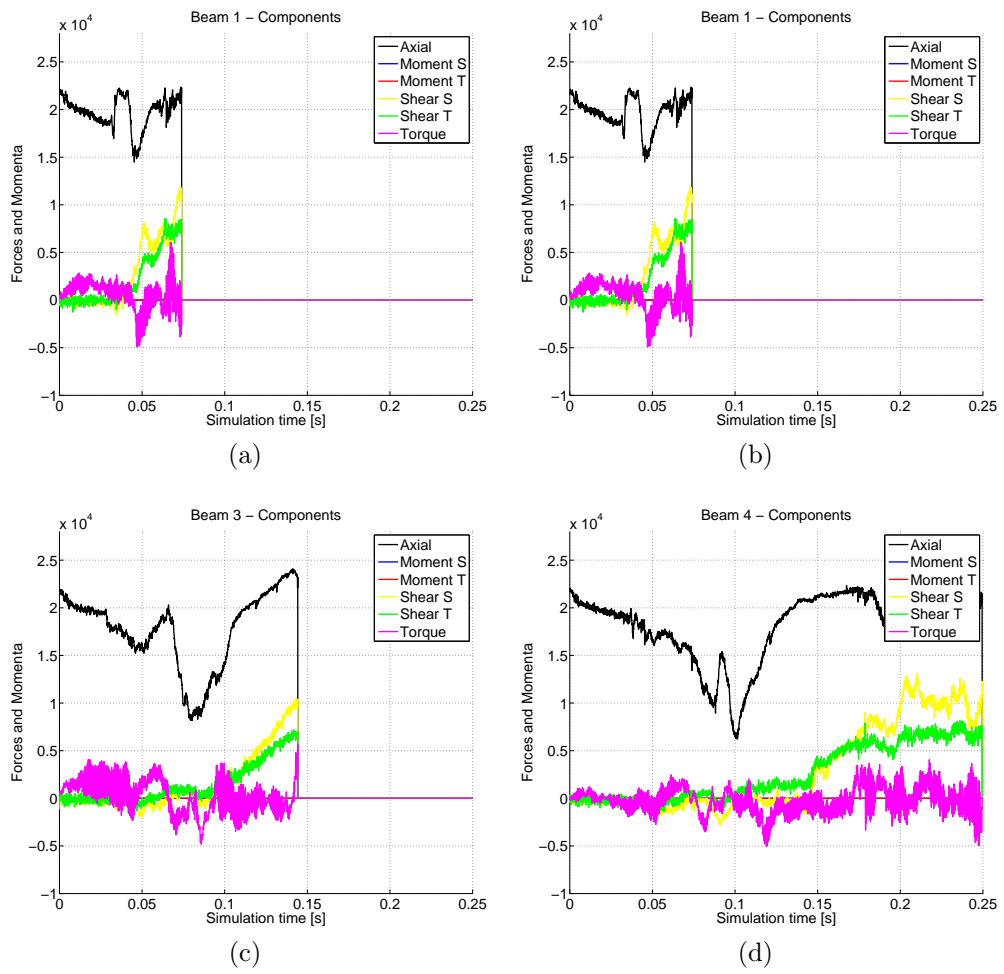the field of crashworthiness and road restraint systems; the usage environment is critical because of the typical lack of information provided in the initial phase of the project.

One of the first goals of the model, the possibility of working with the minimal amount of information has been achieved, in fact no more than the dimensions and the class of the bolt are requested.

Several configurations to model the junction were presented, using all the available solutions offered by the finite element code used, LS-Dyna, considering both solid and shell elements, based on the application: for local tests a model using solid elements is as good as a shell one, meanwhile for full scale simulations the computational increase due to the 3D elements makes the model viable only in limited cases.

Instead, the bi-dimensional approach has proved itself satisfactory in all the situations, it fully fits all the requests in terms of computational efficiency and accuracy of the results, hence it can be used during all the phases involved in the design of a new product, from simple local tests to full scale impact scenario.

As presented, through the local tests the different failure methodologies can be reproduced: rupture of the bolt or bearing of the hole, allowing the bolt to pass through.

The numerical results are always compared with real experimental tests: for both, local cases and full scale simulations, the correlation is excellent. Due to its versatility, compared to the solid model, the contact beam one has been object of further improvements, optimizing the geometry of the

disposition of the elements in charge or representing the shank of the bolt. Compared to the previous solution adopted to represent a bolted connection, the spotweld, the improved is huge: the geometry of the finite elements model is comparable to the real one and the effects of all the components are simulated and taken into account; the introduction of the preload and the improved rupture criterion are remarkable features not considered in the previous version.

All the objectives proposed at the beginning of the work have been satisfied: the model is actually being used and it is, to all effects, a tool for the enterprise.

8.1   Further developments

With a deeper campaign of experimental tests the model could be further improved and made more consistent: some dedicated pure shear trials could help to improve the failure criterion in specific load configurations. In a near future, thanks to the increase of computational power, the tridimensional solution could be preferred over the bi-dimensional one, but to work properly a more sophisticated material law in LS-Dyna has to be used, to consider and permit the eventual deletion of the elements to represents the rupture of the pieces. The definition of such a material goes through many curves and parameters, only available after dedicated and expensive experimental tests.

From a pure numerical point of view the effects of the massive parallel processing (MPP) compared to the shared memory processing (SMP) should be deeply investigated, since LS-Dyna didn't prove itself fully consistent, switching from a version to another one.

It has to be said that the software is continuously updated, improved and new features added with each release; the same should be done to the model, verifying its performances with each solver and eventually including new available features.

Appendix A

Experimental equipment

The pulling test were perfomed using an INSTRON 1126, as shown at the beginning of chapter 3.
The acquisition system name is INSTRON 8800.
The peculiar characteristics are reported in table A.1.

Maximum force [kN]	250
Maximum displacement [mm]	2640
Weight [Kg]	1820

Table A.1: INSTRON 1126 specifications

Appendix B

Calculation machines used

Description	Number of cpu	Frequency [GHz]	RAM [GB]
AMD Phenom X6 T1055	6	2.8	4
Intel Core 2 Duo P7450	2	2.13	4
Intel Xeon X5650	12	2.67	96
Intel Xeon E5520	8	2.67	16
Intel i7-920	4	2.66	12
Intel i7-2600	4	3.40	16

Appendix C

Used Software

- LS-Dyna Version 4.2.1 SMP version
- LS-Dyna Version 5.1.1 SMP and MPP version
- LS-Dyna Version 6.1.1 SMP and MPP version
- LS-PrePost
- TRAP
- Matlab
- Excel
- Word
- Powerpoint
- LaTeX
- MS. Paint
- Hypermesh
- Dropbox
- Teamviewer

Bibliography

[1] Livermore software technology Corporation, *LS-Dyna keyword user's manual Volume I*, 2013.

[2] Livermore software technology Corporation, *LS-Dyna keyword user's manual Volume II*, 2013.

[3] John O. Hallquist, *LS-Dyna theory manual*, 2006.

[4] F. Seeger, M. Feucht, Th. Frank, B. Keding, A. Haufe, *An investigation on spotweld modeling for crash simulation with Ls-Dyna*, 2005, Stuttgart.

[5] Shailesh Narkhede, Nitin Lokhande, Bhavesh Gangani, Ganesh Gadekar, *Bolt joint representation in Ls-Dyna to model bolt pre stess and bolt failre characteristics in crash simulations*, 2011.

[6] Euroviti, *Scelta e verifica dei bulloni*.

[7] F. Previtali, M. Anghileri, L;-M. L. Castelletti and A. Milanese, *Combined numerical/experimental approach for rivet strenght assessment*, 2009, Milano.

[8] Moisey B. Shkolnikov, *Strain Rates in Crashworthiness*, 2010.

[9] Ashok L. Ramteke, *Improving analysis accuracy by modeling rivets/bolts as solids in sheet metal structure*, 2009.

[10] Matej Vesenjak, Zoran Ren *Improving the roadside safety with computational simulations*.

[11] P.K.C.Wood, C.A. Schley, R. Beaumont, B. Walker, T. Dutton, M.A. Buckley, *Modeling and predicting spotweld failures in automotive crash structures*.

[12] U. Sonnenschien, *Modeling of bolts under dynamic loads*, 2008, Bamberg.

[13] Ken-An Lou and William Perciballi *Finite element modeling of preloaded bolt under static three-point bending load,*.

[14] Skye Malcolm, Emily Nutwell, *Spotweld failure prediction using solid elements assemblies.*

[15] Sergio Marco Bassi, Davide Benetton, *Studio di un'innovativa tipologia di giunzione per elementi di barriere stradali*, 2012.

[16] Clemens Barthel, till Clausmeyer, Bob Svendsen *Numerical investigation of draw bending and beep drawing taking into account cross hardening.*

[17] Jerome Montgomery, *Methods for modeling bolts in the bolted joint.*

[18] O.S. Bursi, J.P. Jaspart, *Banchmarks for finite element modeling of bolted steel connctions.*

[19] John D. Reid, Nicholas R. Hiser, *Detailed modeling of bolted joints with slippage.*

[20] José Maria Minguez, Jeffrey Vogwell, *Effect of torque tightening on the fatigue strength of bolted joints*, 2006.

[21] Jeong Kim, Joo-Cheol Yoon, Beom-Soo Kang, *Finite element analysis and modeling of structure with bolted joints*, 2006;

[22] Klas Erik Engstrand *Improvements to the weak post W-beam guardrail*, 2000.

[23] Falko Seeger, Markus Feucht, George Dumitru, Tobias Graf *Enhancement of spot weld modeling using MAT 101 DAI*, 2008, Bamberg.

[24] Jean-Pierre Muzeau, *Constructions métalliques, Assemblages par procédés mécaniques*

[25] British Standard, *Mechanical properties of fasteners made of carbon steel and alloy steel - Part 1: Bolts, screws and studs*, 1999.

[26] Suri Bala, *Deformable spotwelds in LS-Dyna for impact and NVH applications.*

[27] Suri Bala, *Stress initialization in LS-Dyna.*

[28] Tobias Erhart, *Review of solid element formulation in LS-Dyna*, 2011, Stuttgart.

[29] Yih-Yih Lin, *A performance study of LS-Dyna on Vehicle Crash.*

[30] Mortenrikard Jensen, *Introduction to LS-Dyna Implicit*, 2007, Livermore.

[31] European Standard, *EN 1317*, 2010, Bruxelles.

[32] Ente nazionale italiano di unificazione, *Eurocodice.*

[33] International Road Federation, *www.irfnet.org.*

[34] European Union Road Federation, *www.erf.be.*

[35] RRS Road Safety, *www.rrs.erf.be*

[36] DYNAlook, *www.dynalook.com.*

[37] LS-DYNA Examples, *www.dynaexamples.com.*

[38] LS-DYNA Support, *www.dynasupport.com.*

[39] ArcelorMittal, *www.arcelormittal.com.*